НАЦІОНАЛЬНЕ
КОСМІЧНЕ АГЕНТСТВО
УКРАЇНИ

НАЦІОНАЛЬНА
АКАДЕМІЯ НАУК
УКРАЇНИ

КОСМІЧНА НАУКА І ТЕХНОЛОГІЯ

äÄäçÆÄè äÄ åôÉìÇïô

КИЇВ L Æ Þ ø 7, ¶ 2, 2001 L KYIV

SPACE PLASMA PHYSICS

Proceedings of the VIII Ukrainian Conference and School on Plasma Physics and Controlled Fusion

(Alushta, Crimea, September 11—16, 2000)

CONTENTS

№ замовлення 216 Підп. до друку 04.06.01. Формат 84×108/16. Папір офс. № 1. Друк офсетний.
Ум. друк. арк. 12.18. Обл.-вид. арк. 11.5 Тираж 500 екз.

öIçêèÇ èÄæîIùìÄÛ ÅïÇçîê

Матеріали VIII Української конференції-школи
«Фізика плазми та керований синтез»
(Алушта, Крим, 11—16 вересня 2000 р.)

Під редакцією доктора фіз.-мат. наук
О. К. Черемних

PREFACE

The present collection of papers includes the original articles of the participants of the «VIII Ukrainian Conference and School on Plasma Physics and Controlled Fusion» which was held in Alushta, Ukraine, September 11—16, 2000 and had the status of an international conference. The Space Research Institute NSAU-NASU firstly organized the section of «Space Plasma» within the framework of the conference under financial support of National Space Agency of Ukraine. The main goal of the section was oriented on discussion of new results on space plasma, which have been received in Ukraine, and on coordination of the future research. About 40 reports concerning theoretical and applied important problems of space plasma had been presented at the section meetings.

Leading scientists and many young researchers in the area of space and astrophysical investigations represented the following organizations of Ukraine: Space Research Institute, Radio-astronomical Institute, Main Astronomical Observatory, National Taras Shevchenko University, Institute of an Ionosphere, Institute of Physics, V. N. Karazin Kharkov University, G. V. Karpenko Physical-mechanical Institute, NSC «Kharkov physical-technical institute» etc.

The subjects of the section «Space Plasma» is subdivided into the following directions:

— Investigations of nearest space plasma (ionosphere and magnetosphere of the Earth);

— Analysis of astrophysical aspects of plasma physics.

Most of scientific reports were dedicated to precisely these principal trends of plasma physics. The problems raised suggest several interesting leads for further research. Unfortunately, because of limited size of the volume not all the papers were included in this issue.

Finally, we would like to thank all participants of section «Space Plasma» for cooperation, and to express my acknowledgements to N. V. Turoverova, O. I. Zhudra and O. V. Klymenko for the help in preparation of the proceedings.

O. K. CHEREMNYKH
Editor-in-Chief

Космічна наука і технологія. ДОДАТОК. 2001. Т 7. № 2. С. 5—14.

THE CHARACTERISTICS OF LITHOSPHERIC ORIGIN ULF EM RADIATION IN THE LITHOSPHERE-ATMOSPHERE-IONOSPHERE-MAGNETOSPHERE SYSTEM

O. K. Cheremnykh[1], V. V. Grimalsky[2], I. Kremenetsky[1]

[1]Space Research Institute NAS and NSA of Ukraine, Glushkov 40, 03680 Kiev, Ukraine
mailto: phys@space.is.kiev.ua

[2]National Institute for Astrophysics, Optics, and Electronics, Puebla, Mexico

The penetration of ultra low frequency (0.01—100 s^{-1}) electromagnetic (ULF EM) radiation throughout ionosphere are calculated numerically for source in the lithosphere and in the magnetosphere. The changes of perturbation area shape during propagation in the ionosphere are investigated for different «antennas» types in the lithosphere which excite this EM radiation. The wave and spatial characteristics of penetrated into upper ionosphere ULF EM field are determined. The influence of altitude profile's main parameters of ionospheric plasma and geophysical condition onto the penetration effect of ULF EM radiation throughout ionosphere is discussed.

1. INTRODUCTION

It is known that before earthquake the anomalous phenomena in the atmosphere, ionosphere and at the ground surface have been observed. These phenomena have a form of changes of ionosphere parameters, intensity of atmospheric emission and EM radiation. However, the electromagnetic phenomenon such as EM radiation has been observed most often than other ones. To identify the observed radiation as one excited by lithospheric source it is necessary to know the characteristics of EM radiation as one excited by the lithospheric source.

Following Gokhberg hypothesis, we consider that the large-scale ULF currents appear in the seismic zone before earthquakes. The possibility of this effect is considered by Molchanov et al, 1994 in (1) where it was obtained that macrocurrents with typical sizes ~ 10—100 km can be excited in the lithosphere during earthquake preparation period. The penetration of ULF EM waves is considered earlier in (2) on the basis of model of lithosphere-atmosphere-ionosphere-magnetosphere (LAIM) system with axial symmetry and essential simplifications. The better penetration for the frequency ~ 1 Hz is obtained. However, it is not clear how the shape of EM perturbation in the ionosphere (400—800 km) is compared with the shape of current source and its location in the lithosphere. We suppose that only the accurate calculations of penetration of EM field throughout the LAIM media which is modeled without essential simplifications permit to obtain the characteristics of EM radiation of lithospheric origin and by means of these characteristics the identification and determination of the parameters of lithospheric source are possible.

In this paper we present the calculation results of penetration of ULF EM radiation throughout LAIM media obtained by use of the model of LAIM system taking into account the smooth changes of permittivity tensor with respect to altitude, inclination of geomagnetic field and volume lithospheric current of different geometry (we consider both cases of $\mathrm{div}J = 0$ and $\mathrm{div}J \neq 0$). We carry out the search of influence of the geophysical conditions and geometric type of current on the penetration effect of ULF EM radiation throughout LAIM system and obtain the wave and spatial characteristics of this radiation and comparative characteristics of geometrical sizes and spatial structure of EM radiation at the satellite altitudes with geometrical sizes and type of lithospheric current. We also evaluate the amplification effect of EM radiation of lithospheric source which could take place in the area with captured particles of

radiation belts. The losses on the reflection of ULF EM radiation propagating in magnetosphere from the ionosphere in the magneto-conjugated points. The latter consideration is important for the possibility of observation of the lithospheric EM radiation at the satellites during long time period.

2. THE MODEL AND BASIC EQUATIONS

The Cartesian coordinate system is used, so that the axis z was directed perpendicularly to the surface of the Earth. We suppose that the permittivity of all medium is changing along z-direction only, but in tangential plane xy, the permittivity of all medium remains constant.

The lithosphere and atmosphere being isotropic spaces, therefore their tensors of permittivity are diagonal. The lithospheric permittivity is $\varepsilon_l = 1 - i4\pi\sigma_l/\omega$, where σ_l is lithosphere conductivity, and the atmospheric permittivity is $\varepsilon_A = 1$. In the lithosphere we put the volume current with an arbitrary geometry which shape is defined later. Taking into account an inclination of geomagnetic field to the vertical direction $\angle \mathbf{zH} = \theta$ in the ionosphere, we rewrite the ionospheric permittivity tensor as

$$\varepsilon_{\alpha\beta} = \begin{vmatrix} \varepsilon\cos^2\theta + \eta\sin^2\theta & ig\cos\theta & (\eta - \varepsilon)\cos\theta\sin\theta \\ -ig\cos\theta & \varepsilon & ig\cos\theta \\ (\eta - \varepsilon)\cos\theta\sin\theta & ig\cos\theta & \varepsilon\sin^2\theta + \eta\cos^2\theta \end{vmatrix}. \tag{1}$$

where ε, g and η are well-known permittivity tensor elements in cold two component MHD plasma without inclination of the geomagnetic field.

The solving of exact electromagnetic equations is needed because the penetration of ULF radiation occurs in the near zone of radiation and wave zone is forming for considered frequency range 1—100 s^{-1} on the altitudes over 4000 km, where the geometric optics method can be applied. We calculate the penetration of ULF EM field throughout lithosphere, atmosphere and ionosphere, where the sharp changes of permittivity take place, but for propagation in the magnetosphere the geometric optics approximation is used.

Starting from the well-known differential equation for electric field

$$\Delta\mathbf{E} - \nabla(\nabla\cdot\mathbf{E}) = \frac{1}{c}\frac{\partial}{\partial t}\left(\frac{1}{c}\frac{\partial(\hat{\varepsilon}\mathbf{E})}{\partial t} + \frac{4\pi}{c}\mathbf{J}\right), \tag{2}$$

which follows from the Maxwell equations, and applying the Fourier-transform in xy plane, we obtain the equations for the tangential electric field amplitudes

$$\frac{d}{dz}\left[\frac{\varepsilon_{33} - k_y^2/k_0^2}{D}\frac{dE_x}{dz} + \frac{k_x k_y}{k_0^2 D}\frac{dE_y}{dz} + i\frac{k_x}{D}\Upsilon + \frac{4\pi k_x}{\omega D}J_z\right] + i\frac{\varepsilon_{13}}{D}\frac{d}{dz}\Lambda +$$
$$+(k_y^2 + k_0^2\tilde{\varepsilon}_{11})E_x + (k_x k_y + k_0^2\tilde{\varepsilon}_{12})E_y + i\frac{4\pi\omega}{c^2}\left(\frac{\varepsilon_{13}}{D}J_z - J_x\right) = 0, \tag{3}$$

$$\frac{d}{dz}\left[\frac{\varepsilon_{33} - k_x^2/k_0^2}{D}\frac{dE_y}{dz} + \frac{k_x k_y}{k_0^2 D}\frac{dE_x}{dz} + i\frac{k_y}{D}\Upsilon + \frac{4\pi k_y}{\omega D}J_z\right] + i\frac{\varepsilon_{13}}{D}\frac{d}{dz}\Lambda +$$
$$+(k_x k_y + k_0^2\tilde{\varepsilon}_{21})E_x + (k_x^2 + k_0^2\tilde{\varepsilon}_{22})E_y + i\frac{4\pi\omega}{c^2}\left(\frac{\varepsilon_{13}}{D}J_z - J_y\right) = 0. \tag{4}$$

Here, the following definitions are used: the $\propto\exp[i(...)]$ dependence for all wave components; k_i and ω are the components of wave vector in i-projection and frequency respectively; $\varepsilon_{\alpha\beta}$ are components of the permittivity tensor; $0 = \varepsilon_{33} - (k_x^2 + k_y^2)/k_0^2$; $\tilde{\varepsilon}_{\alpha\beta} = \varepsilon_{\alpha\beta} - \varepsilon_{13}\varepsilon_{3\beta}/D$; $\Upsilon = \varepsilon_{31}E_x + \varepsilon_{32}E_y$; $\Lambda = k_x E_x + k_y E_y$; $k_0 = \omega/c$; c is light velocity in vacuum.

3. THE BOUNDARY CONDITIONS

We introduce the upper bound in the magnetosphere over sharp changes of plasma parameters and lower bound in the lithosphere under current source. We consider that semi-infinite homogeneous spaces are situated outside the bounds. We assume that waves of the Alfven (AW) and magnetosonic (MS) types radiate from the upper bound into magnetospheric semi-infinite space and the waves of E- and H-types radiate from the lower bound into lithospheric semi-infinite space due to dispersion properties of these medium in the considered frequency range. The wave numbers in the introduced coordinate system are $k_{z1} = -k_x/\tan\theta + k_0/\varepsilon^{1/2}\cos\theta$ and $k_{z2} = (k_0^2\varepsilon - k_x^2 - k_y^2)^{1/2}$ for AW and MS respectively. The tangential components of EM field (E_t, H_t) over upper boundary could be expressed in the term of wave amplitudes

$$\begin{pmatrix} E_x \\ E_y \end{pmatrix} = \hat{\rho}\begin{pmatrix} C_A \\ C_{MS} \end{pmatrix}, \qquad \hat{\rho} \equiv \frac{1}{k_0\sqrt{\varepsilon}} \left\| \begin{matrix} k_x - k_0\sqrt{\varepsilon}\sin\theta & -k_y \\ k_y & k_x - k_{z2}\tan\theta \end{matrix} \right\|, \tag{5}$$

$$\begin{pmatrix} H_x \\ H_y \end{pmatrix} = \hat{\gamma}\begin{pmatrix} C_A \\ C_{MS} \end{pmatrix}, \qquad \hat{\gamma} \equiv \left\| \begin{matrix} \dfrac{k_y a_{11}\tan\theta + k_{z1}a_{21}}{k_0} & \dfrac{k_y a_{12}\tan\theta + k_{z2}a_{22}}{k_0} \\ \dfrac{-k_x a_{11}\tan\theta - k_{z1}a_{11}}{k_0} & \dfrac{-k_x a_{12}\tan\theta - k_{z2}a_{12}}{k_0} \end{matrix} \right\|. \tag{6}$$

The coefficients of matrix before vectors of MS and AW amplitudes are found using projections of equation $[\mathbf{E}, \mathbf{k}] = -k_0\mathbf{H}$. In the latter derivations the wave numbers of AW and MS waves and the relation $E_z = -E_x\tan\theta$ were used, which is valued due to great conductivity along a geomagnetic field for the considered altitudes. Under upper bound the equations (3), (4) are satisfied and simplified using the relations $\eta \gg \varepsilon \gg g$ and $E_z = -E_x\tan\theta$. After equating the tangential magnetic field above upper boundary, we get the upper boundary conditions

$$\begin{aligned} i\frac{dE_y}{dz} + (\mu_{11} - k_y\tan\theta)E_x + \mu_{12}E_y = 0, \\ i\frac{dE_x}{dz} - \mu_{21}E_x + (\mu_{22} + k_x\tan\theta)E_y = 0. \end{aligned} \tag{7}$$

Here the following definition $\mu = \hat{\rho}\hat{\gamma}^{-1}$ is used.

The conditions at lower boundary is found after applying analogous procedure and is not cited here.

4. PROPAGATION IN THE MAGNETOSPHERE

The trajectory of quasi-AW ray is shifted perpendicularly to geomagnetic field lines during propagation between magneto-conjugated points as a result of $k_\perp$. To estimate this value, it is necessary to consider the accurate local dispersion relation for the Alfven wave in a cold plasma: $\omega = V_A k_\parallel/(1 + k_\perp^2 c^2/\omega_{pe}^2)^{1/2}$. The ray trajectories of AW were calculated and the dependence of transverse displacement of ray on the geomagnetic longitude of initial point of the ray was obtained. For the initial transverse component of the wave vector $k_\perp \sim 100$ km^{-1}, the calculations give for the shift ΔX the value of the order 10 km for the McIlvan parameter $L = 4.5$. Therefore, transverse ray shift really might not be taken into account in the calculation of wave amplification along one path between magneto-conjugated points.

The most simple case of the cyclotron instability is AW — proton interaction in the outer radiation belt when a wave vector $\mathbf{k}$ is parallel to the geomagnetic field $\mathbf{H}_0$. For the AW-proton interaction and bi-Maxwellian distribution function of energetic ions (which are a small admixture to the background plasma), maximum possible increment of cyclotron instability K_{AMP} (where $K_{AMP} \equiv \mathrm{Im}(k)$) is achieved at the magnetic equator and it is equal to [gulielmy]:

$$K_{AMP} = -\frac{\sqrt{\pi}}{2k^2c^2}\frac{\omega_{pi}^2}{S_{i\|}}\omega_{Hi}\left(\frac{T_{i\perp}}{T_{i\|}} - 1\right)\exp\left[-\left(\frac{\omega - \omega_{Hi}}{kS_{i\|}}\right)^2\right]. \quad (8)$$

Here ω_{pi} and $S_{i\|}$ are plasma frequency and longitudinal thermal velocity of warm ion species, respectively, c is the velocity of light, k is a wave number of EM waves. The estimation for the wave amplification coefficient during one pass along the field line: $\propto \exp \int k'' dl$.

5. THE RESULTS

We carry out the numerical simulation to use the following approach. In the horizontal plane xy we introduce the periodical boundary conditions and replacement of the continuous spectrum to the discrete one is used. The volume current with spatial distribution function

$$j_{x,y,z} = \cosh^{-1}[(x - L_x/2)/l_x]\cosh^{-1}[(x - L_y/2)/l_y]\cosh^{-1}[(x - h_z/2)/l_z]$$

is located under ground surface. In the area restricted by boundary conditions the equations (3), (4) are calculated numerically by means of flexible grid and using the sweep method. Such typical parameters for numerical calculation are used: the conductivity of lithosphere is $\sigma_l = 10^4$ s^{-1}, the sizes of current source in xy plane are 50×50 km, the size of current source in z direction is 20 km, the depth of the source location is 40 km, the size of periodic boundary conditions are $L_x = L_y = 2000$ km, the angles of geomagnetic field inclination are $\theta = 0...-20°$, the number of mode in the Fourier-transform are $n_x = n_y = 50$, the satellite altitude is $h_z = 600$ km. The input data of ionospheric parameters is taken from Fatkulin, 1981.

The frequency filtration property of LAIM system is determined by filtration properties of the lithosphere and ionosphere. In the ionosphere, the amplitude-frequency characteristics (AFC) have a maximum of the penetration of ULF EM into magnetosphere from ground surface in the frequency range 1—10 s^{-1} (see figs. 2-4). The precise value of frequency of the maximum penetration of EM radiation through ionosphere depends on the ionospheric conditions. The penetration effect throughout the middle latitude is the most effective for night-time condition then for day-time (fig. 1). The first factor, which determines a value of EM field penetrated into the magnetosphere, is electron concentration profile (fig. 2). In the case of sharp electron concentration profile the main part of EM radiation to be reflected from it. The second important factor, which sufficiently influences the penetration effect is profile of total ion collisions. The value of penetrated on the satellite altitudes EM field for the case of current with

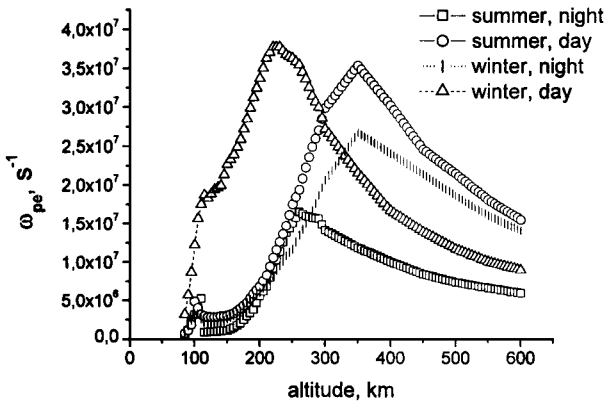

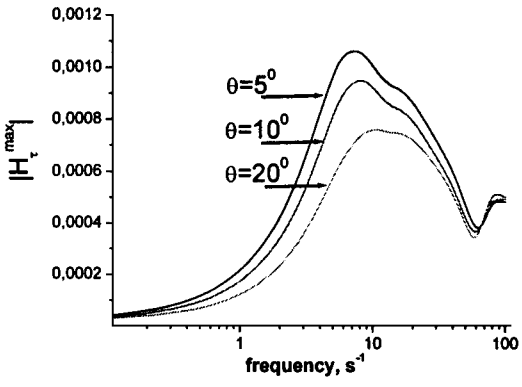

Fig. 1. Profile of plasma frequency in the ionosphere
Fig. 2. The dependencies of amplitude-frequency characteristics (AFC) on angle of geomagnetic field inclination at the altitude 600 km

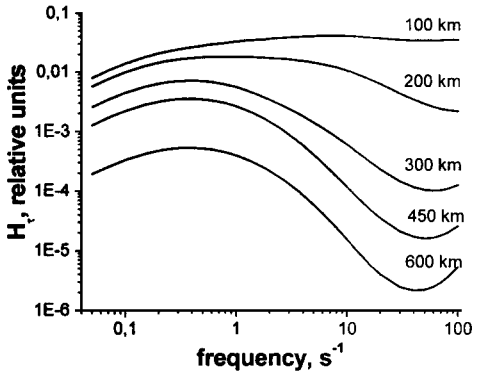

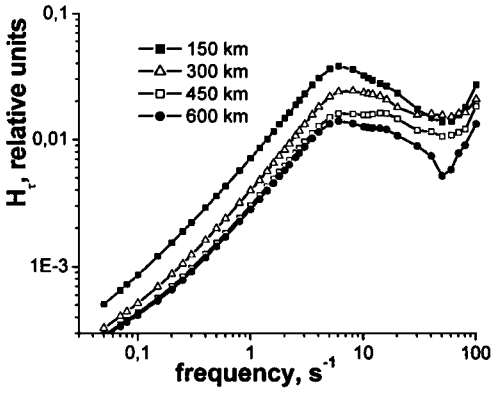

Fig. 3. AFC for different altitudes under day-time summery geophysical conditions. $\theta = 0$

Fig. 4. AFC for different altitudes under night-time summery geophysical conditions. $\theta = 0$

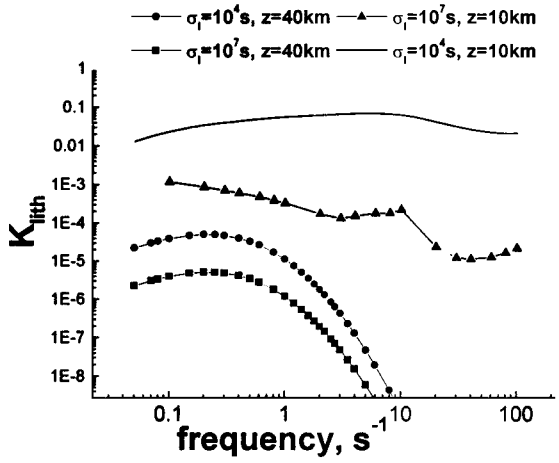

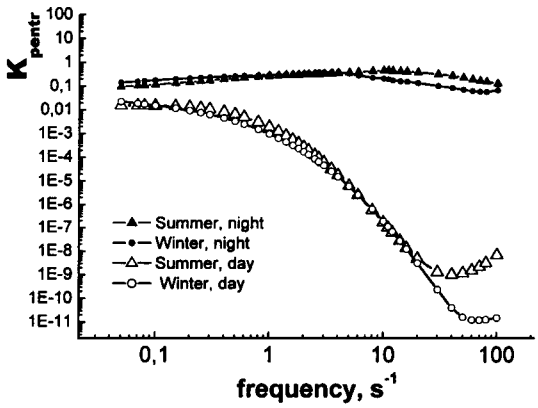

Fig. 5. Frequency dependence of the coefficient of the EM energy penetration from the lithosphere into the lower ionosphere for different localization depths of the source and for different lithosphere conductivity

Fig. 6. Frequency dependence of the coefficient of the EM energy penetration from the lower ionosphere into the satellite altitude into the ionosphere for different geomagnetic conditions

div$J$ = 0 and with div$J \neq 0$ is approximately equal to each other and weakly depends on the geometric sizes. The strong dependence on the summary direction of current takes place. Thus, the EM radiation from the horizontal current is penetrated at least one order bigger than from vertical current.

The amplitude value of a current in a lithosphere is unknown, therefore we have studied the relation of value of EM field disturbances in the ionosphere to the value of current in the lithosphere and marked by transmission coefficient $K_{\text{pentr}} = W_{\text{sat}}/W_{\text{D}}$, $K_{\text{lith}} = W_{\text{D}}/W_{\text{lith}}$, where $W = \int [\mathbf{E}, \mathbf{H}^*]_z ds$ and the indexes correspond to altitude. The dependencies of this parameters on frequency is presented in figs. 5, 6. The relation of tangential magnetic value at the ground level to the tangential magnetic value at the altitude 600 km for frequencies are 100—1000, 10—100, 10^4—10^6 for the frequencies 0.1 s^{-1}, 1—10 s^{-1}, 10—100 s^{-1} respectively. Note that the value of penetration coefficient K_{lith} depends on the lithospheric conductivity, the depth of the current source and the distribution of source density along z-direction. Therefore, only the EM radiation for the current source from near-surface region with high density along the altitude and with the value of current 10^{-6}—10^{-4} A/cm^2, the value of EM radiation 0.1—1 nT at the altitude 600 km is possible.

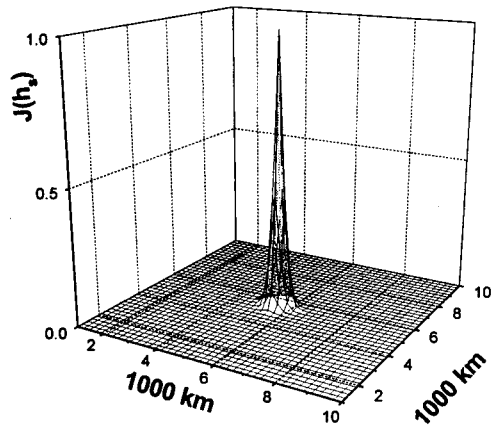

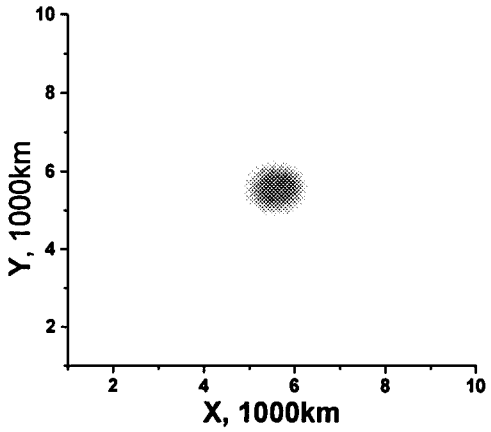

Fig. 7. The spatial distribution of current source amplitude. div**J** ≠ 0

Fig. 8. The spatial distribution of EM field amplitude at the satellite altitude (600 km). $\theta = 0$ for the source shown in Fig. 5

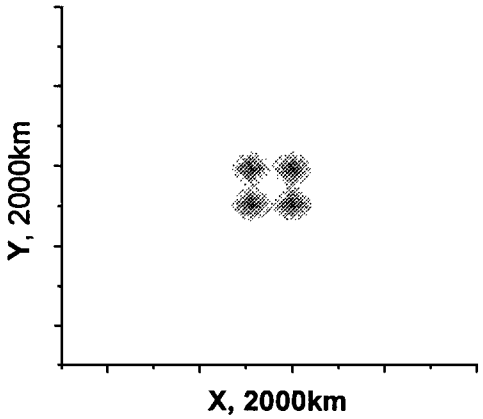

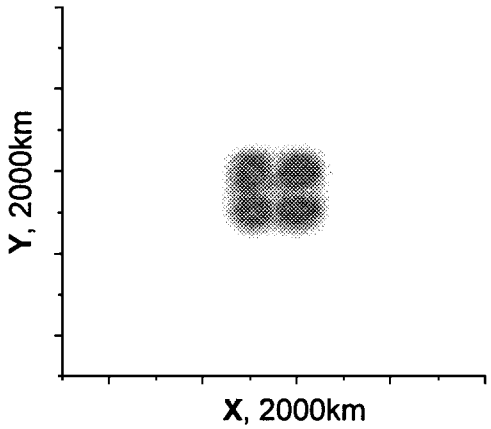

Fig. 9. The spatial distribution of current amplitude for four sources in the lithosphere

Fig. 10. The spatial distribution of the amplitude of EM field radiated by four lithospheric current sources at the satellite altitude for $\theta = 0$

The shape of a spatial distribution of EM field in the satellite altitude is similar to the shape of spatial distribution of current source if geomagnetic field is not oblique (figs. 7, 8). This result also takes place for several spatially separated current sources with a distance from each other about the natural sizes of sources (see figs. 9, 10). The area of distribution of EM field in the satellites altitude (~100×100 km) is much larger than the area of spatial distribution of current source (50×50 km) for the vertical lithospheric current and not larger for horizontal lithospheric current, see figs. 13, 14.

In the oblique geomagnetic field the center of spatial distribution of EM field shifts along geomagnetic field proportionally to its angle value and greatly elongates so that its size along geomagnetic field becomes 200—300 km (fig. 11) and depends on the value of inclination angle. Perpendicular to the geomagnetic field direction the shape of EM radiation is not elongated. The described effect is more intense for the case of vertical lithospheric current than for the opposite case and takes place for currents with div**J** = 0 and div**J** ≠ 0 (fig. 16). The total radiation in the ionosphere from several spaced currents are changing the shape of radiation from each current source and looks like a spot greatly elongated along the direction of the geomagnetic field (fig. 12).

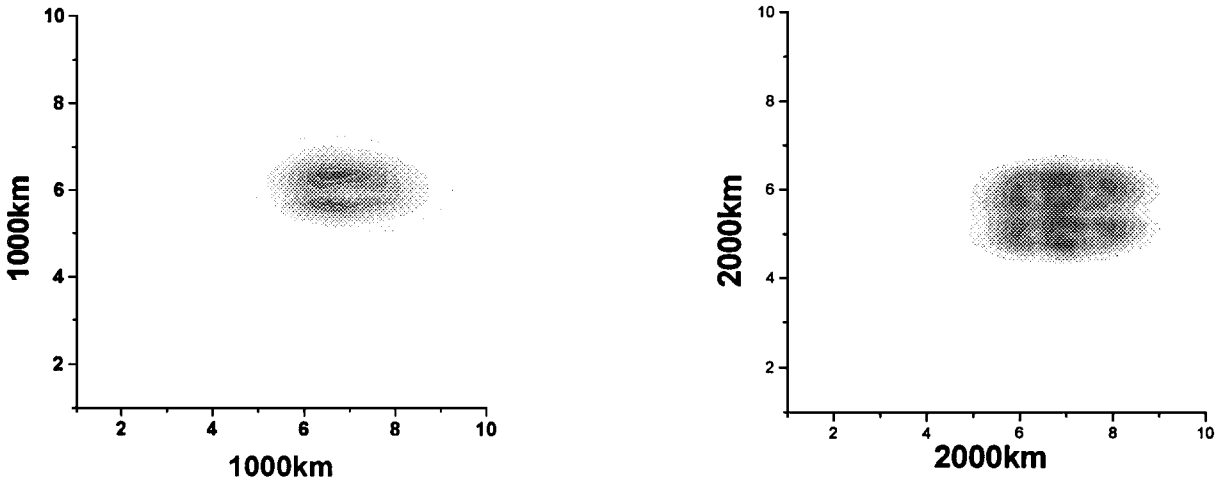

Fig. 11. The spatial distribution of EM field amplitude at the satellite altitude and $\theta = 20°$ for the source shown in Fig. 7

Fig. 12. The spatial distribution of the amplitude of EM field radiated by four lithospheric sources at the satellite altitude and $\theta = 20°$ for the current source shown in Fig. 9

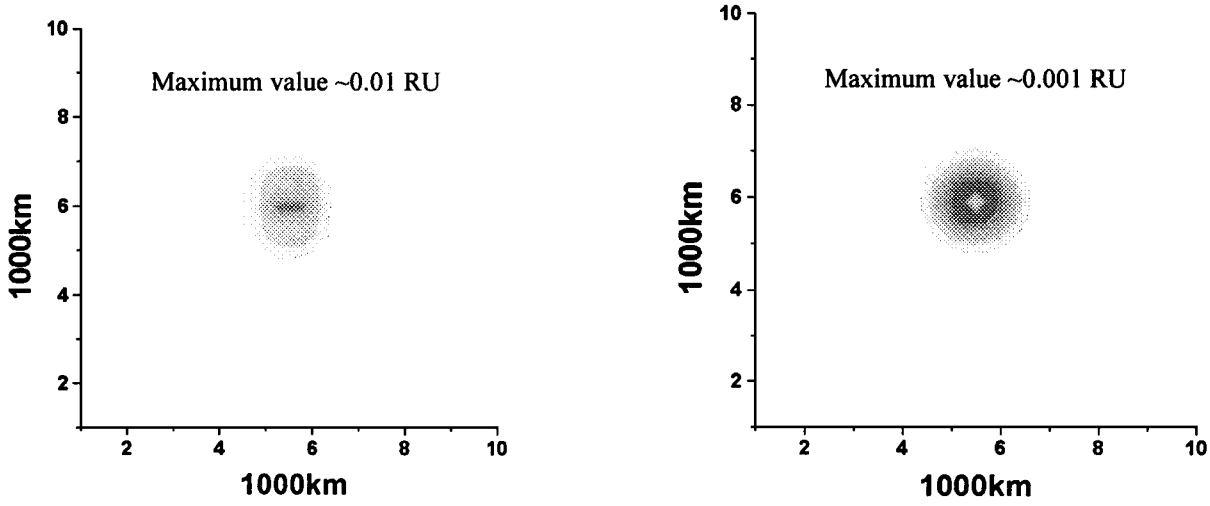

Fig. 13. The spatial distribution of tangential magnetic field amplitude at the satellite altitude for tangential lithospheric current. RU — relative units, $\theta = 0$

Fig. 14. The spatial distribution of tangential magnetic field amplitude at the satellite altitude for vertical lithospheric current. $\theta = 0$

The shape and the value of EM radiation penetrated from source with divJ $\neq$ 0 into satellite altitudes (figs. 15—16) do not essentially deviate from the case of source divJ = 0. This effect takes place also if geomagnetic field is oblique. The spatial distribution of EM field on the ground surface strongly depends on spatial distribution of current source in the lithosphere. We note also that the maximums of horizontal distribution of EM field amplitude at the ionospheric altitude correspond geometrically to the maximums of derivatives of vertical lithospheric current by horizontal directions (fig. 14). In turn, the minimum in the center of the horizontal magnetic field «spot» in the ionosphere corresponds to the maximum in the center of vertical current distribution in the lithosphere. At the same time, the spatial dimensions of EM radiation distribution in the ionosphere for $J_z \gg J_\tau$ are bigger than in the case $J_\tau \gg J_z$ (figs. 13—14). It is interesting to note that the effective widths of the tangential EM field distributions determined, say, by the «half of power density level» are approximately the same at the

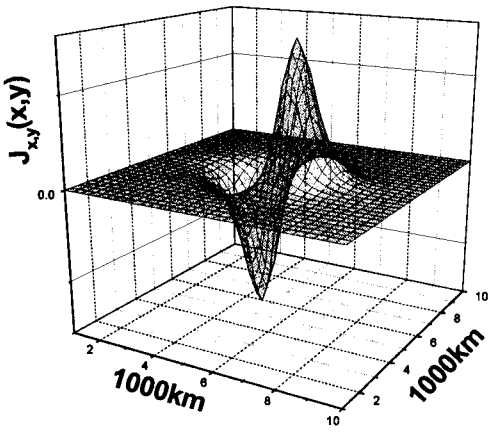

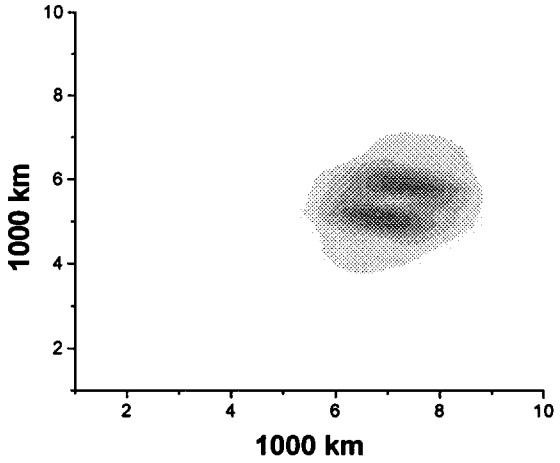

Fig. 15. The spatial distribution of the lithospheric current source for the case div **J** = 0

Fig. 16. The spatial distribution at the satellite altitude of the amplitude of EM field, radiated by the current source shown in Fig. 9. $\theta = 20°$

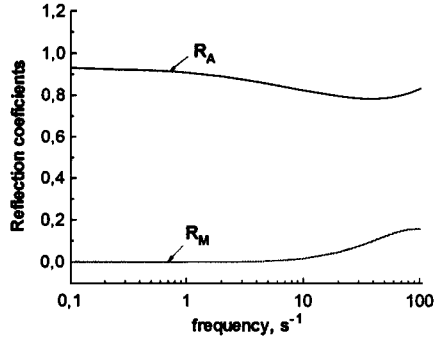

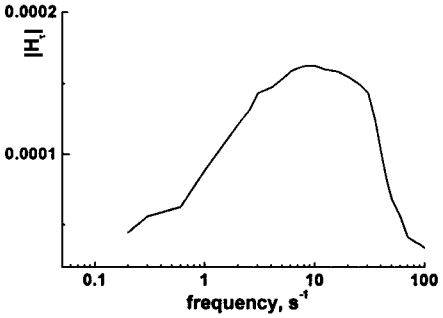

Fig. 17. The reflection of AW and transformation into MSW coefficients R_A and R_{MS} for a case of an incidence of AW from the ionosphere

Fig. 18. The value of amplitude of magnetic field taking into account the penetration of the EM field radiated from the lithosphere into the magnetosphere, reflection from the magneto-conjugated point and amplification caused by cyclotron instability

ground and satellite altitude levels in both cases $J_\tau \gg J_z$ and $J_z \gg J_\tau$.

In the magnetosphere, a main part of EM energy propagates as the waves of AW type because harmonics with AW wave number has a maximum amplitude value. When AW propagates in the radiation belts with the concentration of captured protons 0.1 cm^{-3} the amplification coefficient increases with the frequency and for $\omega \approx 50$ s^{-1} it is equal to 1.25. We have to conclude that this linear mechanism of amplification cannot provide sufficiently good amplification of amplitude value. However, this amplification mechanism for ULF EM waves can be sufficient for maintenance of value of a penetrated in the magnetosphere EM radiation at the high geomagnetic latitude if losses due to reflection from ionosphere are not large. The losses of EM energy in the magnitosphere are small because the energy propagates in the form of AW in the frequency range of maximum penetration effect through ionosphere.

The reflection coefficient essentially depends on the frequency in the considered frequency range 0.1—100 s^{-1} and it changes in the range 0.8—0.92 (fig. 17). Taking into account the reflection losses and amplification due to cyclotron instability, it is possible to conclude: when the ULF EM radiation of lithospheric origin penetrates into the magnetosphere at the magnetic shell with captured protons, then its amplitude varies slowly. The shape of amplitude-frequency characteristics obtained from numerical

calculation for tangential magnetic field value, when the penetration into magnetosphere, the amplification in the magnetosphere, and the reflection at the ionosphere boundary in magneto-conjugate point are taken into account, is presented in fig. 18.

SUMMARY AND CONCLUSIONS

We got the following characteristics for ULF EM radiation excited from the lithosphere on the basis of 3D static continuity numerical model:

Type of waves with maximum amplitude value penetrated from the lithospheric source in the magnetosphere is Alfven waves.

The ULF EM radiation penetrated to magnetosphere has a maximum in frequencies ~ 1—10 s^{-1} (K_{pentr} ~ 10^{-4}). The coefficient of EM penetration from the ionosphere depends essentially on the geomagnetic condition, on the summary direction of current and on the conductivity of the lithosphere and weakly on geometrical configuration of current source and the angle of geomagnetic field inclination. The EM radiation penetrates most effectively in the magnetosphere from the horizontal current. At a ratio of value of ULF EM field on the ground to value of ULF EM field in the satellite altitude (600 km) is 10—100 under conditions of maximum penetration effect. The main losses in ionosphere are connected with the profile of electron density. The second important parameter for penetration of ULF EM throughout ionosphere is the value of total ion collision;

The shape of spatial distribution of EM radiation penetrated in the magnetosphere is similar to the lithospheric current one if geomagnetic field is not oblique. The spatial sizes in the xy plane of EM radiation penetrated in the magnetosphere are small for horizontal current and larger for vertical lithospheric current.

In the oblique geomagnetic field the shape of ULF EM radiation elongates parallel to the ground plane in the direction of geomagnetic field inclination and does not changes perpendicular to it. The center of spatial distribution of EM radiation shifts to the location of source in the lithosphere in the direction of obliqueness similar to $H \cdot \tan\theta$, where H is altitude. The same situation takes place for the currents with div**J** = 0 and div**J** ≠ 0. The shape of spatial distribution of EM radiation from the several isolated current sources takes a form of one greatly elongated spot and discerning of its structure in the lithosphere by satellite observation is difficult.

The cyclotron instability can be effective for maintenance of value of ULF EM penetrated in the magnetosphere under the geophysical condition when the reflection from ionosphere is not smaller than 0.8. This condition is sufficient for middle latitude, however, the question about amplification of lithospheric origin ULF EM demands more accurate investigation;

The obtained numerical results are close to satellite observations, see, for example, Bilichenko et al, 1990 and Liperovsky et al, 1992. We conclude that EM radiation penetrates into the magnetosphere as AW and can have the amplitudes 0.1—1 nT if the effective mechanisms of transformation of elastic energy to EM energy take place in the lithosphere and the currents with amplitudes 10^{-6}—10^{-4} A/cm^2 appear before earthquake. The ULF EM radiation excited in the lithosphere can be identified by the frequency and spatial characteristics of LAIM system and the center of current location and its characteristic sizes will be easily determined from observation at the satellites and ground observatories. We believe that recording and identification of radiation of lithospheric origin is possible.

REFERENCES

Bilichenko S. V. et al. Dokl. Akad. Nauk USSR, 311, 1077-1080, 1990.
Fatkullin M. N. et al. The models of middle-latitude ionosphere, Nauka, Moskow, 1981.

Grimalsky V. V., Kremenetsky I., Rapoport Yu. G. Exitation of Electromagnetic waves in the lithosphere and their penetration into ionosphere and magnetosphere. J. Atmosph. Electr., 19, No.2, p. 101, 1999.

Gulielmi A. V., Pokhotelov O. A. Geoelectromagnetics Waves. Inst. of Physics Publ., Bristol, Philadelphia, 1996.

Molchanov O. A., Hayakawa M. Generation of ULF Seismogenic Electromagnetic Emission: A Natural Consequence of Microfracturing Process. Electromagnetic Phenomena related to Earthquake Prediction, p. 537, 1994.

Molchanov O. A., Hayakawa M., Rafalsky V. A., 100A, p.1691, 1995.

Liperovsky V. A. et al. Ionospheric earthquake precursors (Ionosfernye predvestniki zemletryaseniy, in Russian). Moskow, Nauka Publ., 1992.

Surkov V., Pilipenko V. The physics of pre-seismic electromagnetic ULF signals. Atmospheric and Ionospheric Electromagnetic Phenomena Associated with the Earthquakes, p. 357, 1999.

Vainshtein L. A. Electromagnetic Waves (Electromagnitnie volny, in Russian). M., Sov. Radio. 1958.

Космічна наука і технологія. ДОДАТОК. 2001. Т 7. № 2. С. 15—18.

PITCH-ANGLE SCATTERING AFFECT ON THE RADIATION BELT PROTONS DISTRIBUTION

O. K. Cheremnykh[1], V. Ya. Goloborod'ko[2], S. N. Reznik[2]

[1]Space Research Institute, National Academy of Sciences of Ukraine and National Space Agency of Ukraine, Kyiv, Ukraine

[2]Institute for Nuclear Research, National Academy of Sciences of Ukraine, Kyiv, Ukraine

Numerical simulation was carried out in the present paper to demonstrate the effect of the pitch-angle scattering on the phase space distribution of the proton fluxes measured in the Earth magnetosphere. It was shown that for Mc' Ilvine parameter of order 2-4 even a small order of magnitude of the pitch-angle diffusion coefficient may essentially affect the phase space distribution of the radiation belt proton fluxes. Numerical simulations carried out demonstrate that for future predictions on the satellite measurements it is expedient to obtain the reliable theoretical pitch-angle quasilinear diffusion coefficients with the appropriate experimental verification.

INTRODUCTION

At present there are strong experimental evidences that protons are the main ion population of the Earth radiation belts that come from the Solar wind [1]. That is why it is important to investigate there behavior in the Earth magnetosphere. The Solar wind delivers protons to the Earth magnetosphere through two channels. The first one is a direct Solar wind protons trapping at the outer boundary of the magnetosphere confinement domain (i.e. the confinement domain of the ion drift motion in the Earth magnetosphere magnetic field). The second one is the proton source caused by the Solar wind neutrons albedo in the Earth magnetosphere. We will neglect this volume proton source because the experimental observations demonstrate that Solar protons come mainly from the Earth confinement domain boundary. Previous theoretical investigations as well as numerical simulations dealt only with the high energy proton flux distributions caused by the stochastic radial diffusion, charge exchange and slowing down by electrons [2]. Numerical simulation carried out in [3] was in qualitative agreement with the satellite measurements [3, 4] at least for high values of Mc'Ilvine parameter. At the same time, the latest experimental evidences [5] demonstrate that quasilinear pitch-angle diffusion should be taken into account to describe the measured Solar proton flux distribution over space and energy. This problem was treated numerically in [6] and at least qualitative agreement with the satellite measurements for the low-altitude trapped protons was obtained [7]. Now it is evident, that for the purpose of interpretation of the protons behavior in the whole Earth magnetosphere confinement domain one should take into account also the effect of quasiliniar pitch-angle scattering [8]. The latest theoretical investigation [9] shows that the main impact on the Solar protons pitch-angle diffusion occurs due to the interaction of particles with ion-cyclotron waves or whistlers [7]. At present this problem is still under consideration and we restrict our simulation with the model approach.

SIMULATION APPROACH

We start from the assumption that we may write the averaged Fokker—Planck equation for trapped protons distribution function in the Earth magnetosphere that will take into account stochastic distortion of the field lines, Coulomb scattering, wave-particle interaction as well as charge exchange with neutral atoms. To formulate this problem we proceed from the Fokker—Planck type conservation equation in

phase space.

$$\frac{\partial f}{\partial t} = \frac{1}{\sqrt{g}} \frac{\partial}{\partial c_i} \sqrt{g} \left(d^i + D^{ij} \frac{\partial f}{\partial c_j} \right). \tag{1}$$

This equation is written under the assumption that all processes are independent and random at the same time. This equation should be treated as an orbit averaging, i.e., as a drift Fokker—Planck equation. Here c_i are the constants of motion chosen as follows: c_1 — is the proton magnetic moment, c_2 is the Mc'Ilvine parameter, defined as

$$c_2 = L = \frac{2\pi M}{R\Phi} \tag{2}$$

where Φ is the magnetic flux through the proton drift trajectory, c_3 is the particle pitch-angle cosine at the equatorial mid plane (this variable may be recalculated to the real pitch-angle value by use of the approach proposed in [8].

The determinant of metric tensor is:

$$\sqrt{g} = c_3 \tau_b c_2^{-5/2} \tag{3}$$

where τ_b is the bounce period of the proton drift motion.

There is no volume proton source presented in this equation because, as it was pointed out earlier, we will neglect the neutron albedo. Following [10] we will take the boundary conditions as a proton flux energy spectra at $L = 7$ in the form

$$j = \varepsilon \left(e^{-\varepsilon/60} + 3.5e^{-\varepsilon/10} + 100e^{-\varepsilon/1.1} \right). \tag{4}$$

This energy spectrum of the proton flux was reproduced from the satellite measurements and is in a good agreement with that of obtained by use of the experimental data interpolation package EP6 for the quiet Earth magnetosphere [12].

METHOD USED

To carry out the numerical simulation of the high energy protons behavior in the Earth magnetosphere we simplify Equation (1) in the following way.

We'll treat a steady-state proton distribution function , i.e., $\partial f/\partial t = 0$. Coulomb collisions will be taken into account only as a slowing down process [7]

$$d^1 = 8.8 \cdot 10^{15} L^{9/2} c_1^{1/2} \begin{cases} 205 \left(\frac{L}{4.1} \right)^{-4.64}, & L < 4.1, \\ 13.0 \left(\frac{L}{4.1} \right)^{-4.64}, & L > 4.1. \end{cases} \tag{5}$$

Charge-exchange process on the neutral hydrogen with density n_{H_2} is considered in «BGK» approximation [4], with the effective process time τ_{cx}

$$\tau_{cx} = \sigma_\varepsilon \langle n_{H_2} \rangle, \tag{6}$$

here bracket $\langle \ldots \rangle$ denotes the bounce averaging over the proton drift trajectory,

$$\sigma_\varepsilon = \begin{cases} a_1 e^{-\varepsilon/\varepsilon_0}, & L < 2, \\ a_2 \varepsilon^{-\gamma}, & L > 2 \end{cases} \tag{7}$$

with $a_1 = 9.48 \cdot 10^{-16}$, $a_2 = 7.55 \cdot 10^{-23}$, $\varepsilon_0 = 0.0275$ MeV, $\gamma = 5.64$ [11], and neutrals assumed to be distributed as follows

$$n_{H_2} = n_0 \cdot H^\alpha, \qquad n_0 = 62544.2, \qquad \alpha = -3.7. \tag{8}$$

Expression (7) fits the experimental data presented in [5].

In our simulation the radial diffusion coefficient is taken in the form [2]

$$D^{22} = D_0 L^{10},\ D_0 = 3 \cdot 10^{-14} \tag{9}$$

that corresponds only to the magnetic field stochastic distortion (it is suitable for the qualitative description presented here). Pitch-angle diffusion coefficient will be taken in the model form [3]

$$D^{33} = \sigma \left(\frac{c_3}{c_{\text{cone}}} \right)^{\delta}. \tag{10}$$

This coefficient has two parameters for our investigation: (a) the amplitude value of the pitch-angle diffusion coefficient chosen as $\sigma = 10^{-6}$ and (b) the sharpness of the coefficient, that describes the affect of the cone on proton distribution chosen as $\delta = 1.5$ and pitch-angle cosine on the atmospheric loss cone

$$c_{\text{cone}} = \sqrt{1 - \frac{1}{L^3 \sqrt{4 - 3/L}}}\ . \tag{11}$$

SIMULATION RESULTS

The effective time of all processes that is considered in present paper it is shown in Figures 1a, 1b. From these Figures one can see that for definite values of pitch-angle scattering this process may dominate in some region of phase space even for the equatorial protons (Figure 1a) and always should be taken into account for protons with $c_3 > 0$.

From this figures one may see that charge-exchange process always play the important role and should be taken into account. This term is also very sensitive to the position of the proton trajectory mirror points and so will differ significantly for quite time and for storm time of Earth magnetosphere.

The numerical solution of Equation (1) was done by use of the alternative direction implicit method for two cases. The first one is model case with the proton flux equal to zero at the loss cone. It is a model for comparison with previous two-dimensional calculations carried out in [6] where pitch-angle scattering was omitted. The results of our calculations presented in Figure 2a at least qualitatively reproduced the results of [6]. The second one is a case with proton distribution function equal to zero at the loss cone. Calculated omnidirectional proton flux of energy for different values of L is presented in Figure 2b. Comparing results of Figures 1a and 1b one may see that for $L > 4$ pitch-angle diffusion does not play an important role for protons distribution. On the other hand, for low values of L parameter pitch-angle diffusion is significant and decries the omnidirectional proton flux more than to one-tenth of its former value.

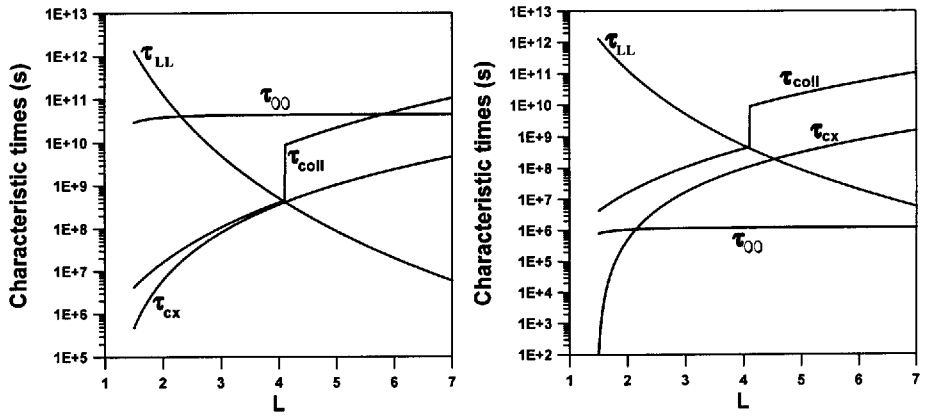

Fig. 1. Effective process times vs. L for protons with $E = 1$ MeV and $c_3 = 0$ (*a*); $c_3 = 0.9$ (*b*)

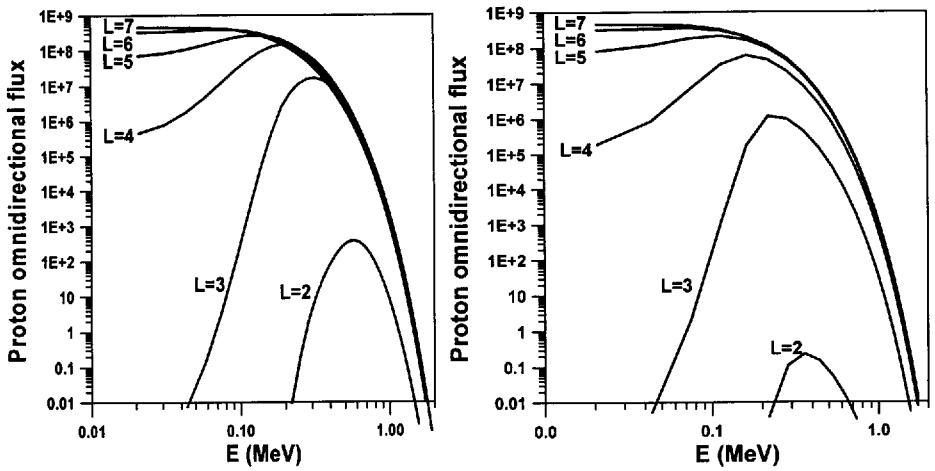

Fig. 2. Proton flux versus energy for the model: *a* — when atmospheric cone loss set to be absent, and *b* — when atmospheric cone loss is taken into account

Present calculations demonstrates that pitch-angle scattering plays the dominant role for proton flux distribution at low values of Mc'Ilvain parameter and should be taken into account in the theoretical investigations.

CONCLUSIONS AND DISCUSSIONS

The model and numerical calculations presented in the paper clarify the role of the pitch-angle scattering for the proton distribution in the Earth plasmasphere. They demonstrates that even a small value of pith-angle diffusion coefficient may strongly affect the proton distribution at least for small values of L and in the vicinity of the atmospheric loss cone.

At the same time approach proposed was based on the assumption that proton distribution function is steady-state. In Figures 1a, 1b one may see that the time required for distribution function to come to steady-state is too long in comparison with the characteristic times of the Solar wind variations. In this connection to obtain the reliable proton distribution function one should solve the nonstationary Fokker—Planck equation with taking into account also the time variation of the proton source and Earth magnetic field geometry.

REFERENCES

1. Albert J. M. // J. Geophys. Res.—1999.—**104**, N A2.—P. 2429.
2. Jordanova V. K., Kistler L. M., Kozyra J. U., et al. // J. Geophys. Res.—1996.—**101**, N A1.—P. 111.
3. Cheng C. Z., Johnson J. R. // J. Geophys. Res.—1999.—**104**, N A1.—P. 413.
4. Chen L. // J. Geophys. Res.—1999.—**104**, N A2.—P. 2421.
5. Toivanen P. K., Pulkkinen T. I., Friedel R. H. W., et al. // J. Geophys. Res.—1999.—**104**, N A5.—P. 10205.
6. Davidson G., Walt M. // J. Geophys. Res.—1977.—**82**.—P. 48.
7. Cornwall J. M. // J. Geophys. Res.—1972.—**77**.—P. 1756.
8. Beutier T., Boscher D. // J. Geophys. Res.—1995.—**100**, N A8.—P. 14853.
9. Speldvik W. // J. Geophys. Res.—1977.—**82**.—P. 2801.
10. Chen M. W., Lyons L. R. // J. Geophys. Res.—1994.—**99**, N A4.—P. 5745.
11. Bashkirov V. F., Panasyuk M. I., Teltsov M. V. // Space Res.—1998.—**36**, N 4.—P. 369.
12. Vette J. I. The NASA/National Space Science Data Center Trapped Radiation Environment Model Program (1964-1991) // NSSDC/WDC-A-R &S 91-29, 1991.

Космічна наука і технологія. ДОДАТОК. 2001. Т 7. № 2. С. 19—25.

UNSTABLE AXIALLY SYMMETRIC MHD FLOW BETWEEN ROTATING BOUNDARIES

A. A. Loginov[1], Yu. I. Samoilenko[2], V. A. Tkachenko[1]

[1]Institute of Space Researches NSA and NAS of Ukraine

[2]Institute of Mathematics NAS of Ukraine

For cylindrical and spherical liquid layers confined between two rotating axially symmetric shells the conditions for azimuth flow instability creating meridional component rise were obtained. Methods for solution of nonlinear equation describing steady-state flow for large Reynolds numbers were proposed.

This report is related with hydromagnetic dynamo problem in the geophysics. It is supposed that magnetic field of the Earth appears due to differential rotation in electroconductive liquid core caused by difference between angular velocities of inner core and mantle [1]. In order to clarify general mechanisms and specific features of such processes it is purposeful to investigate some model examples in simplified formulation. First of all we should explain how flat differential rotation can excite poloidal component of the flow, for example, between coaxial surfaces.

In this section the flow of incompressible viscous liquid is examined that in the fixed frame of reference is described by Navier-Stokes equation

$$\frac{\partial v}{\partial t} + (\mathbf{v}\cdot\nabla)\mathbf{v} = -\frac{1}{\rho_m}\mathrm{grad}(p+U) + \frac{\tilde{\eta}}{\rho_m}\Delta\mathbf{v}, \qquad \mathrm{div}\mathbf{v} = 0, \tag{1}$$

where $\mathbf{v}$, p, U, ρ_m, $\tilde{\eta}$ are respectively velocity, pressure, gravitation potential, mass density and viscosity coefficient. This equation in the frame of reference rotating together with the Earth at angular velocity Ω takes for total velocity $\mathbf{V}_\Sigma$ the following form:

$$\frac{\partial \mathbf{V}_\Sigma}{\partial t} - [\mathbf{V}_\Sigma\times\mathrm{rot}\mathbf{V}_\Sigma] + 2[\Omega\times\mathbf{V}_\Sigma] = -\mathrm{grad}\left\{\frac{p+U}{\rho_m} + \frac{\mathbf{V}_\Sigma^2}{2} - \frac{1}{2}[\Omega\times\mathbf{r}]^2\right\} + \frac{\tilde{\eta}}{\rho_m}\Delta\mathbf{V}_\Sigma \tag{2}$$

where $\mathbf{r}$ is radius vector of observation point. Application of rotor operator to (2) results in Helmholtz equation

$$\frac{\partial \Gamma_\Sigma}{\partial t} - \mathrm{rot}[\mathbf{V}_\Sigma\times\Gamma_\Sigma] + 2\mathrm{rot}[\Omega\times\mathbf{V}_\Sigma] = \frac{\tilde{\eta}}{\rho_m}\Delta\Gamma_\Sigma,$$

where $\Gamma_\Sigma = \mathrm{rot}\mathbf{V}_\Sigma$. If z — axis is directed along vector Ω and accepted system of units is such that $\Omega = 1$ and characteristic length $r_0 = 1$ this equation takes a compact dimensionless form

$$\frac{\partial \Gamma_\Sigma}{\partial t} = \mathrm{rot}[\mathbf{V}_\Sigma\times\Gamma_\Sigma] + 2\frac{\partial \mathbf{V}_\Sigma}{\partial z} + \eta\Delta\Gamma_\Sigma. \tag{3}$$

Differential rotation in the liquid is characterized by dependence of circular velocity $\mathbf{V}_\varphi(\rho)$ on radius ρ. Density of the pulse moment in flow is connected with rho by relation

$$\mu(\rho) = \rho V_\varphi(\rho).$$

Application of the energetic principle makes possible to express increment γ of local instability (for unstable profiles) with $\mu(\rho)$ by simple formula

$$\gamma^2 = \frac{4}{\rho^3}\frac{d}{d\rho}\mu^2(\rho). \tag{4}$$

For our purposes small increments are of specific interest. If increment is rather small and constant in definite interval of rho then we have situation which is called below overcritical regime. The neutral stability takes place if $V_\varphi(\rho)$ in rotating frame of reference has profile

$$V_0(\rho) = \frac{1}{\rho} - \rho. \tag{5}$$

The overcritical regime can be expressed by additional term

$$V_\alpha(\rho) = \frac{1-\rho^4}{2\rho} \tag{6}$$

and subsequently total velocity for this regime can be represented as

$$\mathbf{V}_\Sigma = (V_0 + \alpha^2 V_\alpha)\,\mathbf{e}_\varphi + \mathbf{V}, \tag{7}$$

where $\alpha^2 \ll 1$ — overcritical parameter,

$$\mathbf{V} = V_\rho \mathbf{e}_\rho + V_\varphi \mathbf{e}_\varphi + V_z \mathbf{e}_z$$

is small perturbation of the flow velocity to be found, $\mathbf{e}_\rho$, $\mathbf{e}_\varphi$, $\mathbf{e}_z$, — vector basis of cylindrical coordinate system.

Substitution of (7) in (3) brings equation for $\mathbf{V}$

$$\frac{\partial \Gamma}{\partial t} = \mathrm{rot}[\mathbf{V}\times\Gamma] - \frac{2}{\rho^2}\Gamma_\rho \mathbf{e}_\varphi - -\alpha^2\left[2\rho^2\frac{\partial \mathbf{V}}{\partial z} - 4\rho V_\rho \mathbf{e}_z + \left(\rho^2 + \frac{1}{\rho^2}\right)\Gamma_\rho \mathbf{e}_\varphi\right] \tag{8}$$

with $\Gamma = \mathrm{rot}\mathbf{V}$ by $\mathrm{div}\mathbf{V} = 0$.

Linearization of (8) allows to obtain sufficiently simple system for V_ρ, V_φ, V_z depending on time t according to $e^{\gamma t}$:

$$\begin{gathered}
\gamma\frac{\partial V_\varphi}{\partial z} = 2\alpha^2\rho^2\frac{\partial V_\rho}{\partial z}, \\
\gamma\left(\frac{\partial V_\rho}{\partial z} - \frac{\partial V_z}{\partial \rho}\right) = \frac{2}{\rho^2}\frac{\partial V_\varphi}{\partial z}, \\
\gamma\left(\frac{\partial V_\varphi}{\partial \rho} + \frac{1}{\rho}V_\varphi\right) = 2\alpha^2\rho^2\left(\frac{\partial V_\rho}{\partial \rho} + \frac{3}{\rho}V_\rho\right), \\
\frac{\partial V_\rho}{\partial \rho} + \frac{1}{\rho}V_\rho + \frac{\partial V_z}{\partial z} = 0.
\end{gathered} \tag{9}$$

Elimination $\partial V_\varphi/\partial z$ from the first and second equations yields

$$\frac{\partial V_z}{\partial \rho} = \left[1 - \left(\frac{2\alpha}{\gamma}\right)^2\right]\frac{\partial V_\rho}{\partial z}. \tag{10}$$

Taking this into account we obtain wave equation for V_ρ:

$$\frac{\partial^2 V_\rho}{\partial \rho^2} + \frac{1}{\rho}\frac{\partial V_\rho}{\partial \rho} - \frac{V_\rho}{\rho^2} + \left[1 - \left(\frac{2\alpha}{\gamma}\right)^2\right]\frac{\partial^2 V_\rho}{\partial z^2} = 0,$$

which allows separation of variables by substitution

$$V_\rho = X(\rho)\,Y(z).$$

Finally an explicit expressions for increment and modal column are obtained:

$$\gamma_{nk}^2 = \alpha^2 \frac{k^2\pi^2}{b^2} \frac{1}{\lambda_n^2 + \dfrac{k^2\pi^2}{b^2}}. \tag{11}$$

$$V_{nk}^{(\rho)} = e^{\gamma_{nk}t} Z_1(\lambda_n \rho)\cos\left(\frac{k\pi z}{b}\right),$$

$$V_{nk}^{(\varphi)} = e^{\gamma_{nk}t} \frac{2\alpha}{\gamma_{nk}/\alpha} \rho^2 Z_1(\lambda_n \rho)\cos\left(\frac{k\pi z}{b}\right), \tag{12}$$

$$V_{nk}^{(z)} = -e^{\gamma_{nk}t} \lambda_n \frac{b}{k\pi} Z_0(\lambda_n r)\sin\left(\frac{k\pi z}{b}\right).$$

Here λ_n^2 (n = 1, 2, 3, ...) are eigenvalues of characteristic equation system $Z_1[(1 - a)\lambda_n] = 0$, $Z_1[(1 + a)\lambda_n] = 0$ for tube domain ($1 - a \le \rho \le 1 + a$, $0 \le z \le b$).

It can be seen that $V^{(\rho)}$ and $V^{(z)}$ are larger in order than $V^{(\varphi)}$. This exhibits resonance nature of poloidal component generation by azimuth differential rotation. Another important subsequence of this analysis consists in specific dependence of increment on axial k and radial n wave numbers. The largest increment is observed in short wave part of axial spectrum but in long wave of radial one. This general features take place for spherical layers also as we show further.

Starting analysis of the sphere let us pay attention to one obstacle which prevents application of $V_\alpha(\rho)$ expressed by (6). The sense of this caution consists in circumstance that neighborhood of axis does not belong to the tube domain in cylindrical case but is present in polar zones in spherical layer. So one should change the form of overcritical additional term by $V_\alpha(\rho) = -\rho$.

For azimuth component F of vector potential we obtain the following equation:

$$\Delta_1 F + \frac{2\alpha^2}{\gamma^2\rho^2}\Gamma_\alpha(\rho)\frac{\partial^2 F}{\partial z^2} = 0, \tag{13}$$

where

$$\Delta_1 = \frac{1}{\rho}\frac{\partial}{\partial\rho}\left(\rho\frac{\partial}{\partial\rho}\right) + \frac{\partial^2}{\partial z^2} - \frac{1}{\rho^2},$$

$$\Gamma_\alpha(\rho) = \frac{1}{\rho}\frac{\partial}{\partial\rho}[\rho V_\alpha(\rho)] = -2.$$

Correspondingly for potential

$$f(r, \theta) = F(\rho, z)\Big|_{\rho\,=\,r\sin\theta,\ z\,=\,r\cos\theta}.$$

Expressed in spherical coordinates r, θ, φ equation (13) takes the form

$$\Delta_1 f - \frac{4\alpha^2}{\gamma^2 r^2 \sin^2\theta}\hat{L}f = 0, \tag{14}$$

$$\Delta_1 f = \frac{1}{r^2}\frac{\partial}{\partial r}\left(r^2\frac{\partial f}{\partial r}\right) + \frac{1}{r^2\sin\theta}\frac{\partial}{\partial\theta}\left(\sin\theta\frac{\partial f}{\partial\theta}\right) - \frac{f}{r^2\sin^2\theta}, \tag{15}$$

$$\hat{L}f = \frac{\partial^2 f}{\partial r^2}\cos^2\theta - \frac{2}{r}\frac{\partial^2 f}{\partial r\partial\theta}\sin\theta\cos\theta + \frac{1}{r^2}\frac{\partial^2 f}{\partial\theta^2}\sin^2\theta + \frac{1}{r}\frac{\partial f}{\partial r}\sin^2\theta +$$

$$+ \frac{2}{r^2}\frac{\partial f}{\partial\theta}\sin\theta\cos\theta. \tag{16}$$

which is inhibitory to separation of variables. Thereby eigenfunction $f_\sigma = f_\sigma(r, \theta)$ and corresponding eigenvalues $\gamma = \gamma_\sigma$ are represented as linear combination

$$f_\sigma = \sum_{nl} C^\sigma_{nl} u_{nl}(r, \theta) \tag{17}$$

of normalized in metric $\langle f, g\rangle = \int_a^1 \int_0^\pi f(r, \theta) g(r, \theta) r^2 \sin\theta dr d\theta$ spherical harmonics

$$u_{nl} = \frac{R_n(k_{nl} r)}{||R_{nl}||} \frac{P_{n1}(\cos\theta)}{||P_{n1}||} \quad (a \le r \le 1, 0 < \theta < \pi),$$

where

$$R_n(k_{nl} r) = R_n^{(+)}(k_{nl}) R_n^{(-)}(k_{nl} r) - R_n^{(-)}(k_{nl}) R_n^{(+)}(k_{nl} r), \tag{18}$$

$$||R_{nl}|| = \left(\int_a^1 R_n^2(k_{nl} r) r^2 dr \right)^{1/2},$$

$$||P_{n1}|| = \sqrt{\frac{2n(n+1)}{2n+1}},$$

$$R_n^{(+)}(x) = \sqrt{\frac{p}{2x}}\, J_{\frac{2n+1}{2}}(x),$$

$$R_n^{(-)}(x) = (-1)^n \sqrt{\frac{p}{2x}}\, J_{-\frac{2n+1}{2}}(x).$$

Since the Bessel function of half-integer index can be expressed via trigonometric function it is possible to fulfil calculations by means of recurrent procedure as follows

$$R_n^{(+)}(x) = A_n(x)\cos x + B_n(x)\sin x,$$

$$R_n^{(-)}(x) = -A_n(x)\sin x + B_n(x)\cos x,$$

where

$$A_{n+1}(x) = \frac{n}{x} A_n(x) - A_n'(x) - B_n(x),$$

$$B_{n+1}(x) = \frac{n}{x} B_n(x) - B_n'(x) + A_n(x)$$

with initial data $A_1(x) = -1/x$, $B_1(x) = 1/x^2$.

The construction (18) satisfies boundary condition $u_{nl}(1, \theta) \equiv 0$ which expresses the fact of impenetrability of the liquid through external sphere. The same demand at inner sphere of radius $r_i = a$ leads to characteristic equation

$$\operatorname{tg}[k(1-a)] = \frac{B_n(k)A_n(ka) - A_n(k)B_n(ka)}{A_n(k)A_n(ka) + B_n(k)B_n(ka)}.$$

For every index $n = 1, 2, 3 \ldots$ the infinite sequence of wave-numbers k_{nl} corresponds. Finally we obtain $u_{nl} = u_{nl}(r, \theta)$ and k_{nl} satisfying standard demands:

$$\langle u_{n'l'}, \Delta_1 u_{nl}\rangle = -k_{n'l'} k_{nl} \delta_{n'l', nl}, \qquad \langle u_{n'l'}, u_{nl}\rangle = d_{n'l', nl}, \qquad u_{nl}\Big|_{(S_i)} = 0, \qquad u_{nl}\Big|_{(S_e)} = 0.$$

The next step consists in resolution of infinite system

$$\sum_{\nu} (m_{\nu'\nu} - \lambda_\sigma^2 \delta_{\nu'\nu}) f_\nu^\sigma = 0 \ (\nu, \nu' = 1, 2, \ldots),$$

where

$$\nu = \{n, l\}, \qquad \nu' = \{n', l'\}, \qquad m_{\nu'\nu} = \frac{M_{\nu'\nu}}{k_{\nu'} k_\nu}, \qquad f_\nu^\sigma = k_\nu C_\nu^\sigma,$$

$$M_{n'l',\ nl} = \langle u_{n'l'}, \frac{-4}{r^2 \sin^2\theta} \hat{L} u_{nl} \rangle .$$

The method applied consisted in cutting off ($N \times N$) matrix from the infinite one and subsequent step by step raise of number N. Ordering in sequence of $\nu = \{n, l\}$ by raise of k_ν according to table 1 we obtain as a result of calculations table 2 representing dependence of λ_{max} on N.

Finally we are going to obtain governing equation for stationary axial symmetric MHD flow in conductive liquid. Initial equations are taken in form

$$\begin{gathered} [\mathbf{V}\times\Gamma] - [\mathbf{H}\times\mathbf{J}] + \varepsilon\eta\Delta\mathbf{V} = \mathrm{grad}W, \\ \mathrm{rot}[\mathbf{V}\times\mathbf{H}] + \varepsilon\eta_m\Delta\mathbf{H} = 0 \qquad (0 \le \varepsilon \ll 1), \\ [\mathbf{V}\times\mathbf{H}] - \varepsilon\eta_m\mathbf{J} = \mathrm{grad}\psi, \\ \mathrm{rot}[\mathbf{V}\times\Gamma] - \mathrm{rot}[\mathbf{H}\times\mathbf{J}] + \varepsilon\eta\Delta\Gamma = 0. \end{gathered} \tag{19}$$

where grad$W$ — generalized potential force, Γ = rot$\mathbf{V}$, $\mathbf{J}$ = rot$\mathbf{H}$, div$\mathbf{V}$ = 0, div$\mathbf{H}$ = 0, $\Delta\mathbf{H} = -\mathrm{rot}\mathbf{J}$, ψ — scalar potential of electric field. In cylindrical system all components of $\mathbf{V}$, $\mathbf{H}$, Γ, $\mathbf{J}$ can be expressed via four scalar functions A, V, B, H according to

$$V_\rho = -\frac{1}{\rho}\frac{\partial A}{\partial z}, \qquad V_\varphi = \frac{1}{\rho}V, \qquad V_z = \frac{1}{\rho}\frac{\partial A}{\partial \rho},$$

$$H_\rho = -\frac{1}{\rho}\frac{\partial B}{\partial z}, \qquad H_\varphi = \frac{1}{\rho}H, \qquad H_z = \frac{1}{\rho}\frac{\partial B}{\partial \rho},$$

$$\Gamma_\rho = -\frac{1}{\rho}\frac{\partial V}{\partial z}, \qquad \Gamma_\varphi = -\frac{1}{\rho}\hat{\Lambda}A, \qquad \Gamma_z = \frac{1}{\rho}\frac{\partial V}{\partial \rho},$$

$$J_\rho = -\frac{1}{\rho}\frac{\partial H}{\partial z}, \qquad J_\varphi = -\frac{1}{\rho}\hat{\Lambda}B, \qquad J_z = \frac{1}{\rho}\frac{\partial H}{\partial \rho},$$

where $\hat{\Lambda} = \rho\frac{\partial}{\partial\rho}\left(\frac{1}{\rho}\frac{\partial}{\partial\rho}\right) + \frac{\partial^2}{\partial z^2}$ in cylindrical system and $\hat{\Lambda} = \frac{\partial^2}{\partial r^2} + \frac{\sin\theta}{r^2}\frac{\partial}{\partial\theta}\left(\frac{1}{\sin\theta}\frac{\partial}{\partial\theta}\right)$ in spherical one. Taking into consideration that grad$_\varphi$ = 0 in axial symmetric flow one can represent (19) as follows:

Table 1. The wave numbers k_{nl} of elementary harmonics

l	n							
	1	2	3	4	5	6	7	8
1	5.37	6.16	7.16	8.25	9.38	10.52	11.62	12.60
2	10.08	10.60	11.32	12.22	13.24	14.34	15.45	16.71
3	14.91	15.27	15.80	16.48	17.30	18.24	19.22	20.35

Table 2. Dependence of λ_{max} on number N of involved elementary harmonics

Evenness of number n	N					
	1	2	3	4	5	6
even	2.06	3.92	4.66	4.67	5.25	5.56
odd	3.29	4.34	4.92	4.97	6.12	6.39

$$
\begin{gathered}
[\mathbf{V}\times\mathbf{H}]_\varphi - \varepsilon\eta_{\mathrm{m}} J_\varphi = 0,\\
[\mathbf{V}\times\Gamma]_\varphi - [\mathbf{H}\times\mathbf{J}]_\varphi + \varepsilon\eta\Delta_1 V_\varphi = 0,\\
\mathrm{rot}_\varphi[\mathbf{V}\times\mathbf{H}] + \varepsilon\eta_{\mathrm{m}}\Delta_1 H_\varphi = 0,\\
\mathrm{rot}_\varphi[\mathbf{V}\times\Gamma] - \mathrm{rot}_\varphi[\mathbf{H}\times\mathbf{J}] + \varepsilon\eta\Delta_1\Gamma_\varphi = 0.
\end{gathered}
\tag{20}
$$

By means of bilinear skew symmetric differential form

$$
\{f, g\} = \frac{\partial f}{\partial z}\frac{\partial g}{\partial \rho} - \frac{\partial f}{\partial \rho}\frac{\partial g}{\partial z}. \tag{21}
$$

equations (20) can be expressed via introduced scalar functions:

$$
\begin{gathered}
\{A, B\} + \varepsilon\eta_{\mathrm{m}}\rho\hat{\Lambda}B = 0,\\
\{A, V\} - \{B, H\} + \varepsilon\eta\rho^2\Delta_1\left(\frac{V}{\rho}\right) = 0,\\
\left\{A, \frac{H}{\rho^2}\right\} - \left\{B, \frac{V}{\rho^2}\right\} + \varepsilon\eta_{\mathrm{m}}\Delta_1\left(\frac{H}{\rho}\right) = 0,\\
\left\{A, \frac{\hat{\Lambda}A}{\rho^2}\right\} - \left\{B, \frac{\hat{\Lambda}B}{\rho^2}\right\} + \varepsilon\eta\Delta_1\left(\frac{\hat{\Lambda}A}{\rho}\right) = \frac{1}{\rho^3}\frac{\partial}{\partial z}(V^2 - H^2).
\end{gathered}
\tag{22}
$$

Here ε is small parameter which in the case of ideal liquid becomes zero.

Due to property of brackets (21) the first of three equations of the system (22) is satisfied if

$$
B = B(A), \qquad V = V(A), \qquad H = B'(A)V(A), \tag{23}
$$

where $B(A)$ and $V(A)$ are some smooth functions of A and $B' = \frac{d}{dA}B(A)$. Substituting B, V, H into the fourth equation of (22) accordingly (23) enables us to rewrite it in the form of commutative relationship

$$
\left\{A, \frac{1}{r^2}[1 - B'^2(A)]\,[\hat{\Lambda}A + V(A)V'(A)] - \frac{1}{r^2}B'(A)B''(A)\,[\mathrm{grad}^2 A + V^2(A)]\right\} = 0.
$$

In its turn it is satisfied if the second term in brackets is some smooth function $S = S(A)$. Taking this into consideration one can obtain the following quasilinear equation

$$
\hat{\Lambda}A + Q(A)\mathrm{grad}^2 A = \rho^2\Psi(A) + \Phi(A), \tag{24}
$$

where

$$
Q(A) = -\frac{B'(A)B''(A)}{1 - B'^2(A)}, \qquad \Psi(A) = \frac{S(A)}{1 - B'^2(A)},
$$

$$
\Phi(A) = -V(A)[V'(A) + V(A)Q(A)].
$$

For sufficiently nonlinear problems it is useful to transform (24) into integro-differential form

$$
A(\xi) = \int_{\mathrm{D}} G(\xi, \xi')\{Q[A(\xi')]\mathrm{grad}^2 A(\xi') - \rho^2(\xi')\Psi[A(\xi')] - \Phi[A(\xi')]\}d\xi',
$$

with application the Green function $G(\xi, \xi')$ for D — domain of meridional cross-section and boundary condition of impenetrability $A|_{(\mathrm{D})} = 0$.

If $\alpha^2 \ll 1$ then equation (24) can be linearized and obtain representation

$$
\rho\frac{\partial}{\partial\rho}\left(\frac{1}{\rho}\frac{\partial A}{\partial\rho}\right) + \frac{\partial^2 A}{\partial z^2} + (V_1^2 - \Psi_1\rho^2)A = -(V_0 V_1 - \Psi_0\rho^2),
$$

where notations

$$B(A) = B_0 + B_1 A \qquad (B_1^2 < 1, \quad Q(A) = 0),$$

$$V(A) = V_0 + V_1 A, \qquad \Psi(A) = \Psi_0 + \Psi_1 A,$$

$$\Phi(A) = \Phi_0 + \Phi_1 A = -V(A)V'(A), \qquad \Phi_0 = -V_0 V_1, \qquad \Phi_1 = -V_1^2$$

are applied. For example, let us determine stationary resolution for tube domain where the Green function takes the form

$$G_k(\rho, \rho') = \rho\rho' \sum_{n=}^{\infty} \frac{\widetilde{Z}_1(\mu_n \rho)\, \widetilde{Z}_1(\mu_n \rho')}{\mu_n^2 + \dfrac{(2k-1)^2\pi^2}{b^2} - V_1^2}$$

and finally

$$A \approx A_0(\rho, z) = \frac{4}{\pi_k} \sum_{=n1}^{\infty} \sum_{=1}^{\infty} \frac{\left[(V_1 - \rho'^2\Psi_0) Z_0(\mu_n \rho')\right]_{\rho' = 1-a}^{\rho' = 1+a}}{(2k-1)\mu_n \left[\mu_n^2 + (2k-1)^2 \dfrac{\pi^2}{b^2} - V_1^2\right]} \rho Z_1(\mu_n \rho) \sin(2k-1)\frac{\pi z}{b}.$$

Mentioning that if $\varepsilon = 0$ the system (22) is invariant relatively simultaneous interchange $A \leftrightarrow B$, $V \leftrightarrow H$ one can write equation for $B = B(\rho, z)$ being equivalent to (24), where

$$Q(B) = -\frac{A'(B)A''(B)}{1 - A'^2(B)}.$$

At last in the case of linear dependence $A = A(B)$ if $A'^2(B) \neq 1$ we obtain

$$Q(B) = 0$$

and equation

$$\hat{\Lambda} B = \rho^2 \Psi(B) + \Phi(B),$$

which is well known in plasma equilibrium theory as the Grad—Shafranov equation.

COMMENTS

Situation mentioned above is concerned only one of possible scenarios which may occur in real planetary evolution. Another case may appear if differential rotation has subcritical level. Then alternative technique should be applied consisting in asymptotic resolution of boundary layer problem. So one should take into account both Coriolis, Lorentz and viscous forces simultaneously. This makes the problem much more difficult than in cases explored above. But some results obtained in this paper will be necessary on subsequent steps.

REFERENCES

1. Krechetov V. V. Tidal Forces Generation of Planetary Magnetic Fields // Space Res.—1999.—37, N 4.—P. 392—396 (in Russian).

Космічна наука і технологія. ДОДАТОК. 2001. Т 7. № 2. С. 26—33.

UDK 550.388.2

MODEL OF THE INTERNAL GRAVITY WAVES EXCITED BY LITHOSPHERIC GREENHOUSE EFFECT GASES

O. E. Gotynyan, V. N. Ivchenko, Yu. G. Rapoport

Physics Faculty, Taras Shevchenko Kyiv University, Ukraine

The satellite and near-ground study demonstrated IR temperature anomalies associated with fault system of the crust in the seismic region of the Earth. The amplitude of anomalies is about ΔT = 3 K. Such change of temperature needs about 100 % increase of CO_2 concentration. Internal gravity waves (IGW) excited by greenhouse effect gases could cause some ionospheric disturbances including density irregularities. The accurate numerical model of 2D «lithospheric greenhouse effect gas antenna» with heat, mass and concentration sources of IGW in the atmosphere is built in the present work. The system of hydrodynamics equations for IGW excitation in the atmosphere by the source in the form of near-ground layer of lithospheric greenhouse effect gases is reduced to the system of two equations for pressure and vertical velocity component. Corresponding effective boundary conditions are obtained by means of limit pass to the case of very thin layer and absolutely rigid lithosphere. Periodical boundary conditions in the horizontal directions are used to avoid computations with continuous spectrum and numerical convergence of the model is checked carefully. It is shown that at the altitude Z = 200 km the value of vertical velocity of IGW with period 1 hour could reach the value of order 4 m/s what is enough for plasma bubbles formation in accordance with previously published data. In distinction to the qualitative model of Gohberg et al., reactive modes in the IGW spectrum are taken into account. It is shown that, although these modes are non-propagating, they influence significantly the IGW excitation and, as a result, the characteristics of propagating modes. In particular, non-taking into account reactive modes could cause under definite conditions overestimating of energy flow by at least two orders of value. This result is analogous to the well known in microwave technique effect of the influence of reactive modes on scattering of electromagnetic waves on inhomogeneities in microwave waveguides.

INTRODUCTION

Study of satellite thermal images [1, 2] demonstrated IR anomalies associated with largest linear structures and fault system of the crust in the seismic region of the Earth. Typical dimensions of these anomalies are 700 km length and 50 km width. They appear 6-24 days before shock and are sensitive to crust earthquakes with magnitude more than 4.7. The amplitude of observed temperature anomalies is about ΔT = 3 K. In accordance with [3], such change of temperature needs about 100 % increase of CO_2 concentration. It is possible to expect that IGW excited by greenhouse effect gases could cause both periodical changes of the intensity of optical glows of the ionosphere and a shift of the average level of the glows intensity. IGW could also cause different ionosphere disturbances and density irregularities. The spectrum of variations before earthquake of intensity of red and green lines of oxygen optical emissions (with wavelength 630 nm and typical altitude 270 km and wavelength 557.7 nm and typical altitude 97 km, respectively) includes periods from some minutes to two hour [4, 5]. Such periods are also typical for IGW and acoustic-gravity waves (from the side of shorter waves) [6]. It is supposed in [7] that IGW could be responsible also for the observed change of electromagnetic wave characteristics in the waveguide «Earth-Ionosphere» before earthquake.

The model of 2D «lithospheric greenhouse effect gas antenna» with heat, mass and concentration sources of IGW in the atmosphere is built in the present work. The system of hydrodynamics equations for the IGW excitation in the atmosphere by the gas source in the form of thin near-ground layer of lithospheric greenhouse effect gases is reduced to the system of two equations for pressure and vertical velocity component. Corresponding effective boundary conditions are obtained by means of limit pass to the case of very thin layer and absolutely rigid lithosphere. Periodical boundary conditions in the

horizontal directions are used to avoid problems with continuous spectrum, and numerical convergence of the model is checked carefully.

We suppose in accordance with [3] that the release of lithospheric gases is modulated in time due to two factors. The first one is the modulation of the number of elementary processes of lithospheric gas release by the deformation processes in the earth crust during the earthquake preparation. The second one is the modulation of the lithospheric gas release by the seismogravity oscillation in the system «lithosphere-atmosphere». This modulation develops during last days and hours before earthquake [3], [8]. The typical period of seismogravity oscillations is 1 hour [8]. As it was mentioned above, the periods of the same order have been observed in the spectrums of modulations of the airglow intensity before earthquakes [4]. At the same time, these periods are typical for the IGW in the atmosphere [6].

The real gas source of IGW has rather wide frequency spectrum. It is also possible to expect that the lithospheric gas source includes several non-correlated in space (and, possibly, in time) elementary gas sources of IGW. To search the effect of separate spectrum components of lithospheric gas source, we consider in the present article the problem in the simplest possible formulation. Namely, we consider the «model problem» of IGW excitation in the atmosphere by lithospheric gas source correlated in space and harmonic in time and search this process under different source frequencies.

MODEL DESCRIPTION

The model of 2D «lithospheric greenhouse effect gas antenna» of IGW in the atmosphere is built in the present work. Heat, mass and concentration sources of IGW are taken into account. The system of hydrodynamics equations for acoustic-gravity waves [6] excitation and propagation has the following form:

$$\begin{cases} \rho \dfrac{d\mathbf{v}}{dt} = -\nabla p + \rho \mathbf{g} + \rho \mathbf{F}_z, \\ \dfrac{d\rho}{dt} + \rho \mathrm{div}\mathbf{v} = q, \\ \dfrac{dp}{dt} + \mathbf{v}\nabla p = c^2 \left(\dfrac{\partial \rho}{\partial t} + \mathbf{v}\nabla \rho \right) + A\rho \end{cases} \tag{1}$$

where ρ, $\mathbf{v}$, p, $\mathbf{g}$ are density, velocity, pressure and gravity acceleration, respectively, $d/dt \equiv \partial/\partial t + \mathbf{v}\nabla$, γ is adiabatic constant, $\mathbf{F}_z = F_z \mathbf{e}_z$ is the force function, $q(\mathbf{r}, t)$ and $A(\mathbf{r}, t)$ are densities of the mass and heat sources which are determined by gases released from the lithosphere.

After linearization of system of equation (1), we could obtain (from corresponding homogeneous system of equation) well-known dispersion equation for acoustic-gravity waves [6] in the form:

$$\omega^2 = \frac{c^2}{2}\left(k_x^2 + k_z'^2 + \frac{1}{4H^2} \right) \pm \sqrt{\frac{c^4}{4}\left(k_x^2 + k_z'^2 + \frac{1}{4H^2} \right) - (\gamma - 1) g^2 k_x^2}, \tag{2}$$

where $\omega_b = g\sqrt{\gamma - 1}/c$ is the Brunt—Vaisala frequency, H is the atmospheric scale height, $k_z' = -i/(2H) + k_z$, k_x and k_z are horizontal wave number and the real part of vertical wave number, respectively, ω is the frequency of the lithospheric gas source, and 2D problem is considered, c is acoustic speed, $\partial/\partial y = 0$. This corresponds physically to the case of the lithospheric gas source associated with long (linear) crust fault. In the case $\omega \ll \omega_b$ the dispersion equation of acoustic-gravity waves (2) reduced to the dispersion equation for gravity waves (or internal gravity waves, IGW) [6]:

$$k_z = -\frac{i}{2H} \pm k_z' = -\frac{i}{2H} \pm \sqrt{-\frac{1}{4H^2} + \left(\frac{\omega_b^2}{\omega^2} - 1 \right) k_x^2}, \tag{3}$$

All numerical calculations below in the present paper are presented for the case of IGW, when

dispersion equation is in the form (3).

For $\frac{1}{4H^2} > \left(\frac{\omega_b^2}{\omega^2} - 1\right)k_x^2$, the wave number k_z is purely imagine and corresponding modes are «reactive». These modes could not propagate in the atmosphere. At the same time, it is well know in electrodynamics of inhomogeneous transmission lines (including antennas systems) that reactivities could modify remarkably the coefficients of reflection and transmission as well as the effectiveness of excitation of electromagnetic waves. It is shown in the present paper that analogous situation takes place for IGW excitation. It is necessary to take into account reactive modes otherwise the mistake of determination in the energy flow at the altitude 200 km could exceed two order of value. In the qualitative model [3] the influence of the reactive modes on the excitation of gravity wave in the atmosphere has not been taken into account.

To avoid the problems with continuous spectrum the discrete Fourier transform is used in horizontal directions x, y and calculations are done in horizontal region with big, but finite dimensions $L_x \gg l_x$, $L_y \ll l_y$ and with periodical boundary conditions. Here $l_{x,y}$ are horizontal dimensions of the IGW lithospheric source. The values L_x, L_y are chosen in such a way, that their increase does not cause any remarkable change of the IGW field in the region of interest. In our case the region of interest (where the characteristics of IGW are calculated) has the dimension $L_x = 10^4$ km (the approximation of plane Earth and atmosphere is used) and the number of Fourier modes is $N_x = 500...600$. The horizontal wave numbers corresponding to these Fourier modes are $k_x(l_x) = 2\pi l_x/(N_x L_x)$, where $l_x = \overline{0, N_x - 1}$.

BOUNDARY CONDITIONS

The wave equation for the elastic waves propagating in the earth crust (which is considered as isotropic elastic media) has the form [9]:

$$\rho\ddot{\mathbf{U}} = \mu\Delta\mathbf{U} + (\lambda + \mu)\text{graddiv}\mathbf{U}, \tag{4}$$

where ρ is the density of media, $\mathbf{U}$ is volume element displacement, $\mathbf{v} = \partial\mathbf{U}/\partial t = -i\omega\mathbf{U}$, λ and μ are elastic constants [9].

The general solution of the equation (4) has the form:

$$\mathbf{U} = \begin{pmatrix} U_x \\ U_y \end{pmatrix} = A_1 \begin{pmatrix} -\frac{k_{z1}}{k_x} \\ 1 \end{pmatrix} + A_2 \begin{pmatrix} \frac{k_x}{k_{z2}} \\ 1 \end{pmatrix},$$

where k_x and $k_{z1,2}$ are x- and z-components of wave numbers of elastic modes. Indexes 1 and 2 correspond to the transverse and longitudinal elastic modes with dispersion equations having the forms, respectively [9]:

$$\omega^2 = \left(\frac{\mu}{\rho}\right)(k_x^2 + k_{z1}^2), \qquad \omega^2 = \frac{\lambda + 2\mu}{8}(k_x^2 + k_{z2}^2).$$

We suppose for simplicity that lithospheric gases occupy the near-Earth region of the atmosphere $z_a \le z \le z_b$, which is called below the «lithospheric gases layer» (Figure 1). Here $z_a = 0$, $z_b = \Delta z_0$, Δz_0 is the thickness of the lithospheric gas layer.

As one can see from Figure 1

$$\begin{cases} \Delta V_{z,s} = V_z^a - V_z^b, \\ \Delta P_s = P^a - P^b \end{cases} \tag{6}$$

where $\Delta V_{z,s}$ and ΔP_s are amplitudes of velocity and pressure generated by IGW source, respectively, $P^{a,b}$, $V^{a,b}$ are pressure and wave velocity at the points $z = z^b = \Delta z_0$ and $z = z^a = 0$, respectively.

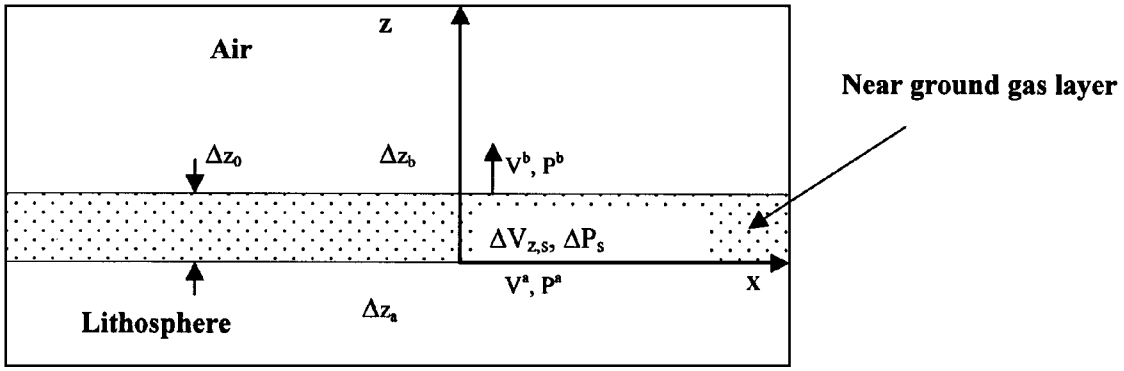

Fig. 1. Gas source of AGW generation in near-ground layer of the atmosphere

The boundary conditions at the both surfaces $z = z_a$ and $z = z_b$ of the lithospheric gas layer have the form:

$$\begin{cases} \sigma_{ij} n_j \mid_{z=z_{a,b}-0} = \sigma_{ij} n_j \mid_{z=z_{a,b}+0}, \\ V_z \mid_{z=z_a-0} = V_z \mid_{z=z_a+0}, \\ P \mid_{z=z_a-0} = P \mid_{z=z_a+0}, \end{cases} \tag{6}$$

where n_j is j-th component of normal to the corresponding surface. The stress tensor σ_{ij} inside the lithosphere ($z < z_a$) has the form

$$\sigma_{ij} = 2\mu U_{ij} + \lambda div \mathbf{U} \delta_{ij},$$

$$U_{ij} = \frac{1}{2}\left(\frac{\partial U_i}{\partial x_j} + \frac{\partial U_j}{\partial x_i}\right).$$

In the gas media both inside lithosphere gas layer, $z_a < z < z_b$, and in the atmosphere above the lithospheric gas layer, $z > z_b$, the stress tensor is

$$\sigma_{ij} = -p\delta_{ij},$$

where p is the pressure in the corresponding gas media.

Using equations, which we have obtained after Fourier transform of the system (1) and boundary conditions (6), we get the following expression for $\Delta v_{z,s}$, ΔP_s:

$$\Delta v_{z,s} = \int_0^{\Delta z_0} \left(\frac{A}{gH} + \gamma \frac{q}{\rho_0}\right) dz, \tag{7}$$

$$\Delta P_s = \frac{1}{gH} \int_0^{\Delta z_0} \left(F_z + D_t^{-1} \frac{A}{\gamma H}\right) dz, \tag{8}$$

$$R_p(k_x) = \frac{P}{v_z} = -\frac{D_t - gD_t^{-1}\left(D_z - \frac{1}{H}\right)}{gH\left(D_z - \frac{1}{H}\right) + gD_t^{-2}D_x^2},$$

where $D_t = i\omega$, $D_z = -ik_z$, $D_x = -ik_x$, $R = \tilde{\rho}/\rho_0$, $P = \tilde{p}/p_0$, P and V_z are the pressure and vertical component of the particles velocity in the atmosphere above the lithospheric gas layer ($z > z_b$), $\tilde{\rho}$, $\tilde{p}$, ρ_0, p_0 are variable and stationary parts of the atmospheric density and pressure, respectively.

It is possible to obtain Fourier-transform of v_z and P from equations (2)—(5):

$$v_z^b = \frac{p_0 \Delta P_{\text{дж}} + \dfrac{S}{\omega(\beta_1 + a)} \Delta v_{z,\,s}}{p_0 R_p + \dfrac{S}{\omega(\beta_1 + a)}}, \tag{9}$$

$$P^b = R_p v_z^b,$$

where

$$\beta_1 = -\frac{k_x}{k_{z1}}, \qquad \alpha_1 = \frac{k_x}{k_{z2}}, \qquad a = A_2'/A_1 = -\frac{k_{z1} + k_x\beta_1}{k_{z2}\alpha_1 + k_x},$$

$$S = \lambda(k_x + k_{z1}\beta_1) + 2\mu k_{z1}\beta_1 + a[\lambda(k_x\alpha_1 + k_{z2}) + 2\mu k_{z2}].$$

In the limit of absolutely rigid lithosphere the equation (9) reduces to the form:

$$v_z^a = 0, \qquad v_z^b = \Delta v_{z,s}. \tag{10}$$

Later we shall use this approximation.

The analysis of equation (7), (8) shows that the IGW are excited at most by the heat source with temperature amplitude ΔT (numerical estimations show that the mass and force sources presented in eqs. (1), (7), (8) give negligibly small contribution to IGW excitation in comparison with the heat source). In accordance with [3], IGW source amplitude $\Delta v_{z,s} = \dfrac{A}{\gamma H}\Delta z_0$ is related to the amplitude ΔT of the observed heat anomaly before earthquake as follows:

$$\Delta v_{z,s} = \Omega \Delta z_0 \frac{\Delta T}{2\gamma T} \exp(z/2H),$$

where Ω is frequency of temperature oscillation (determined by above mentioned processes of lithospheric gas release modulation before earthquake), γ is adiabatic constant, T is an air temperature (we use the approximation of isothermic atmosphere here), z is vertical coordinate.

MODEL SOURCE AND THE FIELD OF GRAVITY WAVES IN THE ATMOSPHERE

Consider one-dimensional thermal source with the space distribution in the form $\Delta T = \Delta T_0 \cdot \text{ch}^{-2}(x_1/l)$, where ΔT_0 is the amplitude of observed temperature anomaly (it is equal to 3 K in the present calculations), l is the lithospheric source width. Such source corresponds to the longitudinal lithospheric fault which has the length much bigger than its width [2]. Corresponding vertical velocity at the earth

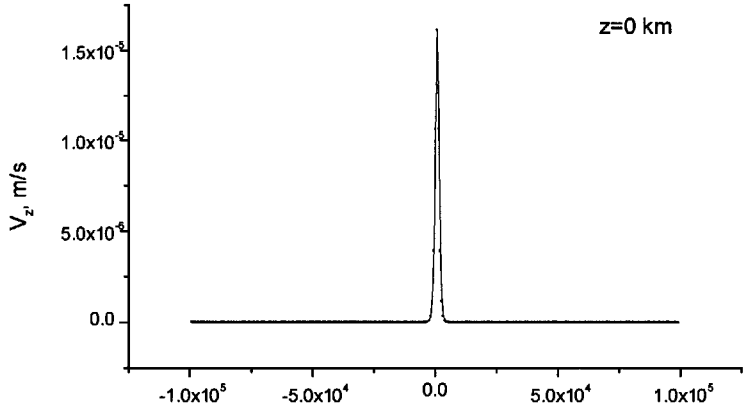

Fig. 2. Vertical velocity profile V_z (m/s) at the level of the Earth crust ($z = 0$), period is equal to 15 min, number of modes is 500, ΔT = 3 K, source size is 100 km

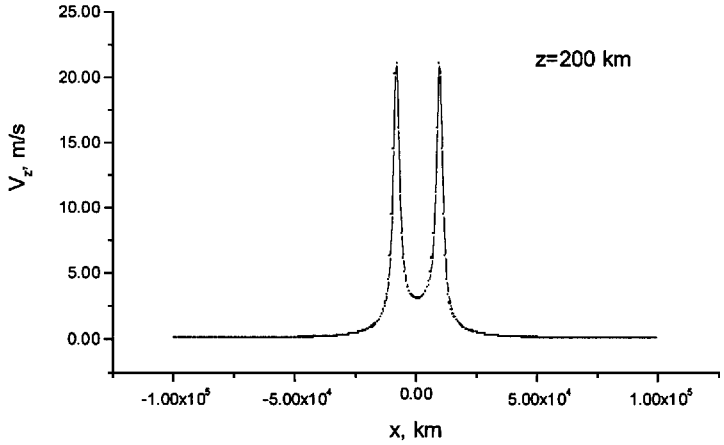

Fig. 3. Vertical velocity profile at the 200 km without reactive modes, period is equal to 15 min, number of modes is 600, ΔT = 3 K, source size is 100 km

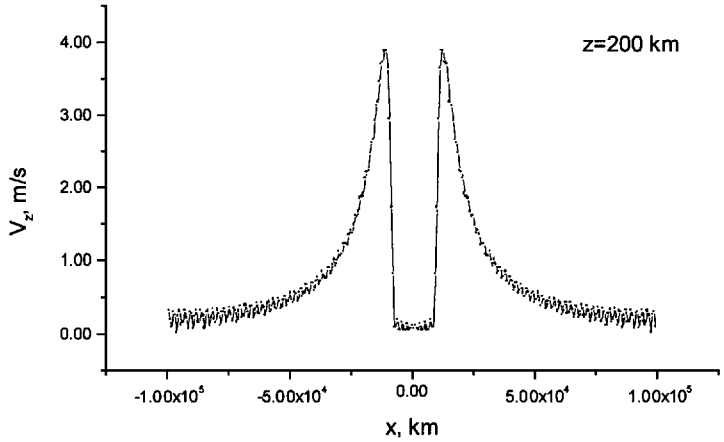

Fig. 4. Vertical velocity profile at the 200 km with reactive modes, period is equal to 15 min number of modes is 500, ΔT = 3 K, source size is 100 km

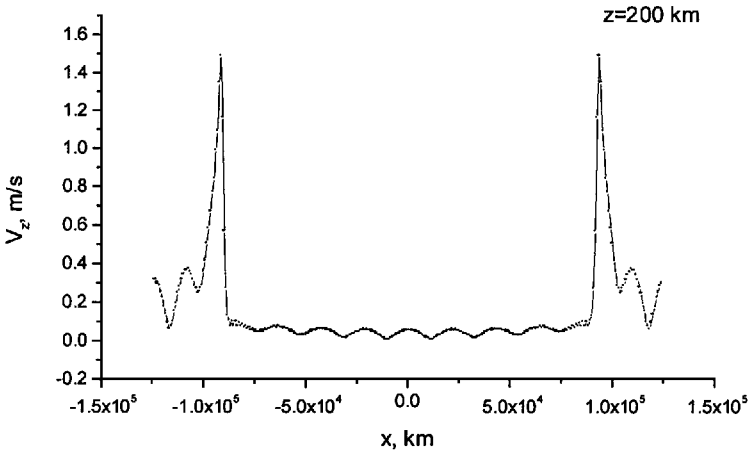

Fig. 5. Vertical velocity profile at the 200 km with reactive modes, period is equal to 60 min, number of modes is 600, ΔT = 3 K, source size is 100 km

surface is $V_{z,s}^{mod}(x_l) = \Delta v_{z,s} ch^{-2}(x_l/l)$ (see Figure 2).

As it follows from the solution of the system of equations (1), the velocity and pressure of IGW excited in the atmosphere by the lithospheric gas source have the following form:

$$v_z(x_l, z) = e^{z/(2H)} \sum_{m=1-Nx/2}^{Nx/2} v_z(k_m) \cdot e^{-ik_m x_l - ik'_z z},$$

$$v_x(k_m) = -\frac{gH}{\omega} k_m R_p v_z(k_m),$$

$$P(x_l, z) = e^{z/(2H)} \sum_{m=1-Nx/2}^{Nx/2} R_p v_z(k_m) \cdot e^{-ik_m x_l - ik'_z z},$$

where $k_m = 2\pi m/L$, $m = \overline{1 - N_x/2, Nx/2}$, $x_l = \frac{l}{Nx} L$, $l = \overline{1 - N_x/2, Nx/2}$, N_x is the number of modes taken into account in discrete Fourier transform, k'_z is real part of k_z, $v_z(k_m)$ is Fourier amplitude of the m-th harmonic of IGW vertical velocity.

The distribution of the vertical velocity V_z taking into account reactive modes are shown on the Figures 4, 5 for the altitude 200 km and the values of the periods $T = 15$ min and $T = 60$ min respectively. Distribution of the V_z with the spectrum where reactive modes are omitted is shown in the Figure 3.

RESULTS AND CONCLUSION

1. It is shown (see Figures 3—5) that it is necessary in general case to take into account the reactive modes in the spectrum, in distinction to the model [3]. For example, for the period $T = 15$ min difference of the V_z amplitudes computed by means of the present model and of the model [3] reaches more than 10 times and IGW peak energy density reaches more than 10^2 times at the altitude 200 km (see Figures 3, 4). In distinction to the model [3], the present model demonstrates much wider distribution with the side lobes in horizontal direction of the IGW vertical velocity. On the other hand, for higher frequencies the difference between the energy flow density computed with and without taking into account the presence of reactive modes in the IGW spectrum is rather small.

2. The gases released from the lithosphere before earthquake are rather effective source of IGW. Namely, for $T = 60$ min the value of vertical component of IGW velocity V_z could reach 4 m/s at the altitude $Z = 200$ km (Figure 5). The IGW with such velocity could excite ionospheric plasma bubbles [10] and influence the intensity of the ionospheric glows before an earthquake [11]. As a result microinstabilities in the ionosphere could be excited on the gradient of electron density [12]. These processes are nonlinear and therefore very sensitive for the amplitude and space distribution of the initial disturbances in the ionosphere. The present accurate model of IGW excitation by the lithospheric gas source is important for calculation of such disturbances excited in ionosphere due to lithospheric processes before an earthquake.

REFERENCES

1. Gornyj V. I., Sal'man A. G., Tronin A. A., Shylin B. V. Residual infrared radiation — of seismic activity // DAN USSR.—1988.—**301**, N 1.—P. 67—69 (in Russian).
2. Tronin A. A. Satellite thermal survey application for earthquake prediction // Atmosphere and ionosphere electromagnetic phenomena associated with earthquakes / Ed. by M. Hayakawa. — TERRAPUB Tokyo, 1999.—P. 717—746.
3. Gohberg M. B., Nekrasov A. K., Shalimov S. L. To the influence of nonstable release of green-house effect gases in seismically active regfions on the ionosphe // Physics of the Earth (Fizika Zemli.—1996.—N 8.—P. 52—55 (in Russian).

4. Toroselidze T. I. Analysis of aeronomy problems using radiation of higher atmosphere. — Tbilisy: Mecniereba Publ., 1991 (in Russian).
5. Gladishev V. A., Fishkova L. M. Optical research of seismoactivity effects of the ionosphere // Electromagnetic phenomena related to earthquake prediction / Ed. by M. Hayakawa, Y. Fujinawa. — TERRAPUB Tokyo, 1994.—P. 375—380.
6. Hines C. O., Interal atmospheric gravity waves at ionospheric heights // Can. J. Phys.—1960.—**38**.—P. 1441—1481.
7. Molchanov O. A., Hayakawa M. Subionospheric VLF signal perturbations possibly related to earthquakes // J. Geophys. Res.—1998.—**103A**.—P. 17489—17504.
8. Linkov E. M., Petrova L. N., Osipov K. S. Seismogravity oscillation of Earth and connected with them ionospheric disturbances // DAN USSR.—1990.—**313**, N 5.—P. 1095—1098 (in Russian).
9. Fedorchenko A. M. Theoretical physics. — K.: Wyshcha shkola, 1992.—Vol. 1. Classical mechanics and electrodynamics.
10. C.-S. Huang, C. Kelley Nonlinear evolution of equatorial spread of F2. Gravity wave seeding of Rayleigh-Taylor instability // J. Geophys. Res.—1996.—**A101**.—P. 293—302.
11. Pertsev N. I., Shalimov S. L. Generation of atmospheric gravity waves in sweismically active region and thir influence on the ionosphere // Geomagnetism i Aeronimiya.—1996.—**36**, N 2.—P. 111—118.
12. Treumann R.A., Baumjohann W. Advanced Space Plasma Physics Imperial. — Singapore: College Press, 1997.

Космічна наука і технологія. ДОДАТОК. 2001. Т 7. № 2. С. 34—35.

DUSTY PARTICLES — POSSIBLE SOURCE OF RYDBERG STATES FORMATION IN LOW IONOSPHERE

E. V. Martysh

Institute of Space Research, Kyiv, Ukraine

It is shown that recombination of free ion with electron on the surface of dusty particle forms the neutral molecule or atom in Rydberg (high-excited) state. The concentration of such neutrals can be higher than concentration originated from usual plasma volume recombination.

During the last few years several works that deal with observation of highly intensive radiation in far infrared and radio frequencies of low ionosphere at disturbance periods appeared. Highly excited atoms or molecules are one of the possible sources of this radiation. Authors [1] had investigated formation of highly excited atomic or molecular state during the solar flares. These states can be one of the potential sources of the above-mentioned radiation. Photoelectrons (and/or electrons born during magnetic storms) were found to be a cause of formation of the strongly excited atoms and molecules. It should be noted that usually atoms with principal quantum number $n \geq 10$ are referred to as Rydberg's states. However the respective value for atmospheric gases (N_2, O_2, NO_x) is $n > 3$ due to the following fact: energy of these states for atmospheric gases appears to be some 2—3.5 eV less than the ionization potentials. In [1] it is shown that there are two maximums for excitement rate constant of molecular Rydberg's states: at the heights of $\approx$ 200 km and $\approx$ 100 km; the values are connected with different parts of the solar spectrum.

Disturbance in the ionosphere may also result from changes in geoelectric field [2—3], thus it is reasonable to consider an additional source of Rydberg's states formation. It is connected with the peculiarities of aeronomy of the area but should also be taken into consideration when analyzing influence of the solar flares. It is known [4] that in the latter case an excursion of electron concentration may also occur at the above-mentioned heights due to floods of high-energy particles. Thus an analysis should allow for recombination processes that also lead to formation of highly excited neutrals.

As it was reported in [5], there are some layers of dust particles 1—5 km in thickness at heights of 80—100 km. The density of these particles varies from 0.5 to 10 cm^{-3}. Unfortunately, our knowledge regarding dust origination, composition, and particle sizes is far from perfect. However, we can make some evaluations based on the experimental data mentioned above. At heights about 80 km, the dust is probably composed of ice, sometimes with metallic impurity [6]. At higher altitudes (90—100 km), the main components of dust are meteor ablation, rocket exhaust products, and materials from destroying part of spacecraft's. The average size of such dust particles (a) is ~ some microns. Such layer of dust overlaps plasma layer of increased electron temperature and concentration. It is known that electron charge of particle surface can be increased by geoelectric field perturbation [2].

We assume that the surface states of electrons on a dust particle are analogous to those on the surface of condensed noble gases and some other dielectric [7]. Therefore, electrons are bound in the normal direction to the surface of the particle and practically free in the tangent directions. The attractive part of surface potential connected with interaction of electron with its «mapping» in dielectric. The origination of repulsion can change in various dielectrics, but usually it is connected with presence of amorphous structure and low (or negative) affinity to electron. It can be shown that energy spectrum (E_n) of such states is close to hydrogen-like one if dusty particle consists of dielectric only [7]:

$$E_n = -Z^2 \mathrm{Ry}/n^2,$$

where $Z = 1/4(\varepsilon - 1)/(\varepsilon + 1)$ — effective charge of electron mapping in dielectric with permeability ε, Ry is Rydberg constant. Distance of electron from the surface is $l \sim b/Z$, where b — Bohr radius. This

distance meets inequality $l \ll N^{-1/3}$, where N is concentration of neutral particles on these altitudes. This inequality provides a possibility to ignore the neutral particles influence on the surface electron spectrum. This hydrohen-like spectrum is more complicate if dielectric has metallic impurities. One needs more detailed information about dusty particle parameters in both cases. Data from [8] provide following magnitude epsilon for chemical substances, mentioned above:

a) Materials with hydrocarbones, $\varepsilon \sim 2.5 — 11$;

b) Metallic oxides (f.e. Al_2O_3, etc.), $\varepsilon \sim 8.5 — 25$;

c). Ice (temperature below −40 °C), $\varepsilon \approx 95$;

We can evaluate a bonding energy of electron on the dusty particle surface as 0.5—0.9 eV. This energy is higher then the thermal energy of surface (near ~ 0.02 eV on these altitudes at night). Thus we can neglect its influence on the first level population.

When an ion collides with a charged dusty particle the electron-ion heterogeneous recombination with particular excited states occurs [9]. This is caused by the peculiarity of the decay of a quasi-molecule: surface electron — ion with formation of neutral particle. This process obviously has dominant probability if the surface electron energy is close to the energy of the particle. The bound energy of a dust surface electron is of the order of 1 eV. Therefore, a neutral particle appears in a highly excited (Rydberg state).

Rydberg state formation also takes place during usual recombination process. Characteristic time of this process is inversely proportional to the charged particles concentration, so an importance of this process is increasing during the time interval of electron concentration disturbances by high-energy particles stream. Analytical solutions for equations, which describe space-temporal structure of electron concentration disturbances by high-energy particles stream [4], can be used for evaluation of Rydberg states concentration. We will assume that Rydberg states are formed by recombination processes on the dusty particles or by «ion — electron» processes and vanish in radiation process. The following ratio between concentration of Rydberg states from dusty particles recombination N_r and usual two-bodies recombination N_r^* results from the balance equations

$$N_r/N_r^* \sim k_{rec}/k_{rec}^* \cdot N_d/N_e,$$

where k_{rec} is the rate of ion-surface electron recombination; k_{rec}^* is the rate of ion-free electron recombination. Concentration of dusty particles is N_d and concentration of free electrons is N_a. It follows from results [4,8] that inequlity $N_r/N_r^* \geq 10$ can exist in low ionosphere (nighttime) and dusty particles make an important contribution to the Rydberg states formation. Evaluation of spectrum and intensity parameter requires specific data about dusty substance and probabilities of transitions in states, mentioned above.

REFERENCES

1. Avakyan S., Serova A., Voronin N. Role of Rydberg's atoms and molecules in high ionosphere // Geomagnetism and aeronomy.—1997.—37, N 3.—P. 99—106 (in Russian).
2. Martysh E. V. Radon emission influence on the low ionosphere parameters // Space science and technology.—1999.—5, N 5/6.—P. 41—51 (in Russian).
3. Sorokin V., Yacenko A. The beginnigs of quasi-stationary electric fields in atmosphere above seismo-active regions // Chemical physics.—2000.—19, N 6.—P. 71—80 (in Russian).
4. Martynenko S. About modeling of electron concentration disturbances, caused by high-energy particles streams in D-region of ionosphere // Geomagnetism and aeronomy.—1989.—29, N 1.—P. 64—70 (in Russian).
5. Havnes O. et al. Charged Dust in the Earth mesopause // Phys. Scripta.—1992.—45.—P. 535—544.
6. Fricke K. et al. Visual and radar observations of rocket induced effects in the upper atmosphere // 12th EAS Symp. May 29 — June 1, Norway, 1995.—P. 81.
7. Shikin V., Monarha Yu. Two-dimensional charged systems in helium. — Moscow: Nauka publ., 1989 (in Russian).
8. Handbook of modern electronics and electrical engineering / Ed. Ch. Belove, 1986.
9. Kogan E., Mal'nev V., Martysh E. About Electron's State on the Dielectric Surface and Geterogenic Recombination / Proc. 3-rd All-Union Symp. on Plasmachemistry. — Moscow, 1979.—Vol. 1.—P. 77—80.

Космічна наука і технологія. ДОДАТОК. 2001. Т 7. № 2. С. 36—41.

UDC 550.388

INVESTIGATION OF CIRCUMTERRESTRIAL SPACE BY MEANS OF INCOHERENT SCATTER RADAR

V. I. Taran, V. K. Bogovsky, V. N. Lysenko,
Ye. I. Grigorenko, L. Ya. Yemelyanov

Institute of Ionosphere of Ministry of Education and Science of Ukraine
and National Academy of Sciences of Ukraine, Kharkov

The results of investigations of ionosphere by means of the Kharkov incoherent scatter radar are presented. The measurements realized jointly with Massachusetts Institute of Technology (Haystack Observatory) and Cornell University (Arecibo Observatory) made it possible to reveal the longitudinal and latitudinal variations of topside hydrogen ion behavior. Ionosphere observations in Kharkov during the solar eclipse on August 11, 1999 first have been carried out up to 1500-km altitude. They have shown the significant changes in state of the F region and topside ionosphere including hydrogen ion concentration, plasma fluxes, that is the evidence of significant infringement of plasma exchange processes between ionosphere and protonosphere.

The parameters of ionized part of circumterrestrial space, i.e., the ionosphere are measured by means of satellites, rockets and ground-based radio physical methods. One of the most informative and accurate methods is the method of incoherent scatter. This method makes it possible to measure simultaneously and with high accuracy the basic parameters of ionosphere plasma: electron concentration N_e, electron and ion temperatures T_e and T_i, vertical velocity of plasma V_z, ionic composition in the altitude range from 100 up to some thousand kilometers.

The incoherent scatter method is based on the scattering of radiowaves on the thermal fluctuations of electron density. Since the effective reflecting surface of ionosphere plasma volumes that are sounded is usually extremely small the signal-to-noise ratio is equal to a few percents. Therefore, the high potential radio devices, i.e., incoherent scatter radars are necessary for determination of plasma parameters of such small signals. The unique incoherent scatter radar has been created near Kharkov city. Radar is equipped with one of the largest in the world zenith parabolic 100-m diameter antenna, with power transmitter device that has the peak pulse power in order of 4 MW and average power about 100 kW, high-sensitive receiver, which noise temperature is about 100 K and high-speed digital correlator. The techniques of measurement and processing of the scatter signal for signal-to-noise ratio less than 0.1 are elaborated.

There are eight observatories in the world: four in America and in other ones in Ukraine, Russia, Japan, Northern Europe, that carry out ionosphere investigations by means of incoherent scatter radars. The coordinated ionosphere observations are performed in accord with the International Geophysical Calendar.

The joint ionosphere measurements together with Massachusetts Institute of Technology (Haystack Observatory) and Cornell University (Arecibo Observatory) enabled revealing the longitudinal and latitudinal variations in behavior of topside hydrogen ions [1].

Figure 1 illustrates longitudinal comparison of the topside hydrogen ion behavior from simultaneous observation results obtained by radars of Millstone Hill (42.6 N and −71.5 E) and Kharkov (49.7 N and 36.3 E) on February 13-14, 1996. The two panels placed above show plots of the H^+ fraction at several topside altitudes as a function of local time. The Kharkov data clearly show much greater concentrations of H^+ ions in comparison with Millstone's observations at nearly identical altitudes.

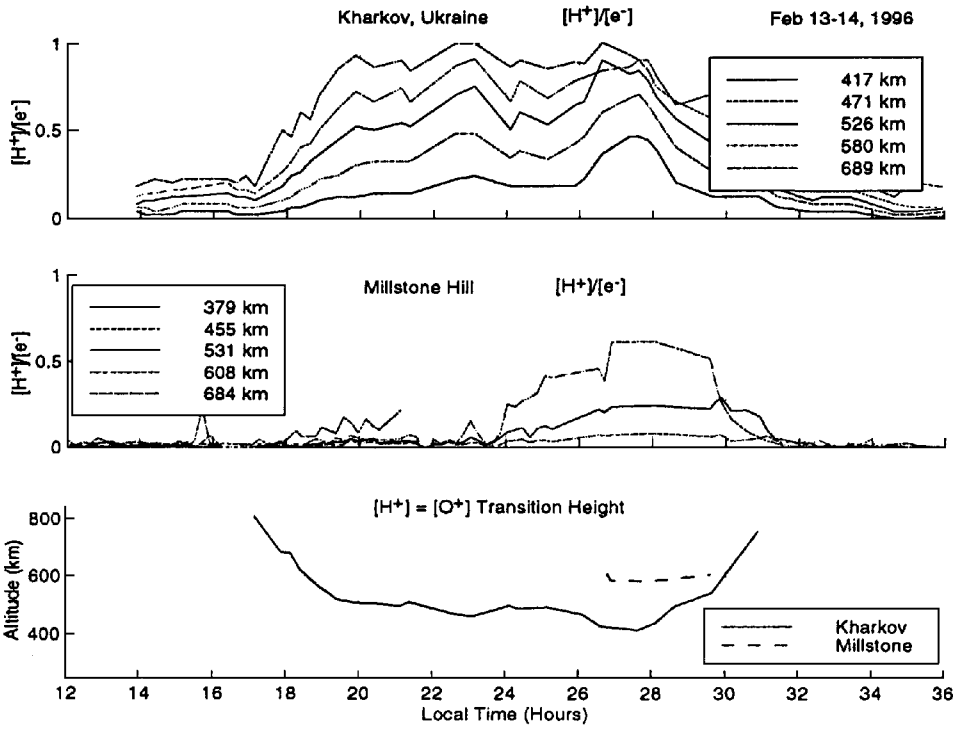

Figure 1. Comparison of observed topside H^+ ion fractions and the O^+/H^+ transition altitude from Kharkov and Millstone Hill data, showing significant longitudinal light ion variations

The bottom panel plots the altitude at which $[H^+] = [O^+]$. It is the important altitude of transition between ionosphere and protonosphere. Below this altitude the charge-exchange chemical processes dominated, above it diffusion and transport prevailed. In this quiet ionosphere, the Kharkov data show transition occurred at 450 to 500 km for most of night. On the contrary, the O^+/H^+ transition for Millstone Hill does not even decrease below 600 km until 0300 LT, and then only for 2 hours. This shows evidence of significant variations of longitudinal topside hydrogen ion.

The observed high concentrations of H^+ ions over Kharkov compared to ones over Millstone Hill can be possibly explained by the following reasons:

— the noncoincidence of the geodetic and geomagnetic poles and as a result the magnetic flux tube for Kharkov (geomagnetic latitude is 45.4 N, L = 1.9) has higher values of H^+ ion density than the magnetic flux tube for Millstone Hill (geomagnetic latitude is 53 N, L = 3.2) because of their different geometric sizes;

— the influence of additional ionosphere heating due to conjugate photoelectron energy input from Southern hemisphere. The point is that for Millstone Hill the conjugate ionosphere region occurs beyond the Southern polar circle, where the sun does not set in February, while in Kharkov the additional heating from the conjugate region (that occurs near Madagascar island) is absent at night.

Investigations during the period of more than solar activity cycle show that in summer electron temperature decreases near noon at solar activity maximum while that is not observed at solar minimum. Increasing of heat transfer due to large values of electron density N_e causes this fall of T_e.

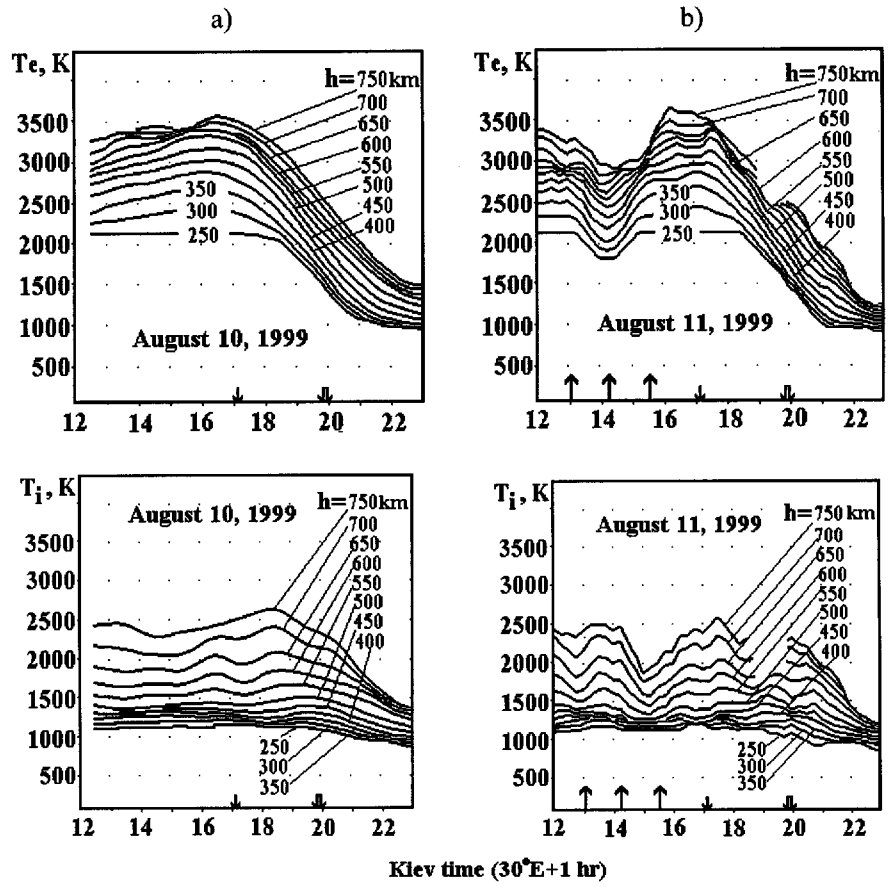

Figure 2. Time variations of electron T_e and ion T_i temperatures at the constant altitudes: a) on the control (preceding) day; b) on the eclipse day. The upward arrows mean the momentum of the first contact, maximum and last contact of eclipse; the downward arrows mean the sunset at Kharkov (double) and conjugate region (single)

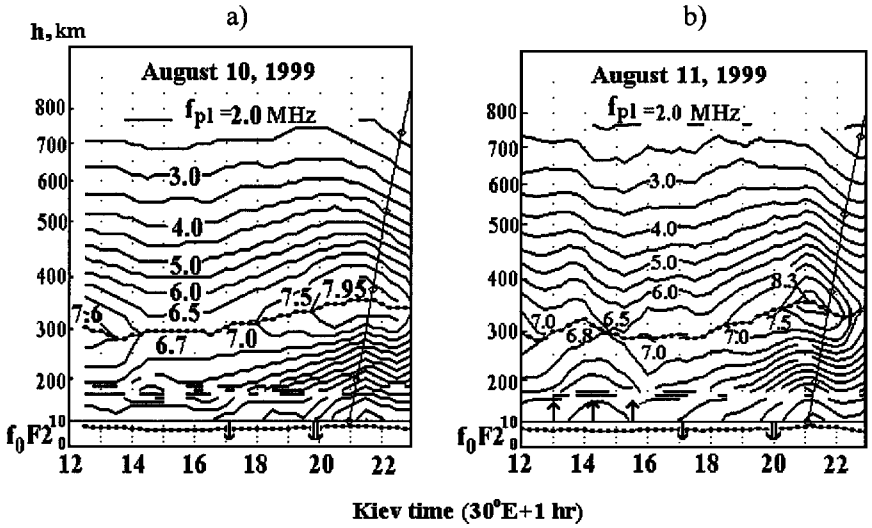

Figure 3. Contours of constant plasma frequency in the F region of the ionosphere as functions of height and time: a) on the day preceding the eclipse; b) on the eclipse day

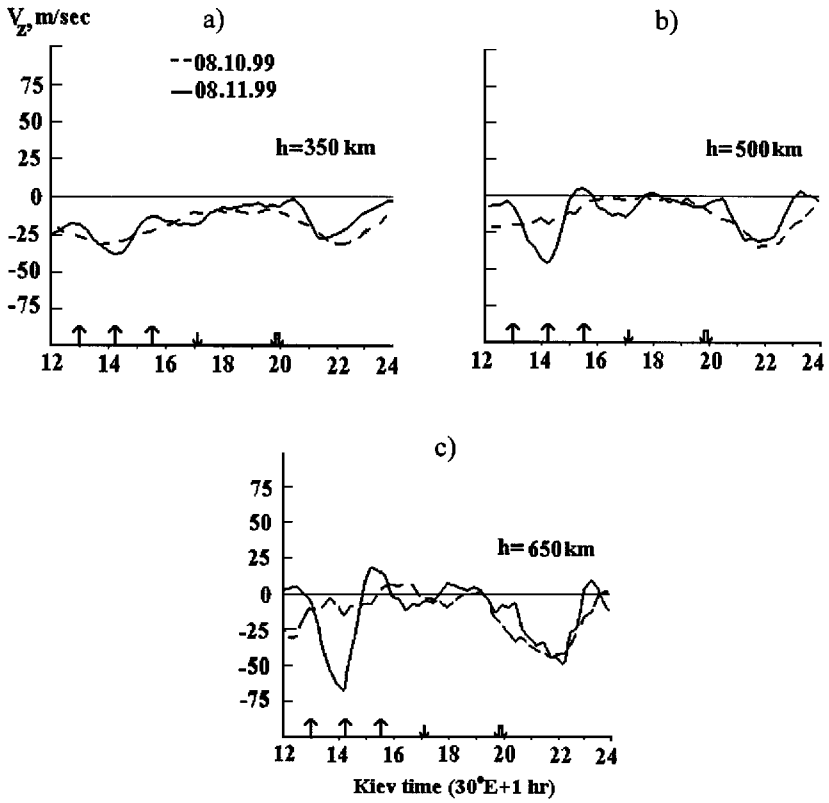

Figure 4. Time variations of vertical plasma velocity on control and eclipse days at altitudes of 350, 500, 650 km

The ionosphere effects of solar eclipse on August 11, 1999 were first observed by the Kharkov radar up to 1500 km. Investigations have shown the significant changes of ionosphere behavior [2].

At Kharkov the eclipse occurred during the period 1257—1529 according to Kyiv time with the maximum phase at 1413, when the disk of the sun was 83 % obscured on the earth's surface.

Eclipse caused the decrease of electron temperature by the value of ≈ 500—600 K at all altitudes with almost similar rapidity. The changes of T_e are centered at the time of eclipse maximum, following closely the variation of solar radiation flux. The ion temperature decreases together with the amplitude, which increases with altitude, but in contradistinction to the electron temperature there is a delay of the ion temperature change relative to the eclipse commencement. For low altitudes the fall of the ion temperature T_i is restricted from below by the value of neutral temperature T_N (Fig. 2).

During the eclipse, the decrease of incident flux of solar radiation leads to increase of losses rate. It causes the significant infringements of equilibrium between processes of production, losses and plasma transfer, which is described by the equation of continuity: $\frac{\partial N}{\partial t} = q - \beta N - \frac{\partial}{\partial z}(N_{V_z})$, where q is the rate of photoionization, β is the coefficient of linear losses, and V_z is the plasma vertical velocity. This infringement of equilibrium causes increase of downward plasma diffusion from upper F region to balance of the loss processes. As a result the electron density of the F layer peak did not change significantly (Fig. 3).

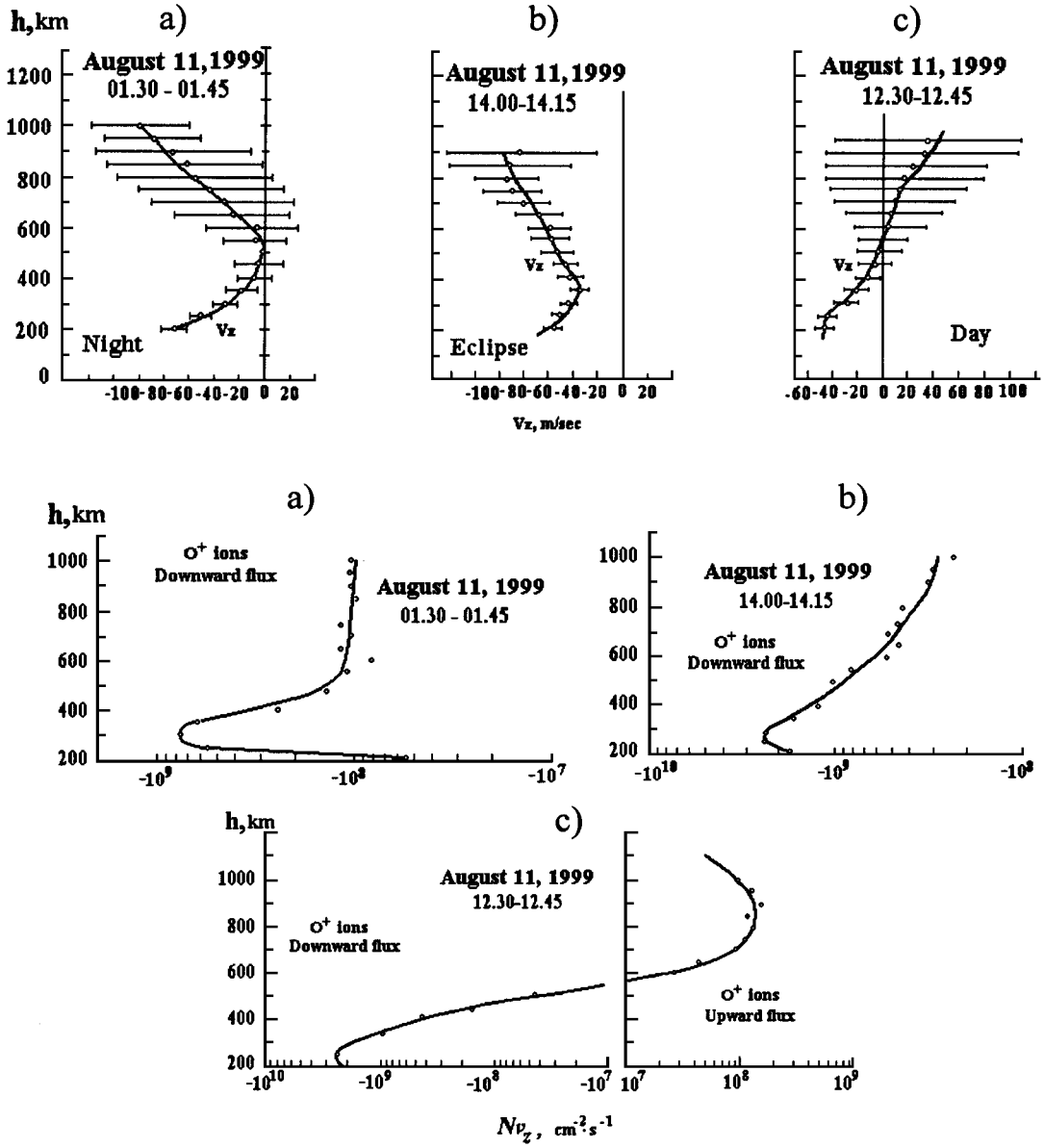

Figure 5. Altitude variations of vertical velocity of O^+ ions and the O^+ flux: a) at night, b) at the eclipse maximum time, c) in the daytime, before eclipse commencement

The downward plasma movement is confirmed by the significant increase of the downward vertical velocity of F region plasma, and at the altitude above sim 650 km V_z oscilating during the eclipse (Fig. 4). Figure 5 shows that during the eclipse maximum the altitude profiles of vertical velocity of O^+ ions and the O^+ flux have changed their shape and became similar to the nighttime profiles.

Figure 6 shows that increase of downward plasma diffusion from upper F region leads to increase of the specific percentage concentration of the hydrogen ion at maximum obscuration by value up to 40 % at low heights and decrease of the transition altitude, where $N(O^+) = N(H^+)$, to about 120 km.

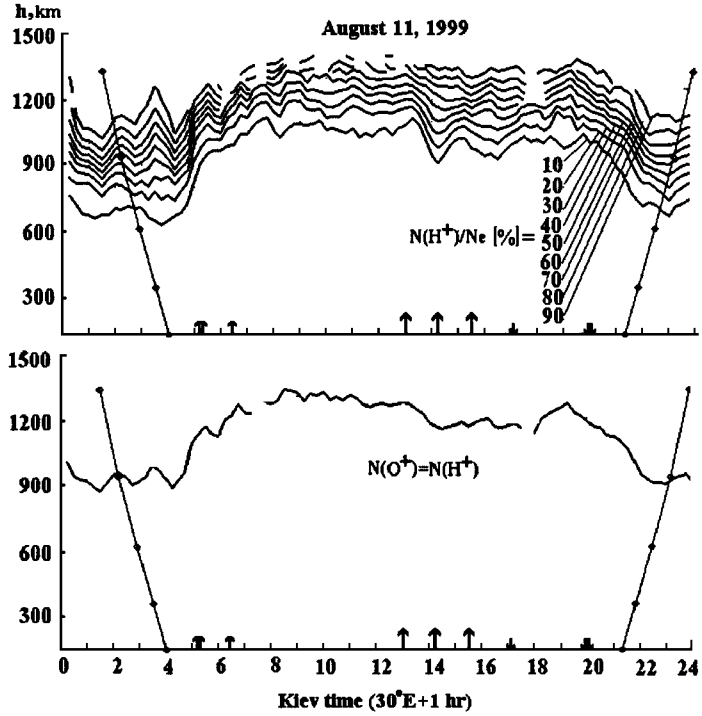

Figure 6. Altitude-diurnal variations of the percentage of H^+ ions and the topside transition height, where $N(O^+) = N(H^+)$, on the eclipse day

This change in the ionosphere behavior is the evidence of the significant infringement of plasma exchange processes between ionosphere and protonosphere during the solar eclipse.

REFERENCES

1. Erickson P. J., Taran V. I., Foster J. C., et al. Simultaneous Longitudinal and Latitudinal Topside Light Ion Variations from Kharkov, Millstone Hill, and Arecibo Radar Observations. AGU Fall 1999 report. San Francisco, USA. December 13, 1999.
2. Taran V. I., Lisenko V. N., Grigorenko Ye. I., et al. Kharkov radar observations of hydrogen ion variations during the solar eclipse of August, 1999. URSI 2000 meeting report. University of Colorado, USA. January 5-8, 2000.

Космічна наука і технологія. ДОДАТОК. 2001. Т 7. № 2. С. 42—46.

UDC 550.388

THE F REGION IONOSPHERE RESPONSE ON THE SEVERE MAGNETIC STORM ON SEPTEMBER 25, 1998

V. I. Taran, Ye. I. Grigorenko, G. A. Kiyashko

Institute of Ionosphere Ministry of Education and Science of Ukraine
and National Academy of Sciences of Ukraine, Kharkov

This paper presents the results of observation of ionospheric response to severe magnetic storm on September 25, 1998 (A_p = 121). Storm caused the significant changes in the ionosphere behavior: the increase of the height of the electron density peak h_mF2, the large fall of the peak electron density N_mF2, increase of plasma temperature and significant infringement of plasma exchange processes between low and upper ionosphere.

The study of ionospheric effects of magnetic storms is of great practical importance because the advanced technological systems, especially electric power lines and radio communications are increasingly sensitive to natural variations in the Earth's magnetic field.

In this paper some results of the F region observations with the Kharkov incoherent scatter radar during the magnetic disturbances are described. The interpretation of observed ionosphere effects from the point of view of the contemporary understanding of generalt common morphology picture and physical scheme of development of ionosphere disturbance was presented too.

Severe magnetic storm with the planetary index of magnetic activity A_p = 121 was observed on September 25, 1998. This storm was accompanied with the large changes in the Earth's ionosphere behavior. The Kharkov radar measurements have been conducted during the period of September 21-25, 1998. The geomagnetic conditions at this period are shown in Figure 1a in the form of the 3-hour magnetic activity index K_p as a function of Kyiv time (30° E + 1 hour). At the top of this Figure the day number, the daily solar activity $F_{10.7}$ index and the 81-day average $F_{10.7}$ index ($F_{10.7A}$) are shown. It was the period of moderate solar activity.

From this Figure it can be seen that the major storm commenced after local midnight on September 25 reached the peak K_p = 9 near local noon.

The magnetic storm is accompanied with the negative ionosphere disturbance. The height of the electron density peak h_mF2 increases at night by about 70 km and in the daytime by about 50 km in comparison with previous quiet days (Figure 1b). The increase of h_mF2 can be caused by the thermosphere disturbance effects, including the rebuilding of the global thermosphere circulation owing to the high-latitude heating, or by altering the neutral winds and electric fields [1].

The storm caused large fall of the peak of electron density N_mF2 in comparison with the average densities for the previous 56-hours period when the geomagnetic field was quiet (the solid line in Figure 1c). The effect of decrease of N_mF2 occurs at night, almost immediately after the storm commencement, increases gradually, before sunrise the depletion of N_mF2 is near a factor of 4 and before local noon it is near a factor of 4.5. During the morning period the major electron density peak is moving to the $F1$ region below 200 km (Figure 1b). It is G condition when $f_0F2 \leq f_0F1$.

At night the fall of N_mF2 is explained by the change of neutral atmosphere composition and the increase of plasma temperature that also produced the rise of peak height shown in Figure 1b. The calculation has shown that the observed large decrease of electron density is to some extent accounted for the fall of ratio of the atomic oxygen [O] to molecular [N_2], [O_2] densities and increase of loss rate β of major O^+ ions because of neutral atmosphere composition change. However, vibrationally excited

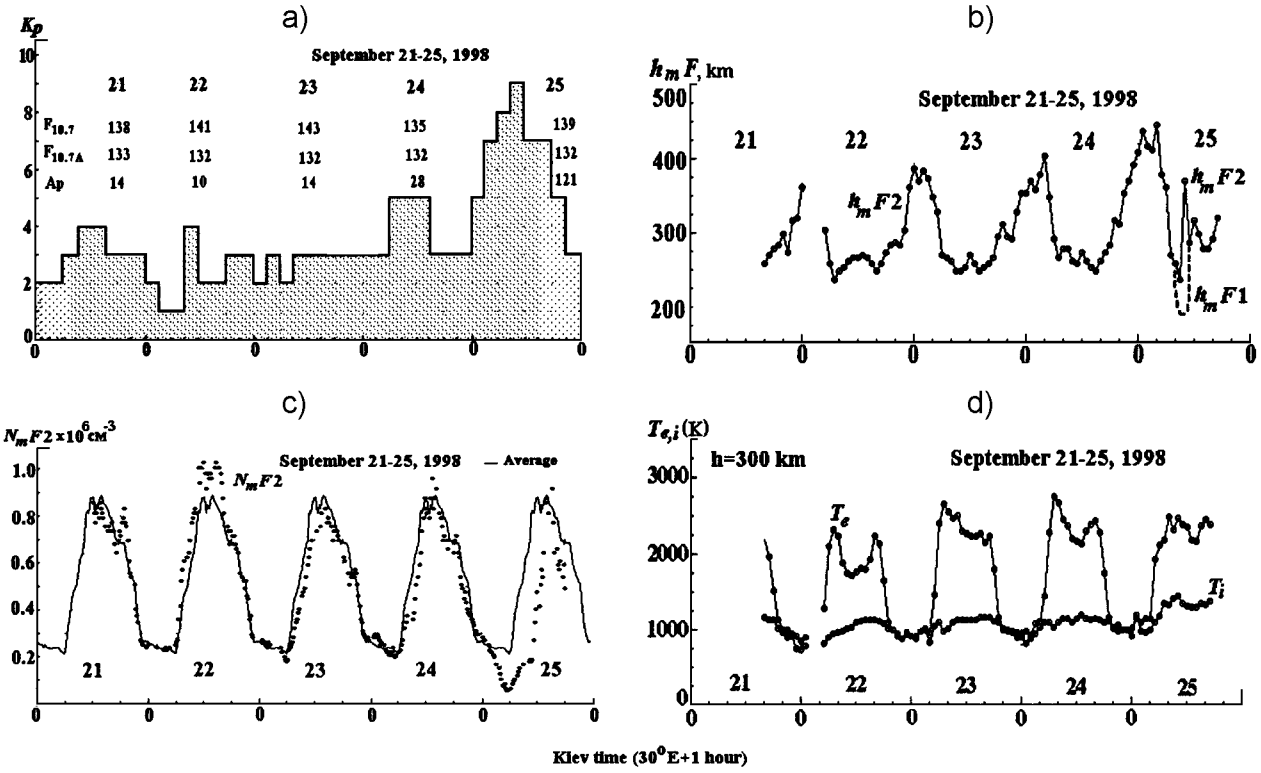

Figure 1. The variations of geomagnetic activity indexes and ionosphere parameters during the period of September 21-25, 1998: a) the 3-hour K_p index as a function of the Kiev time; b) height h_mF of the peak electron density; c) peak electron density N_mF2; the solid line means average values of N_mF2 for previous quiet period (56 hours); d) electron T_e and ion T_i temperatures at 300 km

nitrogen N_2^* could be also important in producing low electron concentrations during this storm [2].

It can be seen from Figure 1d that during the ionospheric disturbance at night, electron temperature T_e at 300 km altitude increases by about 150 K and ion temperature T_i by about 70 K at night and by about 200...300 K in the daytime. The increase of plasma temperature under disturbed conditions could be due to Joule heating associated with penetration of magnetospheric convection electric fields to middle latitudes, particle precipitation and other reasons [1, 2].

Figure 2 illustrates the changes of the vertical velocity of plasma during the severe geomagnetic storm on September 24-25 in comparison with the magnetic quiet days on September 22-23. These data was measured at the height range of 200—500 km.

It can be seen from Figure 2 that in the morning of the quiet day the vertical velocity of plasma was directed practically downward at the all height region from 200 km up to 400 km. During the same morning period (near and after sunrise) of the disturbed day the vertical velocity changed its direction and became the upward one.

Figure 3 illustrates the height profiles of vertical plasma velocity V_z and the plasma flux of O^+ ions, calculated from measured values of N_e and V_z, under undesturbed and disturbed conditions. For the quiet day altitude profile of V_z corresponds to the theoretical representations about the altitude variations of the velocity of F-region plasma parallel to the magnetic field lines [3]. For this period the downward flux observed below 500 km represents that needed for loss (occurring chiefly below 300 km) to balance production.

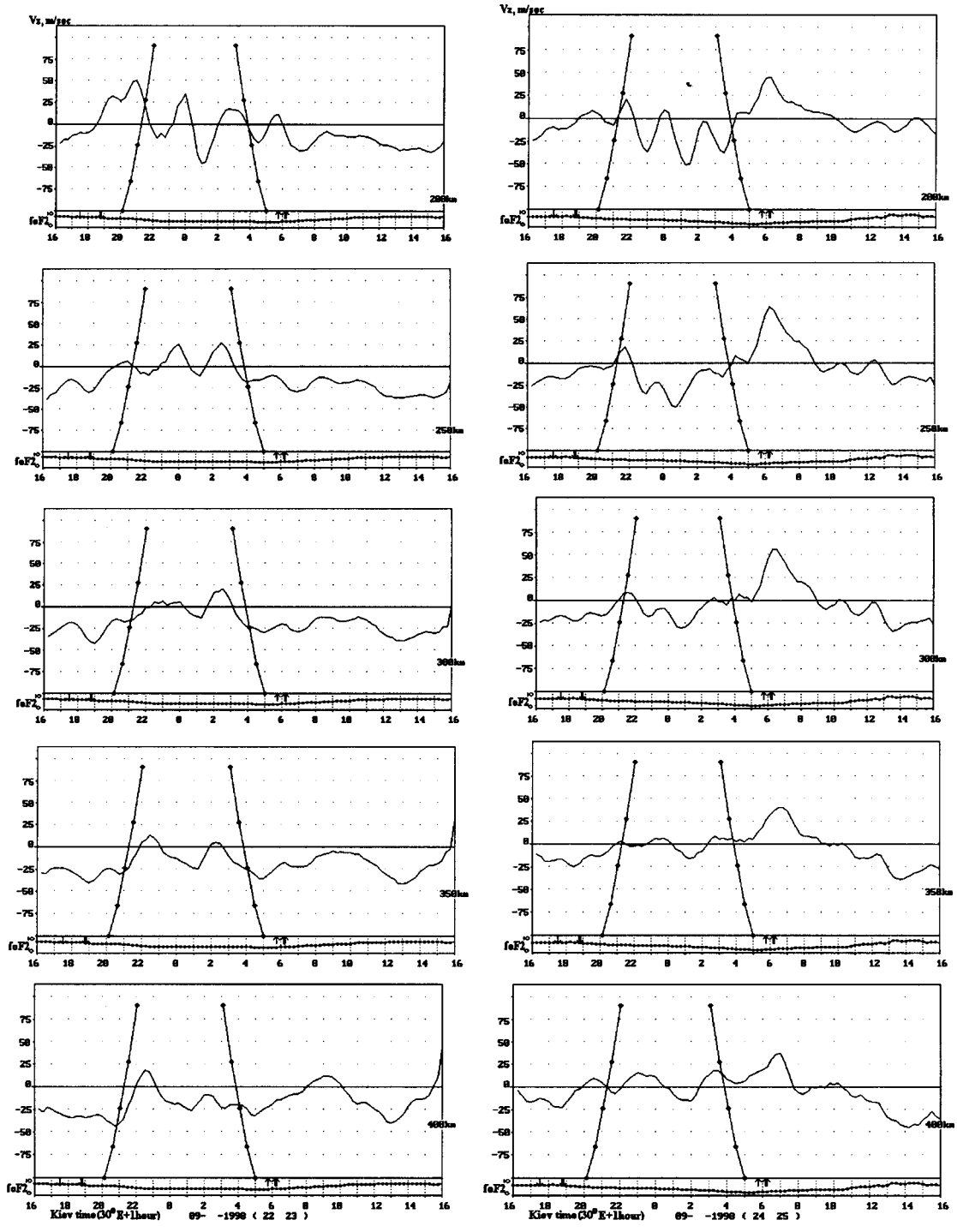

Figure 2. Variations of the vertical velocity of plasma during severe geomagnetic storm (September 24-25, 1998) compared to the magnetic quiet days (September 22-23, 1998)

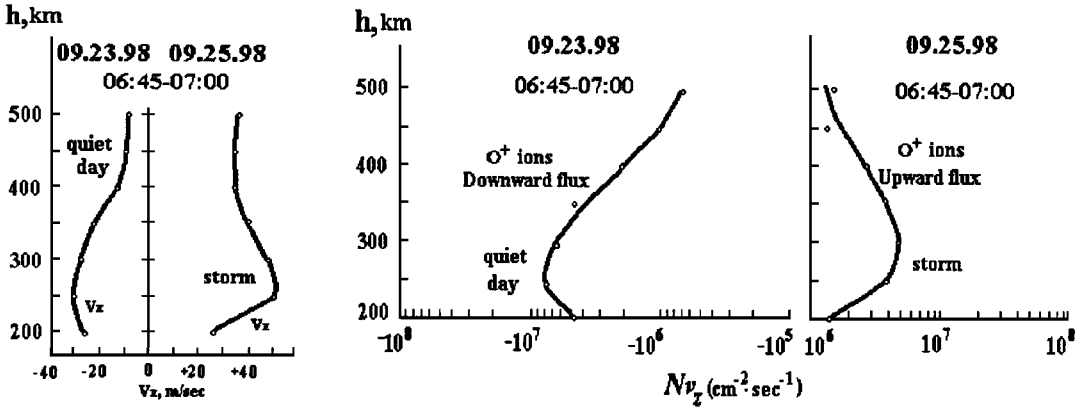

Figure 3. Altitude variations of the vertical plasma velocity and the O^+ flux in the morning on the quiet day (September 23) and during severe magnetic storm (September 25)

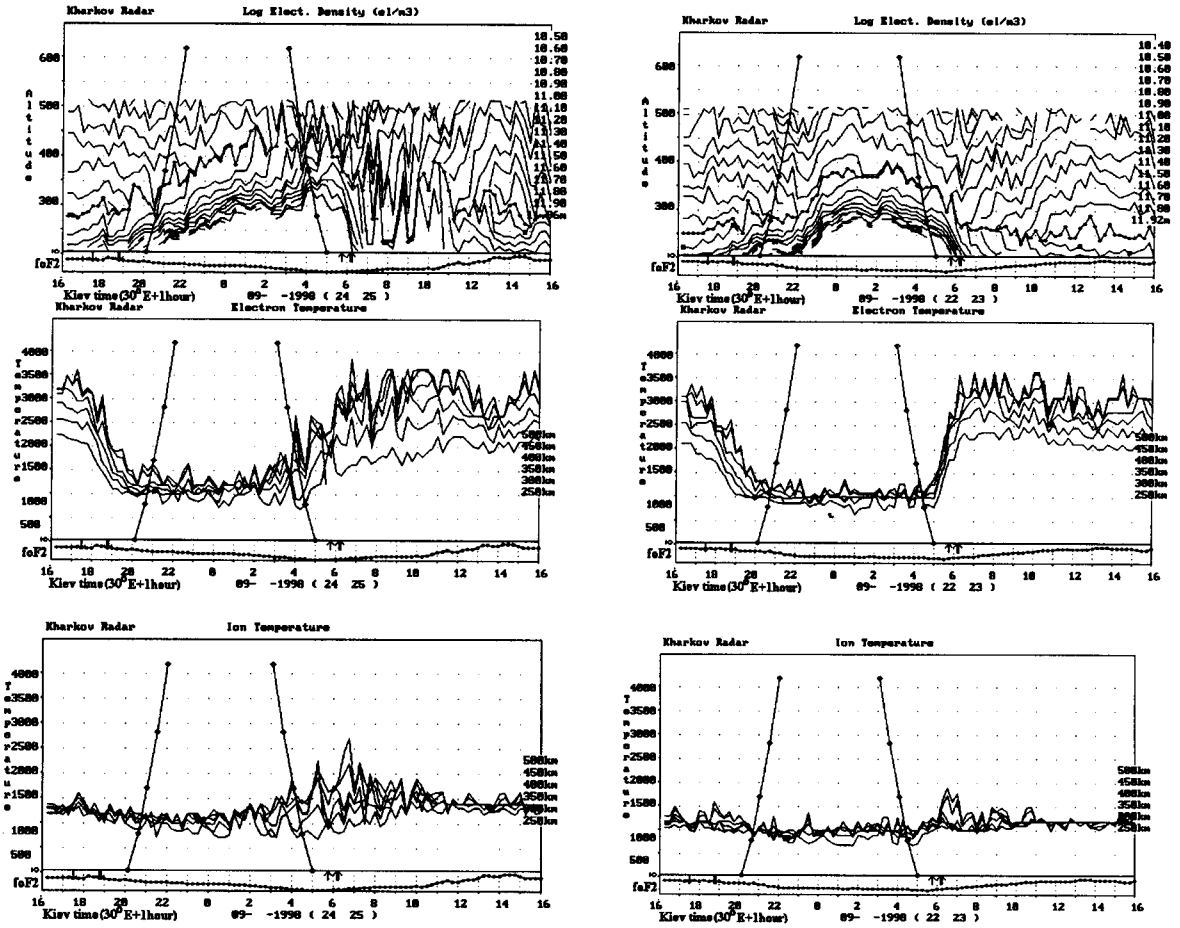

Figure 4. Height-diurnal variations of the electron density N_e (in form of constant plasma frequency lines, MHz), electron T_e and ion T_i temperatures during severe geomagnetic storm (September 24-25, 1998) compared to the magnetic quiet days (September 22-23,1998)

It can be seen that during the disturbed period the vertical plasma velocity V_z and the plasma flux (of O^+ ions) became upward ones at the altitudes from 200 up to 500 km. Such behavior of V_z velocity and the plasma flux is the evidence of the significant change of plasma exchange processes between low and upper ionosphere during this magnetic storm.

Figure 4 shows height-diurnal variations of the electron density N_e (in the form of constant plasma frequency lines, MHz), electron T_e and ion T_i temperatures during severe geomagnetic storm (September 24-25, 1998) compared with the magnetic quiet days (September 22-23,1998).

Obtained results can be used for modeling and prediction of mid-latitude ionosphere parameters under the geomagnetic disturbance conditions.

REFERENCES

1. Richards P. G., Torr D. G., Buonsanto M. J., Sipler D. P. Ionospheric effects of the March 1990 magnetic storm: Comparison of theory and measurement // J. Geophys. Res.—1994.—**99**, N A12.—P. 23359—23365.
2. Buonsanto M. J. Millstone Hill incoherent scatter F region observations during the disturbances of June 1991 // J. Geophys. Res.—1995.—**100**, N A4.—P. 5743—5755.
3. Geisler J. E., Bowhill S. A. Aeronomy Rep., 5, University of Illinois, Urbana, 1965.

Космічна наука і технологія. ДОДАТОК. 2001. Т 7. № 2. С. 47—51.

RADIATION FROM COLLAPSING STARS

V. Kryvdyk

Depart. of Astronomy, Kyiv University, Glushkova 6 Kyiv, 03022, Ukraine

The non-thermal emission in the magnetospheres of collapsing stars with the initial dipole magnetic fields and a certain initial energy distribution of charged particles in the magnetospheres (power-series, relativistic Maxwell, and Boltzmann distributions) are considered. When the star magnetosphere compresses under the collapse, its magnetic field increases considerably. The three factors (particle pressure, collisions between them and stellar rotation) can influence the field structure and the particles dynamics in the magnetosphere. The analysis shows, that these factors may be neglected for the magnetosphere of collapsing star. As it follows from this result, the plasma in magnetosphere is frozen in magnetic field and is collision-free. Therefore, the method of adiabatic invariant may be used to investigate the particle dynamics in magnetosphere. The vortex electric field in magnetosphere accelerates the charged particles, which generate the radiation moving in the magnetic field. The collapsing stars can be powerful sources of a non-thermal radiation produced by the interaction of charged particles with the magnetic field, as it follows from the analysis of particles dynamics and its emission in the stellar magnetosphere under collapse. The radiation flux grows with decreasing of stellar radius and frequency and it can be observed in the form of radiation burst with duration, equal to the stellar collapse time. A value of the radiation flux depends on the distance to the star, its magnetic field, and the particle spectrum in the magnetosphere. In this paper the radiation fluxes are calculated for various collapsing stars. The conclusion is made, that these fluxes can be observed by means of modern astronomical instruments.

INTRODUCTION

Collapse begins when the mass of stellar core exceeds the Chandrasekhar bound, and the star becomes dynamically unstable. The star compresses and its radius decreases. After that, the stars can evolve by several ways. The first possibility is that the stars explodes and lose their masses. The massive stars ($M \leq (3...6)M_{\odot}$) will collapse to neutron stars or black holes. The stars can los their mass and we will observe this phenomenon as supernovae. The stars with the smaller mass will collapse to white dwarfs [16, 17]. The second possibility will realise when stars collapse without the loss of mass. In this case it is very difficult to observe the collapse, and hitherto we not have precise astronomical data conforming the evidences of this stage.

The star emits electromagnetic radiation under the collapse. In this paper the non-thermal radiation from the collapsing stars with the initial dipole magnetic field on the non-relativistic stage is investigated, and the method for the search of collapsing stars is proposed.

PARTICLE DYNAMICS IN MAGNETOSPHERES OF COLLAPSING STARS

The external electromagnetic field of a collapsing star is given [2, 6—12]

$$B_r = 2r^{-3}\mu(t)\cos\theta, \tag{1}$$

Here $F_0 = B_0 R_0^2$ is the initial magnetic flux of star with the radius R having the initial radius R_0 and the initial magnetic field B_0.

Equation (1) has obtained by solving of Maxwell equations in Newton approximation which is valid during the collapse except the region near the gravitational radius. The formulae (1) apply if there are negligible external sources of electromagnetic fields. When the star magnetosphere compresses under the collapse, its magnetic field increases considerably. Thus the cyclic electric field will be generated which

accelerates the charged particles to relativistic energy. These particles moving in the magnetic field generate a radiation. The field structure and particles dynamics in the magnetosphere can be changed due to influence of such factors as the particles pressure, collisions, and star rotation. These factors can be neglected during the collapse as it follows from the analysis [10, 11].

The initial concentrations of charged particles in the magnetosphere have been chosen as the power-series, relativistic Maxwell, and Boltzmann distributions, which can be described as [15]

$$N_{\mathrm{P}}(E) = K_{\mathrm{p}}E^{-\gamma}; \tag{2}$$

$$N_{\mathrm{M}}(E) = K_{\mathrm{M}}E^{2}\exp(-E/kT); \tag{3}$$

$$N_{\mathrm{B}}(E) = K_{\mathrm{B}}\exp(-E/kT); \tag{4}$$

Here K_{P}, K_{M}, K_{B} are the spectral coefficients; k is the Boltzmann constant; is the particles energy and T is the temperature in the magnetosphere; y is the power spectrum.

The power-series distribution is typical for the high-energy particles in cosmic plasmas (in the magnetospheres of neutron stars, the shells of supernova stars and the high-energy cosmic rays). The relativistic Maxwell distribution is typical for some sources of non-thermal radio emission [15].

To investigate particle dynamics in the magnetosphere of collapsing star, the method of adiabatic invariants may be used, so that magnetosphere plasmas is frozen in magnetic field and is collision-free. We considered two mechanisms of the particles interaction with the magnetic field, namely: 1) a betatron acceleration and 2) bremsstrahlung energy losses in magnetic field. The particles energy will change as result of these mechanisms with the rate [10, 11]

$$\frac{dE}{dR} = \left(\frac{dE}{dR}\right)_{\mathrm{a}} + \left(\frac{dE}{dR}\right)_{\mathrm{s}} = a_1\left(\frac{2GM}{R_*}\right)^{1/2}\left(\frac{R_* - 1}{R^3}\right)^{1/2}E - a_2F_0^2R^2E^2r^{-6}. \tag{5}$$

$$a_1 = (5k_1/3)(3\cos^4\theta + 1.2\cos^2\theta - 1)(1 + 3\cos^2\theta)^{-2},$$

$$a_2 = \frac{e^4}{6m^4c^7}(1 + 3\cos^2\theta)\sin^2\theta,$$

$k_1 = 2$ and $k_1 = 1$ for relativistic and non-relativistic particles respectively; $R_* = R_0/R$; G is gravitational constant, M is the mass of collapsing star.

The particle dynamics in the magnetosphere can be considered by means of the equation for particle transition in the regular magnetic field, which can be written as [10, 11]

$$\frac{\partial N}{\partial R} = f_1(E, R)\frac{\partial N}{\partial E} + f_2(E, R)N = 0, \tag{6}$$

Here

$$f_1(E, R) = ER^{-1}\left\{a_1 - a_2F_0^2[R^7R_*/2GM(R_* - 1)]^{1/2}Er^{-6}\right\},$$

$$f_2(E, R) = R^{-1}\left\{a_1 - 2R^3[R/(R_0 - R)]^{1/2}E\right\},$$

Equation (6) has been solved for two special cases. In the first case it is assumed that the energy losses do not influence the particles spectrum in the magnetosphere. Then we can neglected the second term in the right hand part of Equation (5), and thus the solution of Equation (6) for the initials distribution (2)—(4) are as follows

$$N'_{\mathrm{P}}(E, R) = K_{\mathrm{p}}E^{-\gamma}R_*^{-\beta_{\mathrm{P}}}, \tag{7}$$

$$N'_{\mathrm{M}}(E, R) = K_{\mathrm{M}}E^{2}R_*^{-\beta_{\mathrm{M}}}\exp(-E/kT), \tag{8}$$

$$N'_{\mathrm{B}}(E, R) = K_{\mathrm{B}}R_*^{-\beta_{\mathrm{B}}}\exp(-E/kT). \tag{9}$$

Here $\beta_{\mathrm{P}} = a_1(\gamma - 1)$, $\beta_{\mathrm{M}} = a_1(E/kT\ln E - 3)$, $\beta_{\mathrm{B}} = a_1(E/kT\ln E - 1)$;

Equations (7)—(9) determine the particle spectrum in the magnetosphere and itsevolution during collapse for the first case when the energy losses can be neglected. This case is typical for the initial stage of the collapse and we consider it in this paper. The second case will be realise in the final stage of the collapse, when the magnetic field increases to the extreme value and the energy losses will influence the particle spectrum considerably. We will consider this case later, on not in this paper.

ELECTROMAGNETIC RADIATION FROM COLLAPSING STARS

The ratio between the radiation flux from collapsing stars and their initial radiation flux for the power-series, relativistic Maxwell, and Boltzmann distributions (7)—(9) respectively are

$$I_{\nu P}/I_{\nu P0} = (\nu/\nu_0)^{(1-\gamma)/2} R_*^{\gamma-2} \int R_*^{\{} - a_1(\gamma-2)\sin\theta d\theta, \tag{10}$$

$$I_{\nu M}/I_{\nu M0} = (\nu/\nu_0) R_*^{-3} (1/kT) \int R_*^{-\beta_M} \exp(-E/kT)\sin\theta d\theta dE, \tag{11}$$

$$I_{\nu B}/I_{\nu B0} = (\nu/\nu_0) R_*^{-3} (kT) \int_0^{\pi/2} R_*^{-\beta_B} E^{-2} \exp(-E/kT)\sin\theta d\theta dE. \tag{12}$$

Using Equations (10)—(12), the ratio between the radiation flux from collapsing stars and their initial flux can be calculated. This ratio for the different radius R, the temperature 1 eV $\leq kT \leq$ 10 eV by $\nu/\nu_0 = 1$ is given in Tables 1—2. The value obtained by the numerical integration of the Equations (10)—(12) within the range 2 eV $\leq kT \leq 10^9$ eV, $0 \leq \theta \leq \pi/2$.

CONCLUSIONS

The general conclusions from the obtained results are the following. The magnetic field will increase during the collapse. The charged particles will accelerate to relativistic energy in the magnetospheres of collapsing stars. These particles will emit the electromagnetic waves in the wide frequency range, from radio waves to gamma rays. We can see from these results, that the radiation flux increases during the collapse very rapidly (by millions and more comparing with the initial flux). The radiation flux increases most rapidly for the collapsing stars with the cool magnetospheres. For these stars the flux increases by millions yet at the initial stage of collapse, when the stellar radius decreases ten times (Table 2). For the magnetospheres with middle the flux increases at more late stage of collapse, when the stellar radius decreases by tens times. By collapse of the stars with the high-temperature magnetospheres the radiation flux grows at a late stage collapse, when the stellar radius decreases by hundreds times. The radiation flux from stars with Boltzmann distribution increases more rapidly than for stars with the relativistic Maxwell distribution. This radiation can be observed as the impulses in the whole frequency range, from radio impulses to gamma ray bursts. The impulse duration is equal to the duration of stellar collapses defining the mass and radius of stars. The intensity of this impulse is very strong. The radiation flux from collapsing stars exceeds the initial flux by millions at the final stage of collapse. We can see from Tables 1, 2 that the radiation fluxes for stars with the initial fluxes in range 10^{-22} erg/cm^{2}s $\leq I\nu_0 \leq$ $\leq 10^{-30}$ erg/cm^{2}s [2, 6—12] can increase to the value 10^{-16} erg/cm^{2}s $\leq I\nu_0 \leq 10^{-24}$ erg/cm^{2}s and more.

Thus, the collapsing stars can be the powerful sources of the non-thermal radiation impulses. Where can these impulses be observed? First of all, in the middle of powerful gamma bursts and X bursts which are not periodical and can be connected with the precollapse stars. These impulses can be observed also from the presupernovae. The star goes to this stage when the pressure in the stellar core falls and the star becames dynamically unstable on account of the depletion of nucleas Si, the photodissociation of nucleas Fe and the neutronisation of stellar core. After that, the star begins to compress under the

Table 1. The value $I_{\nu P}/I_{\nu P0}$ for various R_*, γ and $\nu/\nu_0 = 1$

R_*	γ								
	2.4	2.6	2.8	3.0	3.2	3.4	3.6	3.8	4.0
10	4.75	12	32.6	93.7	281	864	2.71 E3*)	8.60 E3	2.76 E4
20	8.2	29.5	117	494	2.17 E3	9.74 E3	4.44 E4	2.05 E5	9.56 E5
40	14.6	76.1	443	2.74 E3	1.75 E4	1.15 E5	7.60 E5	5.09 E6	3.43 E7
60	20.7	135	981	7.57 E3	6.03 E4	4.91 E5	4.04 E6	3.36 E7	2.82 E8
80	26.7	203	1.74 E3	1.57 E4	1.46 E5	1.38 E5	1.33 E7	1.29 E8	1.26 E9
100	32.6	281	2.71 E3	2.76 E4	2.89 E5	3.09 E6	3.35 E7	3.67 E8	4.04 E9
200	61.2	774	1.09 E4	1.61 E5	2.46 E6	3.81 E7	5.98 E8	9.47 E9	1.51 E11
400	117	2.17 E3	4.44 E4	9.56 E5	2.11 E7	4.74 E8	1.08 E10	2.47 E11	5.71 E12
600	172	3.98 E3	1.02 E5	2.72 E6	7.45 E7	2.08 E8	5.87 E10	1.67 E12	4.80 E13
800	226	6.14 E3	1.83 E5	5.71 E6	1.83 E8	5.94 E8	1.96 E11	6.50 E12	2.17 E14
1000	281	8.60 E3	2.89 E5	1.02 E7	3.67 E8	1.34 E10	4.98 E11	1.86 E13	7.03 E14

*) 2.71 E3 $\equiv 2.71 \cdot 10^3$

Table 2. The value $I_{\nu M}/I_{\nu M0}$ and $I_{\nu B}/I_{\nu B0}$ for **1 eV** $\leq kT \leq$ **10 eV** and various R_*

R_*	$I_{\nu B}/I_{\nu B0}$	$I_{\nu M}/I_{\nu M0}$	R_*	$I_{\nu B}/I_{\nu B0}$	$I_{\nu M}/I_{\nu M0}$	R_*	$I_{\nu B}/I_{\nu B0}$	$I_{\nu M}/I_{\nu M0}$
	$kT = 1$ eB			$kT = 5$ eB			$kT = 8$ eB	
34	16.4	1.11	135	58.4	1	180	1.99	1
36	86.2	6.04	140	310	1.12	190	21.7	1
38	491	35.2	145	1.72 E3	6.28	200	260	1
40	3.01 E3	221	150	9.93 E3	36.6	210	3.42 E3	5.06
42	1.98 E4	1.48 E3	155	5.99 E4	222	220	4.91 E4	73.3
44	1.40 E5	1.06 E4	160	3.77 E5	1.40 E3	230	7.68 E5	1.15 E3
46	1.05 E6	8.09 E4	165	2.46 E6	9.23 E3	240	1.30 E7	1.97 E4
48	8.35 E6	6.54 E5	170	1.67 E7	6.30 E4	250	2.40 E8	3.65 E5
50	7.06 E7	5.61 E6	175	1.18 E8	4.47 E5	260	4.77 E9	7.30 E6
52	6.32 E8	5.08 E7	180	8.65 E8	3.29 E6	270	1.02 E11	1.57 E8
	$kT = 2$ eB			$kT = 6$ eB			$kT = 9$ eB	
60	4.44	1	150	11.6	1	200	3.7	1
65	70.8	1.43	160	220	12.3	210	34.9	1
70	1.34 E3	27.7	170	4.77 E3	309	220	357	1
75	2.97 E4	626	180	1.18 E5	8.73 E3	230	3.95 E3	4.66
80	7.64 E5	1.64 E4	190	3.31 E6	2.78 E5	240	4.70 E4	55.9
85	2.26 E7	4.92 E5	200	1.05 E8	9.95 E6	250	6.03 E5	721
90	7.67 E8	1.69 E7	210	3.72 E9	3.98 E8	260	8.30 E6	9.98 E3
95	2.96 E10	6.58 E8	220	1.48 E11	1.77 E10	270	1.22 E8	1.48 E5
100	1.29 E12	2.89 E10	230	6.52 E12	8.72 E11	280	1.92 E9	2.34 E6
105	6.31 E13	1.43 E12	240	3.20 E14	4.76 E13	290	3.23 E10	3.95 E7
	$kT = 4$ eB			$kT = 7$ eB			$kT = 10$ eB	
105	2.8	1	160	1.14	1	220	7.12	1
110	17.1	1	170	14.8	1	230	59.7	1
115	111	1	180	216	1	240	536	1
120	770	4.3	190	3.53 E3	6.78	250	5.15 E3	4.96
125	5.66 E3	31.9	200	6.42 E4	124	260	5.27 E4	51.1
130	4.41 E4	250	210	1.29 E6	2.52 E3	270	5.76 E5	561
135	3.63 E5	2.07 E3	220	2.87 E7	5.63 E4	280	6.67 E6	6.54 E3
140	3.15 E6	1.81 E4	230	7.00 E8	1.38 E6	290	8.22 E7	8.09 E4
145	2.88 E7	1.67 E5	240	1.87 E10	3.73 E7	300	1.07 E9	1.06 E6
150	2.78 E8	1.62 E6	250	5.48 E11	1.10 E9	310	1.48 E10	1.47 E7

influence of the gravitational field. The star can throw out the part of mass and we will observed this phenomenon as supernovae. The stage of collapse during which the stars can be the powerful source of the non-thermal radiation must preceded this stage. The impulse of non-thermal radiation can also be observed before the explosion of novae. The powerful sources of the non-thermal radiation can also be the white dwarfs in double systems at the stage of the accretion-induced collapse. The periodical impulse of non-thermal radiation can be generated also by the pulsation of the stars with magnetic field, since in this case the charged particles will accelerate and the non-thermal emission will be generated. We draw the conclusion that the collapsing stars can be observed by means of the impulse of non-thermal radiation. What problems can arise by a realisation of the observational astrophysics program for search of collapsing stars? The first problem is that we can not point at the location of precollapses stars accurately enough, since the theory of stellar evolution does not make it possible to do that. We indicated only the types of stars that can collapse. But the theory does not enable as to make the detailed chronology of collapse, therefore we can not indicate where and when exactly the collapsing star can arise. This fact is a principal problem for the observational astrophysics program for the search of collapsing stars. The second problem is that the stellar collapse passes very rapidly and this stage is very short. This problem can be solved by means of the modern instruments, for example, gamma- and X-telescopes. But new problems arise, how the impulse from collapsing stars can be chooses between the great numbers of bursts of the unknown origin.

REFERENCES

1. Beresinsky V. S., Bulanov S. V., Ginzburg V. L., et al. Asrophysics of cosmic rays. — M.: Nauka, 1984.—380 p.
2. Ginzburg V. L., Ozernoy L. M. About gravitational collapse of magnetic stars // JETP.—1964.—**47**.—P. 1030—1040.
3. Ginzburg V. L., Syrovatskii S. I. Origin of cosmic rays. — M.: Izd. AN USSR, 1963.—384 p.
4. Gudel M., Benz A. O. Radio spectra of dMe and dKe stars // Astron. Soc. Pacif. Conf. Ser.—1996.—**93**.—P. 303—305.
5. Gudel M., Benz A. O., Guiman E. F., Sthmitt J. H. M. M. Nonthermal microwave emission from F dwarfs: 71Tau, a For, and open clustermoving group membership // Astron. Soc. Pacif. Conf. Ser.—1996.—P. 306—308.
6. Gunningam C. T., Price R. H., Moncrief V. Radiation from collapsing relativistic stars.I. Linearized odd-parity radiation // Astrophys. J.—1978.—**224**.—P. 643—667.
7. Gunningam C. T., Price R. H., Moncrief V. Radiation from collapsing relativistic stars. II. Linearized even-parity radiation // Astrophys. J.—1979.—**230**.—P. 870—892.
8. Gunningam C. T., Price R. H., Moncrief V. Radiation from collapsing relativistic stars. III. Second order perturbation of collapse with rotation // Astrophys. J.—1980.—**236**.—P. 674—692.
9. Linsky J. L. Steady radio emission from stars // Astron. Soc. Pacif. Conf. Ser.—1996.—**93**.—P. 436—446.
10. Kryvdyk V. Collapsing stars as sources of electromagnetic radiation // Kinem. and phys. sky bodies.—1998.—**14**, N 6.—P. 475—489.
11. Kryvdyk V. Electromagnetic radiation from collapsing stars. I. Power-series distribution of particles in magnetospheres // Mon. Notic. Roy. Astron. Soc.—1999.—**309**.—P. 593—598.
12. Moncrief V. Radiation from collapsing relativistic stars. IY. Black hole recoild // Astrophys. J.—1980.—**238**.—P. 333—337.
13. Utana G., Trigilio C., Catalano S. Radio emission from Algol-type binaries. I. Results of 1992-1993. VLA Survey // Astron. and Astrophys.—1998.—**329**.—P. 1010—1018.
14. Van den Oort G. M. J. Non-thermal emission mechanism in stellarcoronae // Astron. Soc. Pacif. Conf. Ser.—1996.—**93**.—P. 263—272.
15. Paholchik A. Radioastrophysica. — M.: Mir, 1973.—252 p.
16. Shapiro S. L., Teukolsky S. A. Black Holes, White Dwarfs, and Neutron Stars. — M.: Mir, 1985.—665 p.
17. Zeldovich J. B., Novikov I. D. Theory of gravity and stellar evolution. — M.: Nauka, 1977.—494 p.

Космічна наука і технологія. ДОДАТОК. 2001. Т 7. № 2. С. 52—55.

UDC 550.388.2

IONOSPHERIC IRREGULARITIES INDUCED BY THE TURBULENCE OF THE NEUTRAL ATMOSPHERE: POSSIBLE DEVIATION FROM ISOTROPY

Yu. V. Kyzyurov

Main Astronomical Observatory NASU, Kyiv-127, 03680, Ukraine

The results of study of possible deviation of plasma irregularities caused by the action of neutral air turbulence in the lower ionosphere from isotropy are presented in this report. The consideration was based on an analytic expression for the three-dimensional (3D) spectrum of such irregularities. By integrating the 3D spectrum, 1D spectra were derived for two different directions of its possible measurements. It was shown that the spectra of the irregularities are quite close to an isotropic one, although there are some their deviations from isotropy on the edges of the considered wave-number range. These deviations result from changes in a relative role of the geomagnetic field (more important for larger wave numbers) and the gradient of mean plasma density (more important for smaller ones) in creating the plasma irregularities of different scales. Estimations of slope of the irregularity spectra and of the root-mean-square level of plasma fluctuations were made too. There is good agreement between the obtained results and the data gathered during a rocket-radar simultaneous experiment in the lower ionosphere at high latitudes.

INTRODUCTION

Radar and rocket observations at various latitudes show that plasma irregularities are created as a consequence of the action of neutral air turbulence in the lower ionosphere [4—6]. It is generally assumed that such irregularities are isotropic or at least quasi-isotropic, in contrast to field-aligned ionospheric irregularities generated by current-driven plasma instabilities in the ionosphere. The isotropy of the ionospheric irregularities results in the weak aspect sensitivity of radar returns (whilst the field-aligned irregularities provide the strong aspect sensitivity). It is evident that an isotropy of irregularities results in the isotropy of their spectrum. It means in turn that experimental spectra of the irregularities that are measured during rocket flights and by ground-based radar instruments must be the same. In the case of quasi-isotropic irregularities certain difference between these experimental spectra must exist. The purpose of this report is to investigate possible deviation of the plasma irregularities caused by neutral turbulence from isotropy by comparing irregularity spectra, which can be measured in vertical and horizontal directions. An understanding of features of the deviation is needed not only for the general understanding of the nature of irregularities in the lower ionosphere but also for the better understanding of observational results obtained during combined rocket and radar experimental campaigns.

ONE-DIMENSIONAL SPECTRA OF PLASMA IRREGULARITIES

To study the deviation from isotropy for ionospheric irregularities caused by mixing of plasma resulting from the action of turbulence in the neutral atmosphere, we use an analytic expression for the three-dimensional (3D) spectrum of the irregularities which was recently obtained in the following form [2]:

$$P(k) = \Omega(k) \cdot [L_N^{-2} k^{-2} (\mathbf{n} \times \mathbf{k})^2 + \beta_i^2 (\mathbf{b} \times \mathbf{k})^2] \cdot C_1 \varepsilon^{2/3} k^{-11/3}, \qquad L_N^{-1} < k < k_d, \tag{1}$$

$$\Omega^{-1}(k) = 4\pi(\varepsilon^{1/3}k^{2/3} + 2\alpha_r N_0 + D_A k^2)[2\varepsilon^{1/3}k^{2/3} + 2\alpha_r N_0 + (D_A + \mu_n)k^2],$$

where $n = L_N N_0^{-1}\nabla N_0$ is the unit vector along the gradient of mean plasma density N_0 with a length scale L_N, $\mathbf{b} = \mathbf{B}/B$ is the unit vector along the geomagnetic field $\mathbf{B}$, $\beta_i = \omega_{Bi}/\nu_i$ is the ratio of the ion gyrofrequency, $\omega_{Bi} = eB/m_i c$, to ion-neutral collision frequency, ν_i, C_1 is a dimensionless constant of order unity, ε is the rate of dissipation of turbulent energy, α_r is the recombination coefficient, D_A is the ambipolar diffusion coefficient, μ_n is the kinematic viscosity of neutral gas (in our case $\mu_n \approx D_A$), and $k_d \approx (\varepsilon/\mu_n^3)^{1/4}$ is the Kolmogorov dissipation wave number. The expression (1) is valid when: the neutral turbulence is usual fluid turbulence of the Kolmogorov type, the plasma component has no influence on turbulent movements of neutrals, and a vertical gradient of background plasma density is insufficient for the excitation of plasma instability.

With the use of (1) estimates of the root-mean-square (rms) level of relative plasma-density fluctuations, $\langle \delta N^2/N_0^2\rangle^{1/2}$, have been made in the case of the mid-latitude ionosphere

$$\frac{\langle \delta N^2}{N_0^2\rangle} = \int d\mathbf{k}P(\mathbf{k}) = \int_{k_1}^{k_2} dkP_1(k) \tag{2}$$

with

$$P_1(k) = \frac{8\pi}{3}\Omega(k)(L_N^{-2} + \beta_i^2 k^2)C_1\varepsilon^{2/3}k^{-5/3}. \tag{3}$$

A good agreement with experimental data was found [3]. Shapes of 1D spectra predicted by 1D power spectral density (PSD), (3) was also consistent with experimental spectra. It means that the plasma irregularities induced by neutral turbulence are really very close to quasi-isotropic ones, though the 3D spectrum is not quite isotropic because of its dependence on **n** and **b**.

Using the 3D spectrum, (1) 1D spectrum that can be measured along z-direction in experiments is easily obtained:

$$S_1(k_z) = \int_0^{\sqrt{k_d^2 - k_z^2}} k_\perp dk_\perp \int_0^{2\pi} P(\mathbf{k}d\varphi.$$

In the case of *in situ* rocket experiments we will regard that the 1D spectrum, $S_1'(k_z)$, is measured along the mean plasma density gradient (vertical direction), $\mathbf{z} \parallel \mathbf{n}$, and then

$$S_1'(k_z) = C_1\pi\varepsilon^{2/3}\int_0^{\sqrt{k_d^2 - k_z^2}} \Omega(k)[2L_N^{-2}k_\perp^2 + \beta_i^2 k^2(k_\perp^2 + k_\perp^2\cos^2\theta + 2k_z^2\sin^2\theta)]k^{-17/3}k_\perp dk_\perp, \tag{4}$$

here $k^2 = k_\perp^2 + k_z^2$, $\theta = 90° - I$ is an angle between **b** and **n**, I is the magnetic dip angle ($I \approx 80°$ is chosen in the present case).

In the case of ground-based measurements **z** coincides with the drift direction of the irregularities, which is most commonly eastward (horizontal direction), i.e., $\mathbf{z} \perp$ both **n** and **b**, and the 1D spectrum, $S_1''(k_z)$, is

$$S_1''(k_z) = C_1\pi\varepsilon^{2/3}\int_0^{\sqrt{k_d^2 - k_z^2}} \Omega(k)(L_N^{-2} + \beta_i^2 k^2)(k_z^2 + 2k_\perp^2)k^{-17/3}k_\perp dk_\perp. \tag{5}$$

To illustrate possible deviation of the irregularity spectrum from isotropy, the following set of values of relevant parameters which are quite realistic for the high-latitude lower ionosphere (the height range of 90—95 km) are taken: $L_N \sim 10^4$ m, $N_0 \sim 4\cdot 10^{10}$ m^{-3}, $\beta_i \approx 0.01$, $D_A \approx \mu_n \sim 4$ m^{2}s^{-1}, $\varepsilon \sim 0.1$ m^{2}s^{-3}, $\alpha_r \sim 3.8\cdot 10^{-13}$ m^{3}s^{-1}, $I \approx 80°$ [5, 7, 8]. Figure 1 shows the normalized 1D spectra for the chosen set of

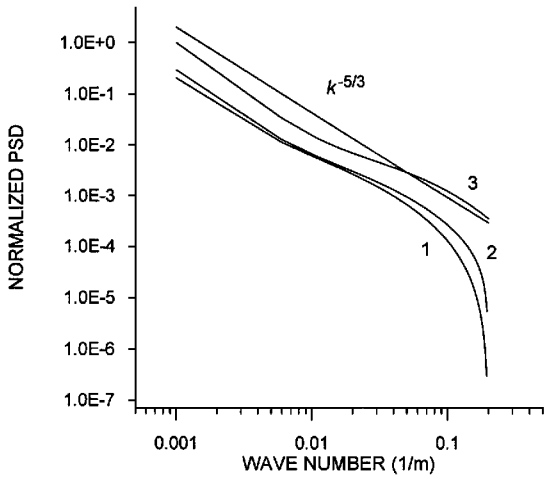

Figure 1. Normalized 1D spectra (or PSD) of relative plasma-density fluctuations predicted by (4), (5), and (3): line 1 represents $S_1(k_z)/P_1(k_1)$ ($k_1 = 10^{-3}$ m^{-1}), line 2 — $S_1(k_z)/P_1(k_1)$, line 3 — $P_1(k)/P_1(k_1)$ straight line represents the slope of the Kolmogorov spectrum

values of parameters: line 1 represents the case of measurement in the vertical direction, $S_1'(k_z)/P_1(k_1)$ ($k_1 = 10^{-3}$ m^{-1}) (see (4)), line 2 corresponds to the case of the horizontal direction, $S_1''(k_z)/P_1(k_1)$ (see (5)), line 3 is for $P_1(k)/P_1(k_1)$ (see (3)), the case of isotropic irregularities, and the straight line represents the slope of Kolmogorov spectrum, $k^{-5/3}$. It is seen that the spectra of the irregularities are quite close to an isotropic one, though there are some their deviations from isotropy on the edges of the considered wave-number range. These deviations result from changes in a relative role of the geomagnetic field (more important for larger wave numbers) and of the gradient of mean plasma density (more important for smaller wave numbers) in creating the plasma irregularities of different scales. The spectral form $S_1'(k_z)/P_1(k_1)$ (line 1) does not contradict experimental spectra obtained during *in situ* rocket measurements in the high latitude ionosphere [1]. Estimates of changes in the slope of the irregularity spectra (changes in the spectral index, $1 \lesssim p \lesssim 8$, if a power-law dependence, k^{-p}, is taken for description of the spectrum) as well as an estimate of the rms level of plasma fluctuations made with the use of (2), ≈ 1.2 % ($k_1 = 10^{-3}$ m^{-1}, $k_2 \lesssim k_d \approx 0.2$ m^{-1}) are consistent with experimental data gathered during the ROSE campaign [5, 7].

CONCLUSION

Thus, it was shown that the spectra of the plasma irregularities that can be caused by neutral turbulence in the lower ionosphere have to be quite close to an isotropic one, although some their deviations from isotropy may exist on the edges of the considered wave-number range. These deviations result from changes in a relative role of the geomagnetic field (more important for larger wave numbers) and of the gradient of mean plasma density (more important for smaller wave numbers) in creating the plasma irregularities of different scales. Estimations of slope of the irregularity spectra and of the rms level of plasma density fluctuations made here do not contradict the data gathered during the rocket-radar simultaneous experiment in the lower ionosphere at high latitudes [1, 5, 7]. It seems useful for testing the present results to conduct an experiment that measures simultaneously the irregularity spectrum in two directions with the use of rocket and radar instruments (see, e.g., [1, 4, 6, 7]), and the pertinent parameters of both the lower ionosphere and the neutral atmosphere turbulence.

REFERENCES

1. Gurevich A. V., Rinnert K., Schlegel K. Low frequency fluctuations in the lower E-region described by neutral turbulence // Plasma Instabilities in the Ionospheric E-Region / Ed. K. Schlegel. — Cuvillier Verlag, Gttingen, 1996.—P. 5—8.
2. Kyzyurov Yu. V., Malovichko P. P., Nosov S. F. Plasma irregularities in a turbulent flow of partially ionized gas. I. Spatial spectrum of plasma density fluctuations in the lower Earth's ionosphere // Kinematika Fiz. Nebesn. Tel.—1999.—**15**, N 5.—P. 455—466.
3. Kyzyurov Yu. V., Malovichko P. P., Nosov S. F. Plasma irregularities in a turbulent flow of partially ionized gas. II. Feartures of spatial spectrum of plasma density fluctuations in the lower ionosphere // Kinematika Fiz. Nebesn. Tel.—1999.—**15**, N 5.—P. 467—475.
4. Ovezgeldyev O. G., Karadzhaev Yu., Korsunova L. P. The amplitude spectrum of a radio signal reflected from the E_s-layer // Geomagn. Aeron.—1988.—**28**, N 6.—P. 1024—1026.
5. Rose G., Schlegel K., Rinnert K., et al. The ROSE project. Scientific objectives and discussion of first results // J. Atmos. Terr. Phys.—1992.—**54**, N 6.—P. 657—667.
6. Ryrvic O., Smith L. G. Comparison of mesospheric VHF radar echoes and rocket probe electron concentration measurements // J. Geophys. Res.—1984.—**89**, N A10.—P. 9014—9022.
7. Schlegel K. Measurements of electron density fluctuations during the ROSE rocket flights // J. Atmos. Terr. Phys.—1992.—**54**, N 6.—P. 715—723.
8. Schlegel K., Gurevich A. V. Radar backscatter from plasma irregularities of the lower E-region induced by neutral turbulence // Ann. Geophysicae.—1997.—**15**, N 7.—P. 870—877.

Космічна наука і технологія. ДОДАТОК. 2001. Т 7. № 2. С. 56—58.

UDK 52-425

PITCH-ANGULAR DIFFUSION OF HIGH-ENERGY PARTICLES IN PLASMA OF THE MAGNETOSPHERE

S. F. Nosov, A. K. Yukhimuk

Main Astronomical Observatory NASU, Kiev-127, 03680, Ukraine

In this work some problems of dynamics of magnetospherical charged particles of high energies (1—1000 MeV) are considered. The coefficients of a pitch-angular and radial diffusion of protons and electrons in a dipole magnetic field are defined. The calculations were grounded on the basic kinetic equation with use of a method by G. M. Zaslavsky [1]. Our calculations were based on the results of the modern theory of nonlinear oscillations in dynamic systems [1, 2]. The aim of the work was to define a role of the mechanism of the breaking down of the first adiabatic invariant in shaping pitch-angular distribution of particles in the magnetosphere. It is shown, that the considered mechanism of scattering reduces in a strong pitch-angular diffusion of protons and heavier ions, while the beams of polar electrons are very stable, can be long-lived in time and oscillate between points of reflection, which are in the polar zones. On the basis of the obtained results it is possible to explain and to interpret origin and stability of auroras, and also radio-frequency radiation from magnetospheres of planets as secondary effect of a stability of polar electron beams.

1. INTRODUCTION

In work [3] on the basis of exact equations of motion two sharply distinguished one from other regimes of motion of particles, entrapped by magnetic field of dipole were explored.The first, basic regime is a condition of gyrorotation and corresponds to the well known Alfven approximation, based on the drift theory of guiding centre motion of a particle. The second regime of motion arises in an equatorial zone for particles with small pitch-angles in a magnetic field of a dipole, and closely corresponds to the central Stormer's trajectory. The trapped particles have only a gyrorotational trajectory, or have elements as Stormer's central trajectory in an equatorial zone, and elements of a trajectory with fast gyrorotation in polar zones. In work [3] the conditions of transition between these modes of motion are defined. Such transitions are characteristic for motion of particles in nonuniform magnetic fields with distinct from zero curvature of force lines. For plane-parallel magnetic fields this appearance is missed.

The transition from a mode of gyrorotation to a mode of a central trajectory actually corresponds to break down of the first adiabatic invariant, and subsequent inverse transition, i.e., its restitution. Such phase conversions on a trajectory of a particle correspond to saddle points on phase portraits of a nonlinear oscillator [2]. The saddle point arises from a point of a type centre at a change of motion parameter, which is in our case a pitch-angle of a particle.

In work [3] it was marked, that the transitions between regimes of motion occur for values of gyrophase equal $\pi/2$ and $3\pi/2$. This deduction is well correlated with outcomes of work [4], where it was shown, that the bifurcations in Hamiltonian systems take place in saddle points at the mentioned above values of phases.

The existence of regions of parameters and phase space with the destroyed integrals of motion, in particular, of the first adiabatic invariant, is a typical physical situation, which is accompanied by occurrence of random dynamics. For one bouns-period a particle with high-latitude points of reflection and the high energy four times transits near saddle bifurcation points on the trajectory. The trajectories of such particles in an equatorial zone between these points go close to a separatrix, where the parameters of trajectories also gain stochastic properties [1,2].

In this work we do not consider in detail modification of a trajectory of a particle at transitions through bifurcation points. We shall be restricted, basing on the strongest assumption about a possibility

of averaging casual phases for an evaluation of diffusion coefficients as in the case of good phase intermixing. The intermixing on phases occurs much faster than slow evolution on a variable action [1]. Basing on this, we suppose, that the operation of averaging phases can be carried out irrespective of evolution of action not only for a regime of fast gyrorotation, but also for a unstable regime of a slow gyrorotation at transiting bifurcation points and stochastic layers in an equatorial zone by a particle.

2. BASIC KINETIC EQUATION

Motion of a charged particle, entrapped by magnetic field of a magnetosphere is in many respects similar to the behaviour of a nonlinear oscillator. The basic kinetic equation for a distribution function $f(I, t)$ of nonlinear oscillator is as [1]

$$\frac{\partial f(I,t)}{\partial t} = \frac{1}{2}\frac{\partial}{\partial I} D_{II} \frac{\partial f(I,t)}{\partial I}, \tag{1}$$

where D_{II} is coefficient of a diffusion on a variable action I, $D_{II} = \langle(\Delta I)^2\rangle/T$, where ΔI is change of action on interval of time T, the angular brackets mean averaging for this interval, which by virtue of our supposition about ergodicity of process is equivalent to average on phases. According to this the change of the action ΔI should be determined for the same interval of time. We find the magnitude dI/dt from the Hamilton equation

$$\frac{dI}{dt} = -\frac{\partial H_1(I,\varphi)}{\partial \varphi}, \qquad H_1(I,\varphi) = mv^2\sqrt{1-\mu^2}u_d(\cos\varphi + \sin\varphi)$$

For calculations we use expression for a precise Hamiltonian $H(I, \varphi)$, obtained in work [5]. Let's obtain expression for derivative dI/dt within the first order of accuracy

$$dI/dt = E\sqrt{2(1-\mu^2)}\,u_d(\sin\varphi - \cos\varphi), \tag{2}$$

Where E = const is the complete kinetic energy of a particle, L is a parameter of the Mc-Ilvain drift, μ is cosine of an pitch-angle of a particle, u_d is normalized relative to a velocity v magnitude of a cross velocity of a drift of a particle [3, 6]

$$u_d = \frac{q}{|q|}\frac{vL^2}{a_0\Omega_0}\frac{1+\langle\mu^2 E\rangle}{2}\frac{(1+\cos^2\theta)\sin^5\theta}{(1+3cos^2\theta)^2}, \tag{3}$$

q is charge of a particle, L is the parameter of the Mc-Ilvain drift envelope, θ is polar angle in a spherical frame, bound with a magnetic dipole, a_0 is the radius of a planet, Ω_0 is gyrofrequency on equator of a planet.

Using (2), (3), obtain expression for D_{II} as

$$D_{II} = \left\langle\left(\frac{dI}{dt}\right)^2\right\rangle T = 2TE^2(1-\langle\mu^2\rangle - u_d^2)u_d^2. \tag{4}$$

In work [3] we have shown, that for a polar group of particles with small pitch-angles in an equatorial region, i.e. for a quasiconstant phase mode the relation $1 - \langle\mu^2\rangle = 2u_d^2$ is valid. Due to a strong dependence of D_{II} on a polar angle θ an essential value of a diffusion coefficient on a variable action is maintained only near an equatorial plane. As an interval for average T for the Stormer mode with a slow phase we select bouns-period $T_b = 2\pi/\omega_b$ for particles with zero equatorial pitch-angle. Here ω_b is bouns-frequency, for which we take the expression obtained in [6] for these particles: $\omega_b = v\cos^4\lambda_*/(r_e|\sin\lambda_*|)$, where $\lambda_* \approx 45°$ is the effective geomagnetic latitude of reflection for such particles, r_e is distance from center of the dipole to a cross point of an equatorial plane along a force line, on which the particle is located.

3. PITCH-ANGULAR DIFFUSION OF PARTICLES IN A MAGNETOSPHERE

The diffusion reduces on a variable action to pitch-angle and radial diffusions of particles. However, as tentative estimation of coefficients of a radial diffusion shows, the path length of an entrapped particle on a drift envelope and before complete scattering is about 10^{18} cm, and reference time for scattering is more than one year. So, the radial diffusion at the expense of violation of the first adiabatic invariant is incidental. It is known [7], that for process of a radial diffusion the most essential mechanism is the betatron, which effectively works at sudden impulses of a field during geomagnetic disturbances.

Thus, further we consider only process of a pitch-angular diffusion occurring at the expense of violations of the first adiabatic invariant. Passing from a variable of action to a variable $\xi = \mu^2$, i.e., quadrate of a cosine pitch-angle of a particle, we shall obtain the following equation instead of (1)

$$\frac{\partial f(\xi, t)}{\partial t} = \frac{\partial}{\partial \xi} \nu_{\xi} \frac{\partial f(\xi, t)}{\partial \xi}, \tag{5}$$

where $\nu_{\xi\xi}$ is the effective collision frequency. For a polar group of particles with small equatorial pitch-angles (mode of a slow phase) we have obtained expression

$$\nu_{\xi\xi\xi} = 4\pi\sqrt{2} v^3 L^3 / (a_0^3 \Omega_0^2). \tag{6}$$

4. CONCLUSION

The estimate of an effective collision frequency $\nu_{\xi\xi}$ and reference time of scattering τ^S for a polar group of particles having small equatorial pitch-angles and a velocity $v \sim 10^{10}$ cm s^{-1} on an envelope $L = 5$ gives: for electrons $\nu^e_{\xi\xi} \approx 2 \cdot 10^{-7}$ s^{-1}, $\tau^e \approx 5 \cdot 10^6$ s, and for protons $\nu^p_{\xi\xi} \approx 1$ s^{-1}, $\tau^p \approx 1$ s.

On the basis of these estimates it is possible to make the conclusion that beams of polar protones are scattering fast, because of an operation of the mechanism of equatorial break down of the first adiabatic invariant. At the same time electron beams of polar particles are very stable relative to the mechanism of scattering. The considerable selectivity of an operation of the surveyed mechanism of scattering relative to polar electrons and protons reduces in the important physical consequences for dynamics of trapped radiation in a magnetosphere. In particular, it can explain why the emptying of electrons is the basic reason of auroras.

The dynamic stability of electron beams in magnetospheric plasma can play the important role in origin of collective plasma effects such, as a beam instability and swing of plasma oscillations with all following from this physical consequences well known in the theory of plasma [8].

REFERENCES

1. Zaslavsky G. M., Sagdeev R. Z. Introduction to nonlinear physics. — M.: Nauka, 1988.
2. Neymark Yu. I., Landa P. S. Stochastic and random oscillations. — M.: Nauka, 1987.
3. Nosov S. F. About two modes of motion of a charged particle in magnetic dipole // Kinematics and physics of celestial bodies.—1999.—**15**, N 3.—P. 273—281.
4. Batalova Z. S. About resonant levels of Hamilton system // Dynamics of systems.—1980.—N 19. Gorkiy: GGU,—P. 60—79.
5. Nosov S. F. The Hamilton formalism in the drift theory of charged particle motion in magnetic field. // Kinematics and physics of celestial bodies.—1992.—**8**, N 6.—P. 14—31.
6. Nosov S. F. Drift Hamiltonian and boundary of its applicability in dipole magnetic field // Kinematics and physics of celestial bodies.—1996.—**12**, N 5.—P. 55—62.
7. Tverskoy B. A. Dynamics of radiation belts. — M.: Nauka, 1968.
8. Yukhimuk A. K. Plasma phenomena in a geophysics. — Kyiv: Naukova dumka, 1982.

Космічна наука і технологія. ДОДАТОК. 2001. Т 7. № 2. С. 59—66.

UDK 550.388.2

GENERATION OF THE KINETIC ALFVEN WAVE AND LOWER HYBRID WAVE IN SPACE PLASMA

A. K.Yukhimuk[1], V. M. Fedun[2], Yu. Voitenko[1,3], O. K. Sirenko[1], V. A. Yukhimuk[4]

[1]Main Astronomical Observatory NAS Ukraine

[2]Department of Astronomy and Space Physics

[3]Centre for Plasma Astrophysics

[4]Los Alamos National Laboratory

Satellite observations show close relationship between the whistlers and lower-hybrid waves in space plasmas. Intense whistler waves generated by lightning discharges [Kelley, 1990] or by quasimonochromatic VLF (very low frequency) transmitters can be unstable and cause the three-wave parametric interaction. Work [Bell, 1994] demonstrates experimental results of excited lower hybrid waves by VLF whistler mode waves in the topside ionosphere and near magnetosphere. The Kinetic Alfven waves are often observed by satellites [Louran], [Volokitin, 1989]. In this paper we analytically consider a possible mechanism of this Relationship, i.e., parametric interaction of whistler pump waves with lower-hybrid and the Alfven waves in magnetized plasma with small plasma parameter. In the dynamics of the Alfven waves the kinetic effects (finite ion Larmor radius and electron inertia) are taken into account A nonlinear dispersion equation describing three-wave interaction is obtained in the framework of two-fluid magnetohydrodynamics. The instability growth rates and the time of instability development are found. Our theoretical investigation shows, that the whistler mode will be an effective source of the lower hybrid and the Alfven waves in the magnetospheric plasma. This nonlinear process can take place in the Earth magnetosphere and in the Sun atmosphere. The products of the decay, i.e., the lower-hybrid and the kinetic Alfven waves, can effectively interact with magnetospheric and sun plasmas.

INTRODUCTION

The interest to the three-wave resonant (TWR) parametric decay closely is related to the study of the origin of the waves observed in the laboratory and space plasmas. Also, different wave modes damp with different rates, and a mutual transformation of the wave modes caused by TWR can significantly change the rate of plasma heating, often providing an explanation for enhanced (or reduced) plasma heating. Therefore, the parametric interactions is of great interest ([Berger, 1976], [Shukla, 1978], [Murtaza, 1984], [Stenflo, 1990], [Guha, 1991], [Leyser, 1991], [Yukhimuk, 1992, 1998]). In introduction we shall be interested in processes, which can be generalized by the same physical phenomenon, i.e., the parametric interaction of whistler mode waves with ionospheric and magnetospheric plasmas. [Sharma, 1992] analyzed the effect of parametric excitation of the electrostatic whistler waves by electron plasma waves. The paper [Chian, 1994] presented a new excitation mechanism of the auroral Langmuir and the Alfven waves in the planetary magnetosphere. It was shown that a large-amplitude electromagnetic whistler wave propagating along the magnetic field lines can nonlinearly generate the Langmuir and the Alfven waves by three wave parametric instability. In the paper [Tara, 1987] about generation of the oblique Alfven waves by the parametric instability of the whistlers in the near Earth pasma decay process with participation of two whistler waves spreading under angles to an external magnetic field and the oblique Alfven wave is considered. It is shown that parametric instability whistlers should reduce to the rapidly growing oblique Alfven waves with perpendicular wave length. The work of [Grach, 1975] is also very interestng. In his paper a parametric instability of quasi-monochromatic VLF waves in the upper ionosphere is considered. It is shown that the initial signal scatters into a low-frequency plasma wave and decays into low frequency and ion-cyclotron waves most effectively. A parametric interaction between

two whistlers and ion-cyclotron wave is considered. The above process also may be responsible for excitation of the low-hybrid resonance in the ionosphere and magnetosphere of the Earth. The processes of whistlers scattering at big angles to an external magnetic field were analyzed in the paper [Tara, 1989]. In the paper [Shukla, 1978] the decay of UHW (upper hybrid waves) into the whistler and KAW was studied. In the paper [Murtaza, 1984] the decay of LHW into the UHW and electromagnetic wave was studied. Later [Leyser, 1991] used theoretical results of Murtaza and Shukla for interpretation of the nature of downshifted maximum, and Stenflo for interpretation of stimulated electromagnetic emission in the ionosphere. In the paper [Yukhimuk, 1998], the nonlinear interaction of kinetic Alfven wave with upper hybrid wave has been investigated, and the results have been used for the interpretation of long-period geomagnetic pulsations.

Whistlers is one of the most widespread type of waves in a magnetized plasma. The generation mechanisms are related to flashes, particle beams, anisotropic velocity distributions of particles, and nonlinear processes in space plasmas. In the Earth magnetosphere, whistlers can propagate from one hemisphere to another, and under favorable conditions can be detected by the ground instruments and satellites in «magnetoconjugated» points. The low-hybrid waves have been often observed simultaneously with whistlers ([Barrington, 1963], [Brice, 1964], [Gurnet, 1966], [Scarf, 1972], [Bell, 1991, 1994]). Satellite observations have shown a close relationship between whistlers and LHWs ([Titova, 1984], [Bell, 1988]), and it was supposed that the whistlers are the source of the lower hybrid wave.

However, despite of the mentioned above observational data, an exact mechanism of such a close relation between lower hybrid emissions and whistlers is still uncertain. In the present paper the nonlinear interaction of the whistlers and the lower hybrid waves has been investigated. The lower hybrid wave is excited as a result of parametric decay of whistlers into KAWs and LHW. A high efficiency of the interaction among KAWs and whistlers is caused by the presence of the longitudinal component of KAW electric field.

BASIC EQUATIONS

Parametric instability, where the whistlers wave decays into the LHW and the kinetic Alfven wave

$$W = LHW + KAW$$

is considered.

The whistler pump wave

$$\mathbf{E}_0 = (E_{0x}\mathbf{e}_x + E_{0y}\mathbf{e}_y)\exp i\psi_0 + c.c. \tag{1}$$

where $\psi_0 = -\omega_{0t} + k_{0x}x + k_{0z}z, \omega_0 = (k_0^2c^2/\omega_{pe}^2)|\cos\theta\omega_{Be}|$ propagates in the homogeneous magnetized plasma ($\mathbf{B}_0 = B_0\mathbf{e}_z$). It is assumed that the wave synchronism condition is satisfied

$$\omega_0 = \omega + \omega_1, \mathbf{k}_0 = \mathbf{k} + \mathbf{k}_1, \tag{2}$$

where ω_0, $\mathbf{k}_0$ are frequency and wave vector of the whistler pump wave, ω, $\mathbf{k}$ are frequency and wave vector of the kinetic Alfven wave, ω_1, $\mathbf{k}_1$ are frequency and wave vector of the lower hybrid wave. Let us consider that all wave vectors are in OXZ plane (Fig. 1).

To study three-waves parametric interaction we use two-fluid magnetohydrodynamics (MHD):

$$\frac{\partial \mathbf{v}_\alpha}{\partial t} = \frac{1}{m_\alpha}(e_\alpha\mathbf{E} + \mathbf{F}_\alpha) + (\mathbf{v}_\alpha \times \omega_{B\alpha}) - \frac{T_\alpha}{m_\alpha n_\alpha}\nabla n_\alpha, \tag{3}$$

$$\frac{\partial n_\alpha}{\partial t} = -\nabla(n_\alpha \mathbf{v}_\alpha), \tag{4}$$

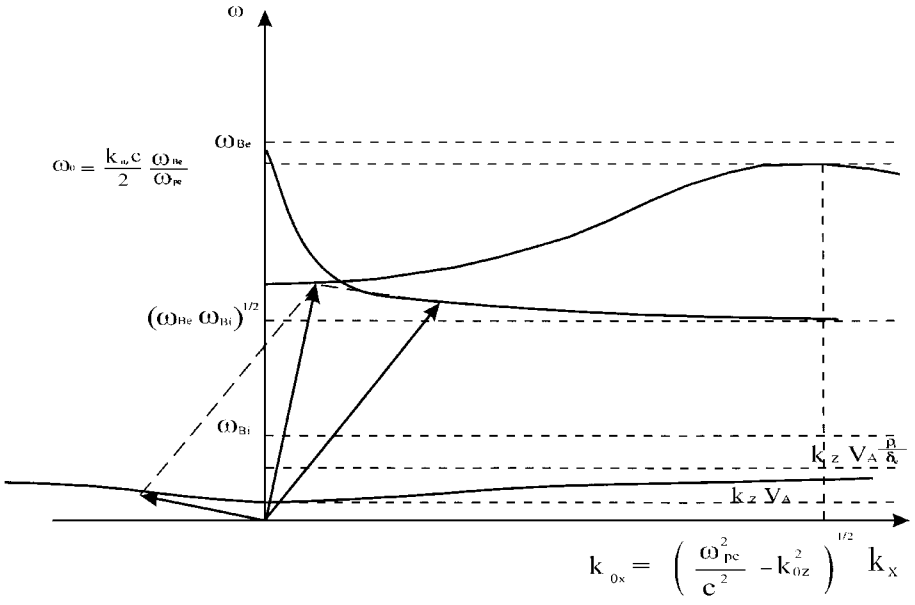

Fig. 1.

$$\nabla\times\mathbf{B} = \frac{4\pi}{c}\mathbf{j} + \frac{1}{c}\frac{\partial\mathbf{E}}{\partial t}, \tag{5}$$

$$\nabla\times\mathbf{E} = -\frac{1}{c}\frac{\partial\mathbf{B}}{\partial t}, \tag{6}$$

$$\nabla\cdot\mathbf{E} = 4\pi\rho, \tag{7}$$

where

$$\mathbf{j} = e(n_i\mathbf{v}_i - n_e\mathbf{v}_e),$$

$$\rho = e(n_i - n_e),$$

$$\mathbf{F}_\alpha = \frac{e_\alpha}{c}(\mathbf{v}_\alpha\times\mathbf{B}) - m_\alpha(\mathbf{v}_\alpha\nabla)\mathbf{v}_\alpha.$$

Index $\alpha = i, e$ which correspond to the ion and electron components of plasma respectively. Electron density and velocity, electric and magnetic field are presented in the form:

$$\begin{aligned} n_e &= n_0 + \tilde{n}_A + \tilde{n}_1, \qquad & \mathbf{v}_e &= \mathbf{v}_0 + \mathbf{v}_A + \mathbf{v}_1, \\ \mathbf{E} &= \mathbf{E}_0 + \mathbf{E}_A + \mathbf{E}_1, \qquad & \mathbf{B} &= B_0\mathbf{e}_z + \mathbf{B}_A, \end{aligned} \tag{8}$$

where n_0 is the mean value of plasma density, index 0 in the expressions for $\mathbf{v}_e$ and $\mathbf{E}$ denotes the variable related to the pump wave and indexes A and 1 denote variables related to KAW and UHW respectively.

DISPERSION EQUATION OF THE ALFVEN WAVES

To obtain dispersion equation we use plasma approximation

$$\tilde{n}_e = \tilde{n}_i, \tag{9}$$

since the Alfven waves are slow. Here $\tilde{n}_e$ and $\tilde{n}_i$ are the perturbations of electron and ion density respectively. From the motion equation (3) and continuity equation (4) we find the expression for $\tilde{n}_e$, $\tilde{n}_i$:

$$\frac{\tilde{n}_e}{n_0} = \left(1 - \frac{v_{ph}^2}{v_{Te}^2}\right)^{-1} eT_e\left[\varphi - A + \frac{k_x}{k_z^2}\frac{\omega}{\omega_{Be}}\frac{1}{e}\left(i\frac{\omega}{\omega_{Be}}F_x + F_y\right) + \frac{F_z}{iek_z}\right], \tag{10}$$

$$\frac{\tilde{n}_i}{n_0} = -\frac{e}{T_e}\frac{\mu_i}{1+\mu_i}\left(\varphi + \frac{\omega_{Bi}^2 k_z^2}{\omega^2 k_x^2}A\right)$$

where $v_{ph} = \omega/k_z$, $A = \frac{\omega}{k_z c}A_z$, $\mu = k_x^2\rho^{2i}$, $\rho_i = v_{Ti}/\omega_{Bi}$ is the ion Larmor radius, φ and A_z are scalar and vector potentials of KAW electric field respectively. The first relation between φ and A follows from (10) = (11):

$$A = \left[1 + \frac{T_e}{T_i}\frac{\mu_i}{1+\mu_i}\left(1 - \frac{V_{ph}^2}{V_{Te}^2}\right)\right]\varphi - \frac{k_x^2}{k_z^2}\frac{\omega^2}{\omega_{Be}^2}\frac{1}{iek_x}\overline{F} + \frac{1}{iek_z}F_z - \frac{T_e}{e}\frac{V_{ph}^2}{V_{Te}^2}\frac{\mathbf{k}}{\omega}\left(\frac{n}{n_0}\mathbf{V}\right)_e \tag{12}$$

where

$$\overline{F} = F_x - i\frac{\omega_{Be}}{\omega}F_y.$$

We can find the second relation between φ and A from the perpendicular projection of Ampere low:

$$-k^2 k_z A_z = \frac{4\pi}{c}k_x j_x. \tag{13}$$

The linear part of the transverse current j_x is determined by the plasma ion component, but the nonlinear perpendicular current is generated by the beating of LHW and whistler in electron motions:

$$j_x = en_0 V_{ix}^L + j_{ex}^{NL}. \tag{14}$$

Inserting the expression for ion velocity and nonlinear electron current we get the second relation between KAW potentials:

$$A = \frac{V_{ph}^2}{V_A^2}\frac{1}{1+\mu_i}\varphi + (k_z^2\delta_i^2)^{-1}\frac{m_i}{e}\frac{\omega}{k_x}\frac{n_e^L}{n_0}V_{ex}^L + (k_z^2\delta_i^2)^{-1}\frac{m_i}{e}\frac{\omega^2}{\omega_{Be}^2}\times$$
$$\times\left[\left(\frac{V_{ph}^2}{V_{Te}^2} - 1\right)^{-1}\frac{1}{im_e k_z}F_z + \left(\frac{V_{ph}^2}{V_{Te}^2} - 1\right)^{-1}\frac{\omega}{k_z^2}\mathbf{k}\left(\frac{n}{n_0}\mathbf{V}\right) + \frac{1}{im_e k_x}\overline{F}\right]. \tag{15}$$

where $\delta_i^2 = c^2/\omega_{pi}^2$. Equating (12) = (15) we obtain the nonlinear dispersion equation for KAW:

$$\left[\frac{V_{ph}^2}{V_A^2}(1+\chi_e) - (1+\overline{\mu}_i)\right]\frac{1}{1+\mu_i}\varphi = \frac{1}{iek_z}F_{ez} - \frac{m_e}{m_i}\frac{V_{ph}^2}{V_A^2}(1+\chi_e)\frac{1}{iek_x}\left(F_{ex} - i\frac{\omega_{Be}}{\omega}F_{ey}\right) -$$
$$-\frac{m_i}{e}(k_z^2\delta_i^2)^{-1}\frac{\omega}{k_x}(1+\chi_e)\frac{n_e^L}{n_0}V_{ex}^L, \tag{16}$$

where $\chi_e = k^{2x}\delta_e^2$, $\overline{\mu}_i = (1 + T_e/T_i)\mu_i$. From the motion equation we find electron velocity components in the field of whistler wave:

$$v_{0x} = -i\frac{eE_{ox}}{m_e(\omega_0 - \omega_{Be})}, \qquad v_{0x} = \frac{eE_{ox}}{m_e(\omega_0 - \omega_{Be})}, \tag{17}$$

and components of the pump wave magnetic field from (6):

$$b_{0x} = -i\frac{ck_{oz}}{\omega_0}E_{0x},$$

$$b_{0y} = \frac{ck_{oz}}{\omega_0}E_{0x}, \tag{18}$$

$$b_{0z} = i\frac{ck_{ox}}{\omega_0}E_{0x}.$$

Velocity components in the LHW field can be obtained from electron motion equation:

$$v_{1x} = -\frac{ek_{1x}\omega_1}{m_e(\omega_1^2 - \omega_{Be}^2)}\varphi_1,$$

$$v_{1y} = -i\frac{ek_{1x}\omega_{Be}}{m_e(\omega_1^2 - \omega_{Be}^2)}\varphi_1, \tag{19}$$

$$v_{1z} = -\frac{ek_{1z}}{m_e\omega_1}\varphi_1.$$

Using expressions (17)—(19) and from (16), we find dispersion equation for the Alfven wave:

$$\varepsilon_A\varphi = \mu_A(E_{0x}\varphi_1^*), \tag{20}$$

where μ_A is the coupling coefficient, that defined by the expression:

$$\mu_A = i\frac{e}{m_e}\frac{k_{1x}}{\omega_{Be}}\frac{k_{0z}}{k_z}\frac{k_z^2V_A^2}{\omega_0}(1+\mu_i)\left[1 + \frac{m_e}{m_i}\frac{k_z}{k_x}\frac{\omega_{Be}^2}{\omega_1\omega}\frac{k_{1z}}{k_{1x}}(1+\bar{\mu}_i)\right],$$

$$\varepsilon_A = \omega^2 - k_z^2V_A^2(1+\bar{\mu}_i).$$

In the calculation of the coupling coefficient μ_A, we have taken account of the ponderomotive force created by scattering whistlers pump wave on LHW. Since we consider magnetosphere, where the plasma parameter $m_e/m_i \ll \beta \ll 1$, in the dispersion equation for KAW we keep therms with finite-Larmor-radius effects.

DISPERSION EQUATION OF LHW

Dispersion equation of LHW can be found from Puasson equation:

$$\Delta\varphi_1 = -4\pi e(\tilde{n}_i - \tilde{n}_e). \tag{21}$$

Expression for $\tilde{n}_i$, $\tilde{n}_e$ we find from the motion equation (3) and continuity equation (4):

$$\tilde{n}_i = \frac{en_0}{m_i}\left(\frac{k_{1x}^2}{\omega_1^2 - \omega_{Bi}^2} + \frac{k_{1z}^2}{\omega_1^2}\right)\varphi_1, \tag{22}$$

$$\tilde{n}_e = -\frac{en_0}{m_e}\left(\frac{k_{1x}^2}{\omega_1^2 - \omega_{Bi}^2} + \frac{k_{1z}^2}{\omega_1^2}\right)\varphi_1 - \frac{n_0}{m_e}\frac{k_{1x}\omega_{Be}}{\omega_1(\omega_1^2 - \omega_{Be}^2)}\times$$

$$\times\left[i\frac{\omega_1}{\omega_{Be}}F_{1x} + F_{1y} + i\frac{k_{1z}}{k_{1x}}\frac{(\omega_1^2 - \omega_{Be}^2)}{\omega_1\omega_{Be}}F_{1z}\right] - \frac{\nabla\langle\tilde{n}_A\mathbf{V}_0\rangle}{-i\omega}, \tag{23}$$

where components of ponderomotive force are defined by interaction of pump wave and Alfven wave. From (21)—(23) we find the dispersion equation for LHW:

$$\varepsilon_1 \varphi_1 = \mu_1 (E_{0x} \varphi^*), \tag{24}$$

where coupling coefficient μ_1 is defined by the expression:

$$\mu_1 = i \frac{e}{m_e} \frac{\mu_s}{1+\mu_i} \frac{\omega}{k_z} \frac{1}{V_{Te}^2} \frac{k_{0z}}{\omega_0} \frac{\omega_1 \omega_{Be}}{k_{1x}} \left[1 + \frac{k_{1z}}{k_{1x}} \frac{k_z}{k_{0z}} \frac{k_z}{k_x} \frac{\omega_0}{\omega_1} \frac{\omega_{Bi}^2}{\omega^2} \frac{V_{Te}^2}{V_s^2} (1+\tilde{\mu}_i) + \frac{\omega_0}{\omega} \frac{k_z}{k_{0z}} \right],$$

$$\varepsilon_1 = \omega_1^2 - \frac{\omega_{pi}^2}{1 + \dfrac{\omega_{pe}^2}{\omega_{Be}^2}} \left(1 + \frac{m_i}{m_e} \frac{k_{1z}^2}{k_1^2} \right).$$

NONLINEAR DISPERSION EQUATION FOR THREE-WAVE INTERACTION

From equations (20) and (24) we find the nonlinear dispersion equation describing three-wave interaction (decay of whistler pump wave into the KAW and LHW):

$$\varepsilon_A \varepsilon_1^* = \mu_A \mu_1^* |\varphi_0|^2.$$

Assuming in (25)

$$\omega = \omega_r + i\gamma_1, \qquad \omega_1 = \omega_{1r} + i\gamma_1,$$

(where $|\gamma| \ll \omega_r, \omega_{1r}$) and decomposing ε_A and ε_1 to the Taylor series with respect to the small parameter $i\gamma_1$ we obtain the expression for the instability growth rate

$$\gamma_1 = \frac{\mu_A \mu_1^* |E_{0x}|^2}{\dfrac{\partial \varepsilon_A}{\partial \omega}} \frac{\partial \varepsilon_1}{\partial \omega_1} \bigg|_{\omega = \omega_r,\ \omega_1 = \omega_{1r}}, \tag{26}$$

where ω_r and ω_{1r} could be found from the equations

$$\varepsilon_A(\omega_r, \mathbf{k}) = 0, \qquad \varepsilon_1(\omega_1, \mathbf{k}_1) = 0.$$

Substituting values of derivatives

$$\frac{\partial \varepsilon_A}{\partial \omega} = 2\omega, \qquad \frac{\partial \varepsilon_1}{\partial \omega_1} = 2\omega_1,$$

and coefficients μ_A and μ_1 into (26) we obtain

$$\gamma^{21} = \frac{W}{4} \frac{\omega_{pe}^2}{\omega_0^2} \mu_s V_A^2 k_{0z}^2 \left[1 + \frac{m_e}{m_i} \frac{k_z}{k_x} \frac{\omega_{Be}^2}{\omega_1 \omega} \frac{k_{1z}}{k_{1x}} (1+\bar{\mu}_i) \right] \left[1 + \frac{k_{1z}}{k_{1x}} \frac{k_z}{k_{0z}} \frac{k_z}{k_x} \frac{\omega_0}{\omega_1} \frac{\omega_{Bi}^2}{\omega^2} \frac{V_{Te}^2}{V_s^2} (1+\tilde{\mu}_i) + \frac{\omega_0}{\omega} \frac{k_z}{k_{0z}} \right],$$

where $W = \dfrac{|E_{0x}|^2}{4\pi n_0 T_e}$.

DISCUSSION AND APPLICATION

In this paper we analytically consider nonlinear parametric interaction of whistlers with LHW and the Alfvenic wave in a low-β plasma. The kinetic effects (finite ion Larmor radius and electron inertia) are taken into account for dispersion law, when we investigate the dynamics of the Alfven wave. Such type of the Alfven wave is usually called the kinetic Alfven waves. They have some properties different from the MHD Alfvenic waves. They include the presence of nonzero parallel electric field E_z and can propagate in xz-plain. Due to this properties KAW interacts effectively with the whistler and amplifys the lower hybrid waves. The considered nonlinear three-wave parametric interaction can be observed in

laboratory and space plasmas with low-β plasmas. In space plasmas such processes can take place in the ionosphere and magnetosphere of the Earth and in the some regions of Sun atmosphere where the plasma parameter is small.

In our paper we consider magnetospheric plasma in the capacity of supplement (or application). Typical parameters for magnetospheric plasma at (3...4)R_E are: $V_{Te} \approx 10^7$ s^{-1}, $\omega_{pe} \approx 10^5$ s^{-1}, $\omega_{Be} \approx 10^5$ s^{-1}, $\omega_{Bi} \approx 10^2$ s^{-1}. We substitut plasma parameters and whistlers intensity $W \approx 10^{-5}$ into (27). The time of instability development is $\tau \approx \gamma_{max}^{-1} = 0.01$ s.

Our theoretical investigation shows, that whistler wave while propagating in the magnetosphere will be a source of the lower hybrid and the Alfven waves. Theoretical results can explain satellite observations of the coexistence of the whistler, lower hybrid and Alfven waves.

Nonlinear parametric processes considered in this paper can take place in the Solar corona as well, where whistlers are generated by energetic electrons in magnetic traps on the Sun. Whistlers will excite the lower hybrid and Alfven waves while propagating through the Solar atmosphere. The lower hybrid wave can effectively accelerate electrons to high energy. The kinetic Alfven waves interact effectively with plasma particles and participate in the heating and acceleration of space plasma particles owing to presence of the longitudinal component of electric field. Thus, i. e., the products of the decay — the lower hybrid and kinetic Alfven waves, can affect the magnetospheric and Sun plasmas stronger than the initially excited whistler waves.

Acknowledgment. This work was supported in part by INTAS Grant 99-0078.

Benz A. O., Smith D. F. Stochastic acceleration of ele trons in Solar flares // J. Geophys. Res.—1987.—**107**, N 2.—P. 299—309.

Berger R. L., Chen L. Exitation of fast waves by slow waves near the lower-hybrid frequency // Phys. Fluids.—1976.—**19**.—P. 1392—1399

Barrington R. E., Berlose G. S. Preliminary results from the very-low-frequency receiver on board Canadas Alouette satellite. emph{ // Nature.—1963.—**198**.—P. 651—656.

Bell T. F., Ngo H. D. Electrostatic waves stimulated by coherent VLF signals propagating in and near the inner radiation belt // J. Geophys. Res.—1988.—**93**.—P. 2599.

Bell T. F., Inan U. S., Sonwalnar V. S., et al. DE-1 observations of lower hybrid waves excited by VLF whistler mode waves // Geophys. Res. Lett.—1991.—**48**.—P. 393.

Bell T. F., Inan U. S., Lauben D., et al. DE-1 and COSMOS 1809 observations of lower hybrid waves excited by VLF whistler mode waves // Geophys. Res. Lett.—1994.—**21**, N 8.—P. 653—656.

Brice N. M., Smith R. L. Recording from satellite Alouette-2-A very low frequency plasma resonance // Nature.—1964.—**203**.—P. 926—927.

Chin Y. // Planet and Space Sci.—1972.—**20**.—P. 711.

Chian A. C.-L., Lopes S. R., Alves M. V. Nonlinear excitation of Langmuir and Alfven waves by auroral whistler waves in the planetary magnetosphere // Astron. and Astrophys.—1994.—**288**.—P. 981—984.

Gurnett D. A. A satellite study of VLF hiss // J. Geophys. Res.—1966.—**71**, N 23.—P. 5599—5615.

Gucha S., Sarkar R. Parametric decay of a whistler wave at the difference frequency of two electromagnetic waves in a plasma // J. Plasma Physics.—1991.—**47**, N 1.—P. 115—123.

Grach S. M. Parametric Instability of VLF Waves in the Upper Ionosphere // Radiophysica.—1975.—**18**, N 11.—P. 1627—1637 (in Russian).

Hasegava A., Chen L. Kinetic processes in plasma heating by resonant mode conversion of Alfven wave // Phys. Fluids.—1976.—**30**.—P. 1924.

Hui C. H., Seyler C. E. Electron acceleration by Alfven waves in the magnetosphere // J. Geophys. Res.—1992.—**97**, N A4.—P. 3953—3963.

Ionson I. A. Resonant absorption of Alfvenic surface waves and heating of solar coronal loops // Astrophys. J.—1978.—**226**, N 2.—P. 650—673.

Kelley M. C., Ding J. G. Intence Ionospheric and Magnetic Field Pulses Generated by Lighting // Geophys. Res. Lett.—1990.—**17**, N 12.—P. 2221—2224.

Kletzing C. A. Electron acceleration by kinetic Alfven waves // J. Geophys. Res.—1994.—**99**.—P. 11095—11103.

Lakhina G. S., Buti B. Stochastic acceleration by lower hybrid waves in the solar corona // Solar Phys.—1996.—**165**, N 2.—P. 329—336.

Leyser T. B. Parametric interaction between hybrid and low hybrid waves in heating experiments // Geophys. Res. Lett.—1991.—**18**, N 3.—P. 408—411.

Louran P., Wahlund J. E., Chust T. Observation of Kinetic Alfven waves by the FREJA Spacecraft // Geophys. Res. Lett.—1994.—**21**, N 17.—P. 1847—1850.

Murtaza G., Shukla P. K. Nonlinear generation of electromagnetic waves. // J. Plasma Phys.—1984.—**31**.—P. 423—436.

Sharma R. P., Tripathi Y. K., Hadi A., et al. Parametric Excitation of Electrostatic Waves by Electron Plasma Waves // J. Geophys. Res.—1992.—**97**.—P. 4275—4281.

Shukla P. K., Stenflo L. Nonlinear Alfven waves // Phys. Scripta.—1995.—**60**.—P. 32—35.

Shukla P. K., Mamedow M. A. Nonlinear decay of a propagating lower-hybrid wave in a plasma // J. Plasma Phys.—1978.—**19**, N 1.—P. 87—96.

Scarf F. L., Fredrics R. W., Smith E. J., et al. OGO-5 observations of LHR noise emissions and whistlers near the plasmapause at several Earth radii during a large magnetic storm // J. Geophys. Res.—1984.—**77**, N 10.—P. 1776—1793.

Stenflo L. Stimulated scattering of large amplitude waves in the ionosphere // Phys. Scripta.—1990.—**30**.—P. 166—169.

Taranenko Yu. N., Chmyrev V. M. Generation of Oblique Alfven Waves by the Parametric Instability of Whistlers in the Near-Earth Plasmas // Geomagnetizm and Aeronomy.—1987.—**27**.—P. 664—665.

Taranenko Yu. N., Chmyrev V. M. Parametric Interaction of Whistler and Electron Cyclotron Waves in the ionospheric Plasma // Geomagnetizm and Aeronomy.—1989.—**29**.—P. 459—464.

Titova E. E., Di V. I., Yurov V. E., et al. Interaction between VLF waves and turbulent ionosphere // Geophys. Res. Lett.—1984.—**11**.—P. 323.

Robert I., Stefant. Alfven wave damping from finite gyroradius coupling to the ion acoustic mode // Phys. fluids.—1970.—**13**, N 2.—P. 440—450.

Volokitin A. S., Dubinin E. M. Theturbulence of Alfven waves in the polar magnetosphere of Earth // Planet. Space Sci.—1989.—**37**, N 7.—P. 761—768.

Yukhimuk, A. K. Plasma phenomenons in geophysics. — Kiev: Naukova Dumka, 1982.—165 p.

Yukhimuk A. K., Kotsarenko N. Ya., Yukhimuk V. A. Nonlinear interaction of Alfven waves in solar atmosphere // Proc. 26th ESLAB Symp. Killarny, 16-19 June, Noordwijk. — 1992.—P. 337—341.

Yukhimuk V. A., Voitenko Yu. M., Fedun V. M., Yukhimuk A. K. Generation of kinetic Alfven waves by upper-hybrid pump waves // J. Plasma Physics.—1998.—**60**, N 3.—P. 485—495.

Космічна наука і технологія. ДОДАТОК. 2001. Т 7. № 2. С. 67—73.

ALFVEN WAVES IN SPACE PLASMAS: DISPERSIVE AND KINETIC EFFECTS

Yu. Voitenko[1,2], M. Goossens[1], A. Yukhimuk[2], A. Voytsekhovskaia[2]

[1]Centre for Plasma Astrophysics, Katholieke Universitet Leuven, Belgium

[2]Department of Space Plasma Physics, Main Astronomical Observatory, Golosiiv, Kyiv, Ukraine

New linear and nonlinear properties of Alfven waves induced by finite-ion-Larmor radius effects in space plasmas are discussed.

1. INTRODUCTION

An Alfven wave with a large transversal wave-vector component, $k_x \gg k_z$ ($k_\perp \perp B_0$, B_0 is the ambient magnetic field), when the perpendicular wavelength become comparable to the ion gyroradius ($\rho_i = V_{Ti}/\Omega_i$), is known as a kinetic Alfven wave (KAW) [10]. The linear dispersion relation for KAWs may be written as

$$\omega_k = |k_z| V_A K_k.$$

The dispersion function $K_k = K_k(\mu)$ has the following asymptotics:

$$K_k \approx 1 + \frac{1}{2}\left(\frac{3}{4} + \frac{T_e}{T_i}\right)\mu^2 \quad \text{for}\, \mu^2 \ll 1,$$

$$K \approx \left(1 + \frac{T_e}{T_i}\right)^{1/2} \mu \quad \text{for}\, \mu^2 \gg 1,$$

where $\mu = k_\perp \rho_i$.

KAWs have become known mainly because of the extensive investigations for their kinetic properties, which are important for processes of plasma heating and particles acceleration (see e.g. Hasegawa 1993 and references therein). It has been shown explicitly that finite-ion-gyroradius and electron-inertia effects produce E_z in Alfven waves, which brings about collisionless wave-particle resonant interaction, resulting in enhanced plasma heating and anomalous transport in the presence of kinetic Alfven waves.

Linear and nonlinear properties of KAWs play an important role in the dynamics of space plasmas. Examples are plasma heating [3, 30] and current drive [5] in the coronal loops of the solar atmosphere, instability of the interstellar plasma [25], particles acceleration in the galactic radio jets [2], impulsive plasma energization in solar flares [28, 29], plasma instability and wave turbulence in the Earth magnetosphere [35, 11], anomalous magnetic diffusion in coronal current layers [27], and many others. In fusion devices, the efficiency of the energy exchange between waves and plasma particles caused by kinetic properties of KAWs has been proved recently both by the theory and by experiment (see e.g. [15] and references therein).

In the present paper we concentrate on the new aspects of wave dynamics in space plasmas that are possible due to ion gyroradius effects in KAWs.

2. NONLINEAR INTERACTION AMONG KAWS

A dynamic equation governing the weak interaction between KAWs in a low (plasma has been derived using a plasma kinetic model [31, 32]). This allowed us to keep kinetic and dispersive finite ion Larmor radius corrections in the nonlinear dispersion relation for KAWs. The general expression for the coupling coefficient of the three-wave resonant interaction among KAWs with arbitrary values of the kinetic variable μ, has been calculated, and the growth rate and threshold amplitude of the KAW decay instability in a Maxwellian plasma have been obtained. In the limit $k_\perp \rho_i \ll 1$ we found the growth rate scaling prop prop $k_\perp^2$, more favourable for three-wave resonant decay than the scaling previously elaborated, $\propto k_\perp^3$. Note that only parallel propagation of interacting KAWs has been implicitly implied previously [6, 36, 39]. The first study of parametric KAW instability in the domain $k_\perp > \rho_i^{-1}$ is presented, where the same growth rate behaviour, $\propto k_\perp^2$ is found. These results show a growing efficiency of the three-wave interaction among Alfven waves with growing $k_\perp$.

Inverse and direct energy cascades, and Kolmogorov type spectra $W_k \propto k_z^{-1/2} k_\perp^{-4}$ and $W_k \propto k_z^{-1/2} k_\perp^{-3.5}$, may be formed in the $k_\perp < \rho_i^{-1}$ and $k_\perp > \rho_i^{-1}$ domains respectively by the interaction including parallel-propagating KAWs. The remarkable property of this interaction is spectral energy escaping out from the region $k_\perp \propto \rho_i^{-1}$. If the interaction including counter-streaming KAWs dominates, the turbulent energy always cascades into lower wavenumbers, forming $W_k \propto k_z^{-1/2} k_\perp^{-3.5}$ and $W_k \propto k_z^{-1/2} k_\perp^{-2}$ spectra in the limits $k_\perp > \rho_i^{-1}$ and $k_\perp < \rho_i^{-1}$. In contrast, entropy tends to concentrate at wavenumbers $k_\perp \propto \rho_i^{-1}$, resulting in $W_k \propto k_z^{-1/2} k_\perp^{-5}$ and $W_k \propto k_z^{-1/2} k_\perp^{-3}$ spectra.

Of critical significance for the energy and entrophy cascades and the resulting turbulent spectra is the type of three-wave interaction, as well as position of the source in k-space with respect to $k_\perp = \rho_i^{-1}$.

3. QUASISTEADY HEATING OF THE SOLAR CORONA: FLR EFFECTS IN ALFVEN WAVES

The physical mechanisms responsible for the heating of the solar corona still *lack* unambiguous identification. Resonant absorption and phase mixing (see [7] and references therein) are two popular theories of Alfven wave heating which involve spectral energy transfer towards small length-scales in the plane $\perp \mathbf{B}_0$. Both are due to the transversal plasma inhomogeneity, typical for the corona. The phase mixing of Alfven wave which leads to enhanced wave dissipation and consequent plasma heating, has been first proposed as a coronal heating mechanism by [12]. Since then, phase mixing has been studied in linear approximation both for closed and open magnetic configurations (see for recent papers [13] and [22]). There are also a few papers which concentrate on nonlinear effects in phase mixing [12], and resonant absorption [21]. But all these investigations have been carried out in the one-fluid MHD approximation, missing important properties of Alfven waves induced by FLR effects.

A significant input of energy into a plasma, as observed in the solar corona, can only be achieved if the launched waves have sufficiently large amplitudes. E. g., AWs can balance the energy loss from the loop structures of active regions and from coronal holes, if the wave magnetic field amounts to 1—5 % of background magnetic field B_0. The energy flux $F \sim 10^8$ erg cm^{-2}s^{-1} is required to heat active region coronal loops of $L \sim 5 \cdot 10^9$ cm length, where $T_e \approx T_i \approx 5 \cdot 10^6$ K [16]. Supposing that this energy flux is supplied by Alfven waves, and taking typical for coronal loops $B_0 = 100$ G and $V_A = 10^8$ cm/s, we get the wave amplitude $B_k/B_0 = 3.5 \cdot 10^{-2}$ and corresponding (non-thermal) plasma velocity $V_{pl} = 35 \cdot 10^5$ cm/s due to motion of plasma in the waves. It is interesting to note that the observed non-thermal broadening of spectral lines yields the same rms velocities [23]

$$V_{pl} = (25...45) \cdot 10^5 \text{ cm/s}.$$

The nonlinear effects become important for the waves of such amplitudes, and the ability of the waves to participate in the different kinds of nonlinear interaction have to be thoroughly examined.

In the coronal plasma with transversal ($\perp \mathbf{B}_0$) inhomogeneity of Alfven speed (scale $L_A \sim 10^6$ cm, see. [38]), the growth of transversal wavenumber $k_\perp \propto (\omega_k/L_A)t$ brings about a kinetic effect of Landau damping for $\omega_k \geq 1$ s^{-1}, or enhanced collisional dissipation for $\omega_k < 1$ s^{-1} [30]. Then the condition of effective wave dissipation over loop length L ($\geq 10^9$ cm), $\gamma_k^L \geq V_A/L$, is $\mu^2\omega_k \geq V_{Te}/L$. Such a waves becomes also nonlinearly unstable if $\gamma_k^{NL} \geq V_A/L$. We found that the condition for decay instability of KAWs, heating coronal loops, is satisfied in a wide frequency range $\omega_k < \omega_{cr}$, where

$$\omega_{cr} = 0.3(V_{Te}/\rho_i)(B_k/B_0).$$

Under typical coronal conditions $\omega_{cr} \approx 0.5 \cdot 10^6$ s^{-1}, and condition $\omega_k < \omega_{cr}$ covers the whole MHD spectrum. Therefore, the nonlinear spreading and turbulent character of Alfven wave spectra should be taken into account investigating plasma heating and current drive in coronal loops.

4. IMPULSIVE PLASMA HEATING IN SOLAR FLARES

One of the most intriguing discoveries of Yohkoh mission is impulsive heating of collisionless coronal plasma in solar flares. The heating mechanism incorporating intermediate turbulence of KAWs has been proposed by [28, 29]. The kinetic theory of the excitation of kinetic Alfven waves (KAWs) in the just-reconnected magnetic flux tubes above soft X-ray loops is further developed in the papers [33, 34]. Using linear and quasilinear theory, it is shown that the proton-beam-driven instability of KAWs provides an effective mechanism for the PB-kinetic energy conversion into the energy of wave turbulence in the coronal part of just-reconnected flaring loops. In the wide range of PB parameters, the distance of quasilinear relaxation ($\sim 10^6$ cm) is by several orders less than the typical length of a flaring loop (10^9—10^{10} cm), and KAW/beam energy flux partition ~ 1 after relaxation. The fast plasma heating by these KAWs provides the temperature and flux of escaping electrons enough to produce observed microwave emission from the loop leg and hard X-ray bremsstrahlung from the footpoints and loop top.

Let us estimate the saturation level of the KAW turbulence excited by proton beams in flaring loops [31]. Taking typical value for (linear) instability growth rate $\gamma_k^L/\omega_i = 500$ in flaring loop with magnetic field $B_0 = 100$ G, Alfven velocity $V_A = 10^8$ cm/s, and ion temperature $T_i = 5 \cdot 10^6$ K, we get the saturation level of wave amplitude in the source ($k_\perp \rho_i \leq 1$) region: $B_k^{(s)}/B_0 = 500$. The calculated from saturation level (non-thermal) velocity of wave motions, $V_{pl} = 50 \cdot 10^5$ cm/s, is 3 times smaller than $V_{pl} = 150$ km/s, observed at flare onset [1]. This discrepancy between the calculated and observed nonthermal velocity we consider as a significant indication that the turbulent cascade and concentration of KAW energy at lower wavenumbers occur in flaring loops. With spectrum $\propto (k_\perp)^{-2}$ we calculate the lower boundary of the inertial range, $k_{\perp min} = k_{s\perp}/3 \leq 0.7 \cdot 10^{-2}$ cm^{-1}, where the energy of KAW turbulence is concentrated.

5. SPECTRAL DYNAMICS AND TURBULENCE OF KAWS IN THE AURORAL MAGNETOSPHERE

Kinetic Alfven waves of a large amplitude $B_k/B_0 = 0.01...0.001$, propagating along the geomagnetic field lines in the auroral zones of the Earth's magnetosphere, have been observed by satellites at altitudes $h = (0.1...2) \cdot 10^4$ km on a background of large-scale field-aligned currents [9, 4]. Current-driven instability of KAWs can develop at altitudes $h = (2...4) \cdot 10^4$ km and excite the observed wave flux [35]. For the magnetospheric conditions at $h = 4 \cdot 10^9$ cm, where $\Omega_i \sim 10$ s^{-1}, $V_A \sim 10^8$ cm/s, $\rho_i \sim 2 \cdot 10^6$ cm, and $T_i = T_e$, the exciting waves have wavenumbers $k_\perp \rho_i \approx 0.5$, $k_\parallel \rho_i \approx 0.05$, and amplitudes $B_k/B_0 \approx 2.5 \cdot 10^{-3}$.

Using the above parameters, we found a growth rate of the parametric decay instability of these KAWs, propagating towards the Earth, $\gamma_k^{NL} \approx 0.025$ s^{-1} [31]. Since the decay growth time, $\tau_{NL} \approx 1/\gamma_k^{NL} \approx$ $\approx$ 40 s, is much less than Alfven wave propagation time, $\tau_A = \Delta h/V_A = 50...100$ s, we conclude that KAWs excited at the distant magnetosphere undergo parametric decay instability, and observed wave spectra should be modified by three-wave couplings among KAWs. The lowest frequency (of the anti-parallel-propagating KAW) is well above the decay growth rate, $\omega_2 \approx 0.5\mu^2\omega \approx 0.5$ s $\gg \gamma_k^{NL} \approx 0.025$ s^{-1}, and hence the weak-interaction approach is justified.

Let us consider spectral energy distributions in KAW turbulence [32]. Let some source in a distant magnetosphere pumps the energy into modes $k_\perp \propto k_{s\perp}$; this may be current-driven KAW instability, excited at altitudes $h = (2...4)\cdot 10^4$ km [35]. The turbulent KAW spectrum formed by three-wave $s_1 = -s_2 = 1$ interaction in the domain $k_{s\perp} < \rho_i^{-1}$ varies as $\propto (k_\perp)^{-2}$ in the vicinity of the source; the spectrum $\propto (k_\perp)^{-4}$, formed by $s_1 = s_2 = 1$ interaction, can appear at smaller wavenumbers, where $s_1 = -s_2 = 1$ interaction may be forbidden by finite correlation length of waves [32]. Then the tendency for turbulent KAW spectra is to become steeper, up to $\propto (k_\perp)^{-4}$, as a result of dominant role of $s_1 = s_2 = 1$ interaction at low wavenumbers. Also, since the growth rate of nonlinear interaction attains its maximum at $k_{2\perp} = 0.776k_{s\perp}$, the energy transfer is most efficient into modes concentrated around $(k_\perp)^{(1)} \propto 0.776k_{s\perp}$, $(k_\perp)^{(2)} \propto 0.776(k_\perp)^{(1)}$, and so on. As a result, the humps on the above-mentioned spectra appear at $k_\perp \propto (0.776)^n k_{s\perp}$, where $n = 1, 2, 3...$ is the decay (step) number.

All of these features of turbulent KAW spectra, following from our theoretical consideration, have been revealed by spacecraft observations [9, 4].

The general tendency for the KAW turbulence is energy concentration in the spectrum $\propto (k_\perp)^{-4}$ at low wavenumbers. Spectra $\propto (k_\perp)^{-4}$ have been often observed in the space plasmas with intense field-aligned currents [9, 18]. These observations supply strong evidence for the nonlinear spreading of spectra generated by the current-driven KAW instability at $k_{s\perp} \leq \rho_i^{-1}$ [35].

6. GENERATION OF KINETIC ALFVEN WAVES BY UPPER-HYBRID PUMP WAVES

It has been shown [19], that lower-hybrid waves can be generated as a result of UHW decay. Three-wave interaction including UHW has been considered in [17], [40], where pump wave was an ordinary electromagnetic wave. Parametric excitation of MHD (non-dispersive) Alfven (and /or magnetosonic) and electron-cyclotron waves has been considered in [26].

Taking into account perpendicular dispersion of KAW, caused by effects of finite ion Larmor radius and electron inertia, we examined a new channel for UHW decay, in which a pump UHW decays into another UHW and an ultra low-frequency wave, KAW: UHW → KAW + UHW [41].

We applied the results of our calculations to investigate a new way of KAW generation in the magnetosphere, where UHW is the most stable wave mode in the high-frequency region $\omega \gg \omega_{Be}$ (ω_{Be} — is an electron-cyclotron frequency): a high level of UHWs is continuously observed at the heights over 1000 km at all latitudes from the equator to the auroral zone [20]. Numerical calculations give sufficiently short times of the instability development:

$$\tau \cong \gamma_{NL}^{-1} \cong (0.1 \div 1) \text{ s}.$$

Taking into account that near the equator UHW emission enhancement is induced by the non-equilibrium electron velocity distribution in the transverse direction, KAW turbulence with $k_\perp \lambda_{De} \leq$ ≤ 0.35 will be generated as a result of the UHW decay. In the auroral regions where UHW generation is caused by field-aligned electron beams [37], parametric decay instability of such UHWs generates

turbulence of KAW with $k_{\perp}\lambda_{De} \leq 0.1$. That is why in the satellite system of co-ordinates, the typical frequencies of KAW turbulence near geomagnetic equator and in the auroral regions can be different. Kinetic Alfven waves generated by parametric instability will be dissipated by electron Landau resonance with consequent heating of the electron component, and, owing to electron-ion collisions, with heating of the ion component as well.

7. PARAMETRIC EXCITATION OF ELECTROMAGNETIC WAVES IN THE MAGNETISED PLASMA

The detection of the electromagnetic waves (EMWs) with a frequency slightly higher than the local electron Langmuir frequency in the Earth's magnetosphere has been reported by Gurnett and Shaw (1973). The satellite measurements [20] show that upper-hybrid waves (UHWs) are the most widespread electrostatic waves in the magnetosphere.

We considered the possible mechanism of the excitation of radio emission by UHWs via parametric decay UHW = EMW + KAW, where EMW can be ordinary (O-mode) or extra-ordinary (X-mode) electromagnetic wave [42]. First we estimate the instability growth rate and characteristic time for the case of UH pump wave decay into the ordinary electromagnetic wave and KAW. The instability growth rate attains its maximum value $\gamma_1 \approx 0.3\ s^{-1}$ at $k\perp/k_{0\perp} \approx -10$, where $k_{0\perp}$ is the perpendicular wave number of the pump wave. The minus sign here indicates that the exciting KAW propagate in the direction opposite to that of the pump wave. The characteristic time of instability development is $\tau_1 \approx 3$ s. The generation of KAWs and X-mode radiation in the perpendicular direction has been considered by [24], and the increment was found to be $\propto \Omega_e$. Since with the perpendicular O-mode the increment $\propto \omega_{pe}$, generation of the perpendicular O-mode is ω_{pe}/Ω_e times more efficient than perpendicular X-mode. The threshold of decay instability is $E_{cr} \propto 1$ mV/m.

The characteristic time of the instability development in the case of UH pump wave decay into the left-hand polarised electromagnetic wave and KAW is $\tau_2 \sim 0.3$ s. Thus, the decay including left-hand polarised electromagnetic wave is much faster than the decay including ordinary and X-mode electromagnetic waves.

This mechanism of electromagnetic emission can also work in the solar corona during radio bursts. Type III radio bursts are most interesting from the theoretical point of view. They are observed in the wide frequency range varying from tenth of kHz (satellite observations) up to hundreds of MHz while an emission source moves from the Sun to the Earth. Excited by high-energy particle beams, UHW can generate KAWs and electromagnetic emission with frequencies close to the UH frequency.

8. CONCLUSIONS

The results discussed in the present paper show that due to the FLR effects, Alfven waves can interact with proton beams, among themselves, and with other wave modes more effectively than it have been known previously.

The main new findings are:

1. The strongest nonlinear coupling among Alfven waves includes counter-propagating waves. It results in the spectral energy transfer into lower wavenumber domain in flares. The turbulent state should develop before KAWs flux is dissipated in the solar corona.

2. Kinetic Alfven turbulence, excited by the reconnection outflow, can result in the impulsive plasma energization in flaring loops.

3. Parametric decay of UHWs, induced by their coupling with KAWs, introduces spectral redistribution of the wave energy, and can excite EMWs in the vicinity of upper-hybrid frequency.

This work was supported in part by INTAS grant 96-530. Yu. Voitenko acknowledge the support by KUL through fellowship grant FWO G.0335.98, and by Ukrainian FFR grant 2.4/1003.

REFERENCES

1. Antonucci E., Dodero M. A. Temperature dependence of nonthermal motions in solar flare plasma // Astrophys. J.—1995.—**438**, N 1.—P. 480—490.
2. Bodo G., Ferrari A. Local coupling of surface MHD waves with kinetic Alfven waves in jets // Astron. and astrophys.—1982.—**114**, N 2.—P. 394—399.
3. de Azevedo C. A., Elfimov A. G., de Assis A. S. Coronal loop heating by Alfven waves // Solar Phys.—1994.—**153**, N 1-2.—P. 205—215.
4. Dubinin E. M., Volokitin A. S., Israilevich P. L., Nikolaeva N. S. Auroralelectromagnetic disturbances at altitudes of 900 km: Alfven wave turbulence // Planet. Space Sci.—1988.—**36**, N 7.—P. 949—962.
5. Elfimov A. G., de Azevedo C. A., de Assis A. S. Noninductive current generation by Alfven wave-electron interaction in solar loops // Phys. Scripta.—1996.—**63**, N 1.—P. 251—253.
6. Erokhin N. S., Moiseev S. S., Mukhin V. V. Decay instability of Alfven waves in a hot plasma // Sov. Phys. Plasma.—1978.—**4**, N 8.—P. 1172—1174.
7. Goossens M. Alfven wave heating // Space Sci. Rev.—1994.—**68**, N 1.—P. 51—61.
8. Gurnett D. A., Shaw R. R. Electromagnetic radiation trapped in the magnetosphere above the plasma frequency // J. Geophys. Res.—1973.—**78A**, N 34.—P. 8136—8149.
9. Gurnett D. A., Huff R. L., Menietti S. D., et al. Correlated Low Frequency electric and magnetic noise along the auroral field lines // J. Geophys. Res.—1984.—**A89**, N 38.—P. 8971—8995.
10. Hasegawa A., Chen L. Kinetic processes in plasma heating by resonant mode conversion of Alfven wave // Phys. Fluids.—1976.—**19**, N 5.—P. 1924—1930.
11. Hasegawa A., Chen L. Ring current instabilities in the magnetohydrodynamic frequency range // Ann. Geophysicae.—1992.—**10**, N 3.—P. 644—646.
12. Heyvaerts J., Priest E. R. Coronal heating by phase mixed shear Alfven waves // Astron. and Astrophys.—1983.—**117**, N 2.—P. 220—234.
13. Hood, D. Gonzalez-Delgado, J. Ireland Heating of coronal loops by phase-mixing // Astron. and Astrophys.—1997.—**324**, N 1.—P. 11—14.
14. Ireland J, Priest E. R. Phase-mixing in dissipative Alfven waves. // Solar Phys.—1997.—**173**, N 1.—P. 31—51.
15. Jaun A., Hellsten T., Appert K., et al. Kinetic Alfven Eigenmodes in a Hot Tokamak Plasma // Plasma Phys. Contr. Fusion.—1997.—**39**, N 3.—P. 549—556.
16. Kano R., Tsuneta S. Temperature distribution and energy scaling law of solar coronal loops // Publ. Astron. Soc. Japan.—1996.—**48**.—P. 535—543.
17. Kotsarenko N. Ya., Yukhimuk A. K., Yukhimuk V. A. Nonlinear interaction electromagnetic waves in space plasma // Kinematika i physika nebesnich tel.—1993.—**6**, N 2.—P. 46—52.
18. Labelle J., Treumann R. A. Plasma waves of the dayside magnetopause. // Space Sci. Rev.—1988.—**47**, N 2.—P. 175—182.
19. Murtaza G., Shukla P. K. Nonlinear generation of electromagnetic waves // J. Plasma Phys.—1984.—**31**, N 3.—P. 423—436.
20. Oya H., Morioka A., Kobayashi K., et al. Plasma wave observation and sounder experiments (PWS) using the Akebano (EXOS-D) satellite // J. Geomag. Geoelectr.—1990.—**42**, N 4.—P. 411—417.
21. Poedts S., Goedbloed J. P. Nonlinear wave heating of solar coronal loops // Astron. and Astrophys.—1997.—**312**, N 3.—P. 935—944.
22. Ruderman M. S., Nakariakov V. M., Roberts B. Alfven wave phase mixing in two-dimensional open magnetic configurations // Astron. and Astrophys.—1998.—**338**, N 3.—P. 1118—1124.
23. Saba J. L. R., Strong K. T. Coronal dynamics of a quiescent active region // Astrophys. J.—1991.—**375**, N 2.—P. 789—799.
24. Saleem H., Chaudhry M. B., Murtaza G., Shukla P. K. Generation of extraordinary mode radiation by an electrostatic pump // Phys. Fluids.—1985.—**28**, N 3.—P. 830—835.
25. Shukla P. K., Murtaza G., Yu M. Y. Finite Larmor radius effects on Alfven radiative thermal instability // Phys. Fluid.—1989.—**B1**, N 3.—P. 702—704.
26. Stenflo N., Shukla P. K. Generation of radiation by upper hybrid pump waves // J. Geophys. Res.—1995.—**100**, N A9.—P. 17261—17264.
27. Voitenko Yu. M. Anomalous magnetic diffusion in coronal current layers. // Solar Phys.—1995.—**161**, N 1.—P. 197—201.
28. Voitenko Yu. M. Flare loops heating by 0.1—1.0 MeV proton beams. // Solar Phys.—1996.—**168**, N 1.—P. 219—202.
29. Voitenko Yu. // Magnetic reconnection in the solar atmosphere / Eds R. D. Bentley, J. T. Mariska: ASP Conf. Ser.—1996.—**111**, N 2.—P. 312—315.
30. Voitenko Yu. M. Kinetic Alfven waves in the solar corona // Space plasma physics. — Kiev, NSAU, 1994.—P. 221—230.
31. Voitenko Yu. M. Three-wave coupling and parametric decay of kinetic Alfven waves // J. Plasma Phys.—1998.—**60**, N 3.—P. 497—514.
32. Voitenko Yu. M. Three-wave coupling and weak turbulence of kinetic Alfven waves // J. Plasma Phys.—1998.—**60**, N 3.—P. 515—525.
33. Voitenko Yu. M. Excitation of kinetic Alfven waves in a flaring loop // Solar Phys.—1998.—**182**, N 2.—P. 411—430.

34. Voitenko Yu. M. 1998 Impulsive flare plasma energization in the light of Yohkoh discoveries // The Hot Universe / Eds K. Koyama, S. Kitamoto, M. Itoh. — Kluwer, 1998.—P. 211—212.
35. Voitenko Yu. M., Kryshtal A. H., Malovichko P. P., Yukhimuk A. K. Current driven instability and generation of the Alfven waves in the Earth magnetosphere // Geomagnetism and aeronomy.—1990.—**30**, N 3.—P. 402—407.
36. Volokitin A. S., Dubinin E. M. The turbulence of Alfven waves in the polar magnetosphere of the Earth // Planet. Space Sci.—1989.—**37**, N 4.—P. 761—765.
37. Wahlund J.-E., Louarn P., Chust T., et al. On ion acoustic turbulence and the nonlinear evolution of kinetic Alfven waves in aurora // Geophys. Res. Lett.—1994.—**21**, N 17.—P. 1831—1834.
38. Woo R. Kilometre-scale structures in the Sun's corona // Nature.—1996.—**379**, N 1.—P. 321—326.
39. Yukhimuk A. K., Kucherenko B. P. Nonlinear interaction of kinetic Alfven waves // Kinem. Phys. Celest. Bodies.—1994.—**9**, N 1.—P. 33—38.
40. Yukhimuk A. K., Yukhimuk V. A. Parametric generations upper hybrid and ion-sound waves in space plasma // Kinematika i physika nebesnych tel.—1994.—**6**, N 3.—P. 67—74.
41. Yukhimuk A. K., Voitenko Yu. M., Fedun V. N., Yukhimuk V. A. Generation of kinetic Alfven wave by upper hybrid pump wave // J. Plasma Phys.—1998.—**60**.—P. 485—495.
42. Yukhimuk A. K., Yukhimuk V. A., Sirenko O. K., Voitenko Yu. M. Parametric excitation of electromagnetic waves in the magnetized plasma. // J. Plasma Phys.—1999.—**62**, N 1.—P. 53—64.

Космічна наука і технологія. ДОДАТОК. 2001. Т 7. № 2. С. 74—83.

UDC 533.951.8

THEORY OF LOW-SCALE MHD WAVES IN THE NEAR EQUATORIAL REGION OF THE EARTH PLASMASPHERE

O. S. Burdo[1], O. K. Cheremnykh[1], O. P. Verkhoglyadova[2]

[1]Space Research Institute NASU & NSAU (03022, Kyiv 22, Acad. Glushkova Avenue, 40)
[2]Taras Shevchenko National Kyiv University (03022, Kyiv 22, Acad. Glushkova Avenue, 6)

Study of low-scale MHD waves in the inner Earth magnetosphere was performed using the standard set of ballooning mode equations obtained naturally for finite pressure plasmas in general magnetic field geometries. Flute- and ballooning-type low-scale disturbances in the near equatorial plasmasphere where they may have maximum growth rates were studied. The ballooning mode stability condition was obtained, the wave excitation spectrum was investigated. Corresponding dispersion equations for low-frequency wave modes were formulated and analysed. Dependencies of eigenfrequencies and growth rates on plasma pressure and McIlwain parameter were discussed.

INTRODUCTION

Our approach to the low-scale MHD disturbances is based on the dipole model of the geomagnetic field sketched on Figure 1. This field with the components

$$B_\theta = \frac{M\cos\theta}{r^3}, \qquad B_r = -\frac{2M\sin\theta}{r^3}$$

and with module

$$B = \frac{M\sqrt{a(\theta)}}{r^3},$$

where $a(\theta) = 1 + 3\sin^2\theta$, M — the Earth's magnetic dipole moment.

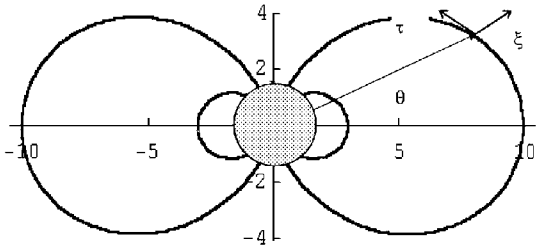

Fig. 1. Sketch of the dipole geomagnetic field geometry

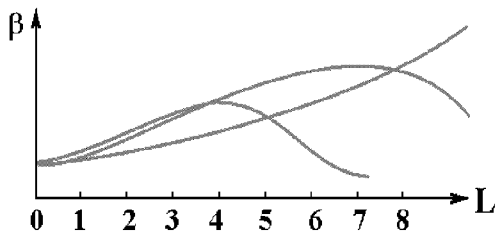

Fig. 2. Different possible radial dependencies of plasma β

Figure 2 represents the characteristic radial dependencies of β which is the ratio of the gas-kinetic plasma pressure to the magnetic one. It results from the most general reasons, the β is higher the plasma energy power is higher and its ability to deform the magnetic field equilibrium configuration containing the plasma is higher. Maxima of the presented curves are of the order of unit, so β is not in the least a small value. At the same time it must be noted that the generally accepted results were derived predominatly for the case of plasma with $\beta \ll 1$. So the aim of this work is to extend the derived results on the finite β domain.

THE BALLOONING MODES EQUATIONS

To obtain the required ballooning equations which we are interested in one can start from ballooning-type equations in the magnetic field of arbitrary configuration, as it was provided in [1] and [4]. Also one can start from the linearized MHD equations for the plasma volume element displacement, as it was done in [2] and [5]. The principal fact is that either approach leads to the same system of equations. After the transformation to the dimensionless form which was used in [6] this system has the form:

$$\Omega^2\hat{\xi} + \frac{4}{a(\theta)\cos^4\theta}\left(\frac{\alpha\beta}{\gamma}\hat{\xi}+F\right) + \frac{a(\theta)}{\cos^{13}\theta}\frac{d}{d\theta}\left[\frac{1}{a(\theta)\cos\theta}\frac{d\hat{\xi}}{d\theta}\right] = 0, \tag{1}$$

$$\Omega^2\hat{\tau} + \frac{1}{\cos^7\theta}\frac{dF}{d\theta} = 0, \tag{2}$$

where

$$F = \frac{\beta\cos^2\theta}{a(\theta)+\beta\cos^{12}\theta}\left\{\cos^3\theta\frac{d\hat{\tau}}{d\theta} - \frac{2\sin\theta\cos^2\theta}{a(\theta)}[4+5a(\theta)]\,\hat{\tau} - \frac{4\hat{\xi}}{a(\theta)}\right\}, \tag{3}$$

$\alpha = -(L/p)dp/dL$ is the dimensionless pressure gradient. System of Equations (1)—(2) complemented by corresponding uniform boundary conditions at the upper ionosphere border $r(\theta) = 1$ (we consider ionosphere to be an ideal conductor) is the boundary eigenvalue problem. If we solve this problem we define it's eigenfrequencies or growth rates of aperiodic solutions and corresponding eigenfunctions.
The equations forming this system are the linear differential equations with the variable coefficients, so there is no hope to solve this eigenvalue problem analytically. This problem may be solved only by applying some numerical method. Such approach enables us to derive any desired eigenvalue dependencies (i. e. squared eigenfrequencies or squared growth rates) upon the parameters but it has not desirable predicting features.

Therefore, it seems absolutely necessary to enunciate a simpler problem, in a certain sense similar to the original one, which will permit the analytical solution.

NEAR-EQUATORIAL REGION AND CONSTANT COEFFICIENT PROBLEM

The most natural simplification for the original system (1)—(2) is the conversion from the variable coefficients to the constant ones. On the strength of the reasons of symmetry let us take their values at $\theta = 0$, i. e. in the geomagnetic equatorial plane. After the substitution of F into the Equations (1) and (2), calculating of all the necessary derivatives and taking coefficient values at zero we will obtain the system of equations with the constant coefficients

$$\beta\frac{d^2\hat{\tau}}{d\theta^2} + [\Omega^2(1+\beta) - 18\beta]\,\hat{\tau} - 4\beta\frac{d\hat{\xi}}{d\theta} = 0, \tag{4}$$

$$\frac{d^2\hat{\xi}}{d\theta^2} + \left[\Omega^2 + 4\frac{\alpha\beta}{\gamma} - 16\frac{\beta}{1+\beta}\right]\hat{\xi} + 4\frac{\beta}{1+\beta}\frac{d\hat{\tau}}{d\theta} = 0. \tag{5}$$

This system of equations is good enough approximation of the original system (1)—(2) at close to zero values θ. Is it possible to adduce the meaningful physical interpretation for such a task? It is possible if we find the near-equatorial region with the physically essentially different properties. The radiation belt of the Earth may be considered as such region. Indeed, in the radiation belt the β values (β is the ratio of gaskinetic plasma pressure to the pressure of the magnetic field) multifoldly preponderate over β outside the belt. Moreover, the advanced β leads to the advanced gaskinetic pressure gradient α, which, as will be shown below, affects decisive the stability of the disturbances under consideration. During the

Solar activity elevation periods high-energy particle concentration increases exactly within the radiation belts. As for our problem such growth of concentration means the highly essential increase of β and α, which gives rise swing and transformation into unstable modes of low-scale waves.

With the boundary conditions on the radiation belt border we may expect that such a problem may be applicable to description of the low-scale disturbances. Furthermore, the properties of constant coefficient problem (4)—(5) solutions may be the desirable starting point for the interpretation of the original problem (1)—(2) solutions.

One may make sure that the system (4)-(5) has the nontrivial solutions

$$\hat{\tau}(\theta) = \begin{cases} \tau_0 \sin\mu_k\theta, & \text{even } k, \\ \tau_0 \cos\mu_k\theta, & \text{odd } k, \end{cases} \qquad \hat{\xi}(\theta) = \begin{cases} \xi_0 \cos\mu_k\theta, & \text{even } k, \\ \xi_0 \sin\mu_k\theta, & \text{odd } k, \end{cases} \tag{6}$$

with the boundary conditions

$$\frac{d\hat{\tau}}{d\theta}(\pm\theta_0) = 0, \hat{\xi}(\pm\theta_0) = 0, \tag{7}$$

where $2\theta_0$ is the angular size of the advanced β domain, and also

$$\hat{\tau}(\theta) = \begin{cases} \tau_0 \cos\mu_k\theta, & \text{even } k, \\ \tau_0 \sin\mu_k\theta, & \text{odd } k, \end{cases} \qquad \hat{\xi}(\theta) = \begin{cases} \xi_0 \sin\mu_k\theta, & \text{even } k, \\ \xi_0 \cos\mu_k\theta, & \text{odd } k, \end{cases} \tag{8}$$

with the boundary conditions

$$\hat{\tau}(\pm\theta_0) = 0, \qquad \frac{d\hat{\xi}}{d\theta}(\pm\theta_0) = 0, \tag{9}$$

where $\mu_k = \dfrac{\pi}{2\theta_0}$, $k = 0, \pm1, \pm2, \ldots$

(It is necessary to note that the system (4)—(5) with the simplest Dirichlet boundary conditions

$$\hat{\tau}(\pm\theta_0) = 0, \qquad \hat{\xi}(\pm\theta_0) = 0 \tag{10}$$

has not nontrivial solutions at all - their existence is precluded by the $d\hat{\xi}/d\theta$-consistent term in the $\hat{\tau}(\theta)$-equation and $d\hat{\tau}/d\theta$-consistent term in the $\hat{\xi}(\theta)$-equation).

DISPERSION EQUATION AND ITS SOLUTIONS

The condition of the existence of nontrivial solutions (its physical sense — the dispersion relation) has almost the same form for both variants of the boundary conditions:

$$[\Omega^2(1+\beta) - 18\beta - \beta\mu_k^2]\left[\Omega^2 - \mu_k^2 + 4\frac{\alpha\beta}{\gamma} - 16\frac{\beta}{1+\beta}\right] - 16\frac{\beta^2\mu_k^2}{1+\beta} = 0. \tag{11}$$

Let us explain the sense of this assertion. Equation (11) with respect to Ω^2 always has two solutions. Meantime the $k = 0$ case (accordingly to $\mu_k^2 = 0$) needs the special consideration. In fact, for the boundary conditions (7) at $k = 0$ we obtain the solutions

$$\hat{\tau}(\theta) \equiv \tau_0 \neq 0, \qquad \hat{\xi}(\theta) \equiv 0. \tag{12}$$

After their substitution into the constant coefficients system (4)—(5) we obtain the condition

$$\Omega^2(1+\beta) - 18\beta = 0 \tag{13}$$

from the $\hat{\tau}$-equation, while the $\hat{\xi}$-equation is satisfied identically. In the same way for the boundary conditions (9) and solutions

$$\hat{\tau}(\theta) \equiv 0, \qquad \hat{\xi}(\theta) \equiv \xi_0 \neq 0 \tag{14}$$

one can obtain the condition

$$\Omega^2 + 4\frac{\alpha\beta}{\gamma} - 16\frac{\beta}{1+\beta} = 0. \tag{15}$$

The solutions of the eigenproblem (4)—(5) with boundary conditions (7) and (9) at $k = 0$ have a common property: all the solutions are the identical constants and are absolutely independent of the variable θ, i. e. they are the purely flute solutions. At $k \neq 0$ the dependencies on θ are essential, so the corresponding solutions are the ballooning ones.

Considering the latter remark about dispersion relations which result from the constant coefficient system (4)—(5) solvability, one may say:

— for the ballooning eigenfunctions satisfying both boundary conditions (7) and (9) the dispersion relation (11)

$$[\Omega^2(1+\beta) - 18\beta - \beta\mu_k^2]\left[\Omega^2 - \mu_k^2 + 4\frac{\alpha\beta}{\gamma} - 16\frac{\beta}{1+\beta}\right] - 16\frac{\beta^2\mu_k^2}{1+\beta} = 0.$$

is valid at the nonzero k and Ω^2 has two roots;

— for the flute eigenfunctions the dispersion equations are different for different boundary conditions, namely:

for the boundary conditions (7)

$$\Omega^2 = 18\frac{\beta}{1+\beta}, \tag{16}$$

is valid; for the boundary conditions (9)

$$\Omega^2 = 16\frac{\beta}{1+\beta} - 4\frac{\alpha\beta}{\gamma}, \tag{17}$$

is fulfilled and Ω^2 has only one root.

Thereby, the set of dispersion equation solutions in a (β, Ω^2) plane consists of the only flute curve (16) or (17) (depending on boundary conditions) and of the infinite set of the ballooning curves pairs — for every nonzero k. These curves behaviour is demonstrated by Figure 3. The bold-typed curves are the ballooning solutions pair corresponding to $k = 3$, the upper thin curve is the flute solution for the boundary conditions (7), the lower one — for the conditions (9). It was noted that the ballooning dispersion equation solutions are completely identical for the both kinds of boundary conditions.

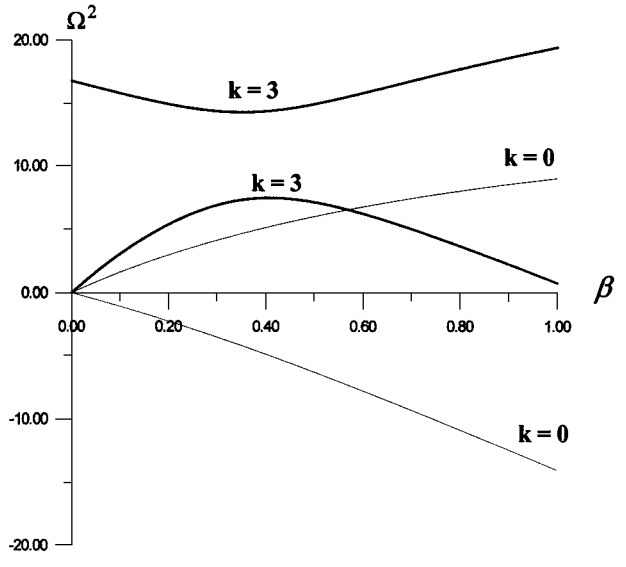

Fig. 3. β-dependent squared dimensionless eigenfrequencies Ω^2 (constant coefficients problem)

THE STABILITY OF FLUTE AND BALLOONING DISTURBANCES

Study of stability of disturbances under consideration is of a special interest. Indeed, Ω^2 in Equations (1)—(2) arises from time dependency of the form $\exp(-i\Omega t)$ when the Fourier method is used. It is obvious that the obtained solutions will not increase with time only under condition $\Omega^2 \geq 0$, otherwise the factor $\exp(\Omega_i t)$ where $\Omega_i = \mathrm{Im}(\Omega)$ will approve itself.

As to flute disturbances the stability question may be solved without any difficulties. For the boundary conditions (7) we have

$$\Omega^2 = 18\frac{\beta}{1+\beta} \geq 0, \tag{18}$$

i. e., the flute solutions are absolutely stable. For the boundary conditions (9) the stability criterion will have the form

$$\alpha \leq \frac{4\gamma}{1+\beta}, \tag{19}$$

and in the ultimate case of very small β it descends into classical flute disturbances stability criterion (note, that isentropic exponent value is $\gamma = 5/3$).

$$\alpha \leq 20/3.$$

To obtain the ballooning disturbances stability criterion it is necessary to write down the conditions of dispersion equation (11) solutions reality which sooner or later can be expressed in the form

$$\alpha \leq \frac{\mu_k^2}{\beta}\frac{\gamma}{4} + \frac{4\gamma}{1+\beta}\frac{1}{1+\mu_k^2/18}. \tag{20}$$

It must be noted that in the ultimate case $\mu_k^2 = 0$ expression (20) coincides with the condition of flute disturbances stability for the boundary conditions (9). It is also evident that at small enough β the ballooning disturbances are stable because with decrease of β the restrictions for α become more and more weak. It results from the monotonous increase μ_k^2 with increasing k that the k is higher, the mode is more stable. The β-dependent flute and ballooning modes growth rates behaviour is shown on Figure 4, where the thin curve corresponds to a flute disturbance (boundary conditions (9)) and the bold-typed curve corresponds to a ballooning one (incidentally $\alpha > 20/3$.

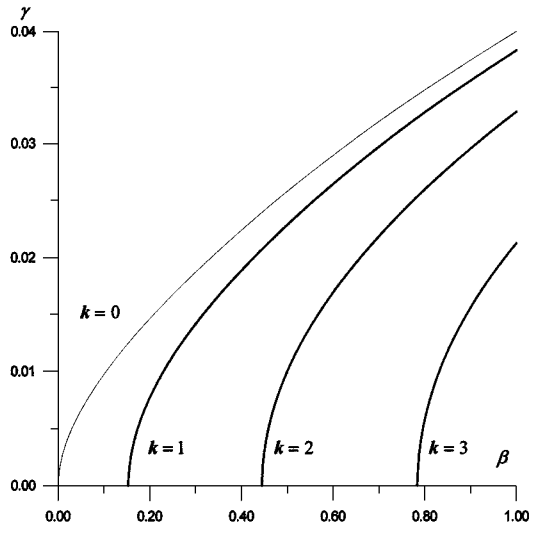

Fig. 4. β-dependent flute mode growth rate ($k = 0$) and ballooning mode growth rates ($k = 1, 2, 3$) (constant coefficients problem)

THE ANALYSIS OF NEAR-EQUATORIAL DISTURBANCES SPECTRUM

Let us study the features of dispersion equation (11) solutions at $k \neq 0$. If we eliminate the term $16\beta^2\mu_k^2/(1+\beta)$ from the dispersion equation then the residuary equation is factorised and has the solutions

$$\Omega^2 = (\mu_k^2 + 18)\frac{\beta}{1+\beta} \tag{21}$$

and

$$\Omega^2 = \mu_k^2 + 16\frac{\beta}{1+\beta} - 4\frac{\alpha\beta}{\gamma}, \tag{22}$$

which are shown on Figure 5 by the dotted lines: the branch (21) corresponding to slow magnetic sound $\Omega^2_{MS}(\beta)$ monotonously increases and the branch (22) corresponding to poloidal shear Alfven mode

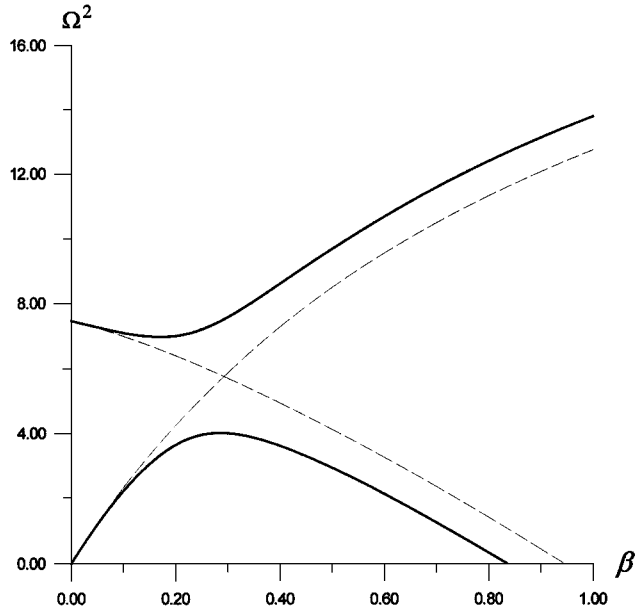

Fig. 5. β-dependent squared dimensionless eigenfrequencies Ω^2 for the complete dispersion equation (bold-faced curves) and for the «truncated» dispersion equations (dotted curves) (constant coefficients problem)

$\Omega^2_A(\beta)$ monotonously decreases. Both these branches intersect at β_0 which equals to

$$\beta_0 = \frac{1}{12\alpha}\sqrt{(6\alpha+5)^2 + 60\alpha\mu_k^2} - (6\alpha+5), \tag{23}$$

and

$$\Omega^2(\beta_0) = \Omega^2_A(\beta_0) = \Omega^2_{MS}(\beta_0) = (\mu_k^2 + 18)\frac{\beta_0}{1+\beta_0}. \tag{24}$$

The dispersion equation (11) derived above describes the effect of coupling slow nagnetosonic and poloidal shear Alfven waves. It is well-known [3] that the small disturbances of the dispersion equations eliminate the degeneration first of all exactly near the intercection of the branches of oscillations. As such disturbance the term $-16\beta^2\mu_k^2/(1+\beta)$ may be considered which leads to the gap between the upper and lower branches in the k-th mode oscillation spectrum (Figure 5, bold-typed curves). The width of this gap at $\beta = \beta_0$ equals to

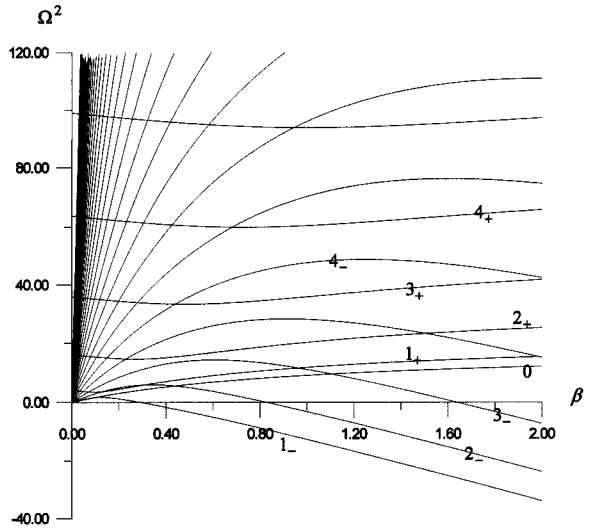

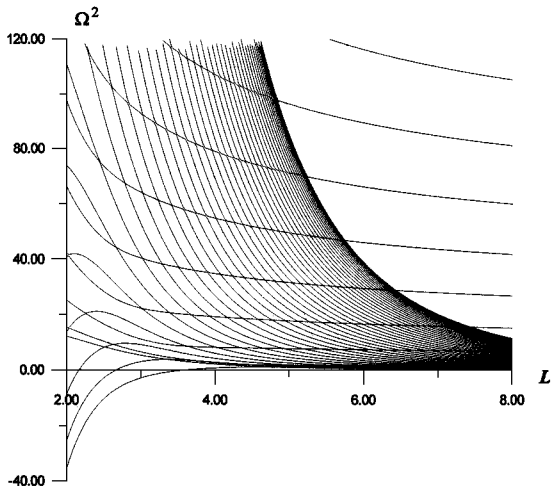

Fig. 6. β-dependent squared dimensionless eigenfrequencies Ω^2 (constant coefficients problem)

Fig. 7. McIlwaine parameter L dependent squared dimensionless eigenfrequencies Ω^2 (constant coefficients problem)

$$\Delta\,\Omega^2(\beta_0) = 8\,\mu_k^2\,\frac{\beta_0}{1+\beta_0}.$$

If we write explicitly the dispersion equation (11) solutions $\Omega_+^2(\beta)$ and $\Omega_-^2(\beta)$ — the upper and lower bold-typed curves on Figure 5 accordingly, one may see for oneself that the solutions behave at $\beta = 0$ as follows:

$$\Omega_+^2(0) = \mu_k^2,\ \frac{d\Omega_+^2}{d\beta}(0) = 4(4 - \alpha/\gamma) \tag{25}$$

and

$$\Omega_-^2(0) = 0,\ \frac{d\Omega_-^2}{d\beta}(0) = \mu_k^2 + 18, \tag{26}$$

and at $\beta \to \infty$ as

$$\Omega_+^2(\beta) \to \mu_k^2 + 18 \tag{27}$$

and

$$\Omega_-^2(\beta) \to \mu_k^2 + 16 - 4\,\frac{\alpha}{\gamma}\beta. \tag{28}$$

Let us now look at the fragment of the spectrum of problem (4), (5), (7). It is shown on Figure 6. The numerical solution of the generalised eigenvalue problem which is the finite-difference approximation of the initial problem is presented here. The curves corresponding to the k-th mode are marked by $k_\pm$ so the sign «plus» means the upper branches $\Omega^2{}_+(\beta)$ and the sign «minus» means the lower ones $\Omega_-^2(\beta)$. The obtained spectrum may be easily interpreted as a set of multitude pairs (in general, infinite) of curves, one of them is shown on Figure 5.

If we are interested in eigenfrequency spatial dependency then using the fact that β depends on McIlwain parameter L employed in our model we can obtain the L-dependent squared dimensionless frequencies which are shown on Figure 7 and the same dependence of dimensional frequencies $f(L)$ which are shown on Figure 8.

We can see that on all three latter Figures 6, 7, and 8, where the dependencies $\Omega^2(\beta)$, $\Omega^2(L)$ and

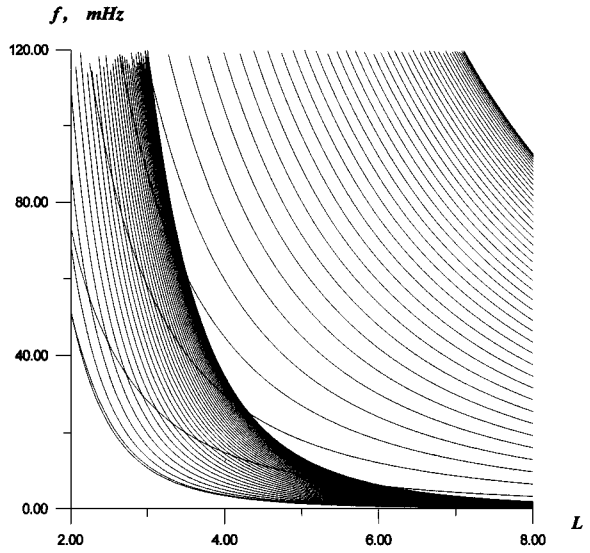

Fig. 8. McIlwaine parameter L dependent dimensioned eigenfrequencies f (constant coefficients problem)

$f(L)$ are shown, the spectrum consists of two families of branches. Let us consider the $\Omega^2(\beta)$ dependence. The ballooning component of spectrum consists of the family $\Omega^2_+(\beta)$, which has not any common point and of families $\Omega^2_-(\beta)$, which have the only one common point — limiting point — the origin of coordinates. At the same time curves pertaining to the different families have the manifold crossing-points (the same is true for the spectra on Figures 7 and 8).

ORIGINAL PROBLEM SPECTRUM

Meantime, it would be useful to search the dispersion equation (or the system of differential equations (4)—(5)) disturbance which is able to remove the degeneration near the points of the branch crossings. We have a chance to jump out the non-common state case by perturbing the system (4)—(5) coefficients. Actually, the non-simplified system spectrum with θ-dependent coefficients (1)—(2) has the form shown on Figures 9 and 10.

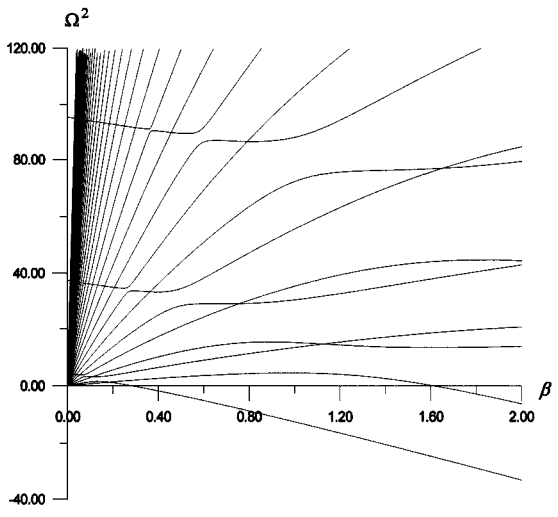

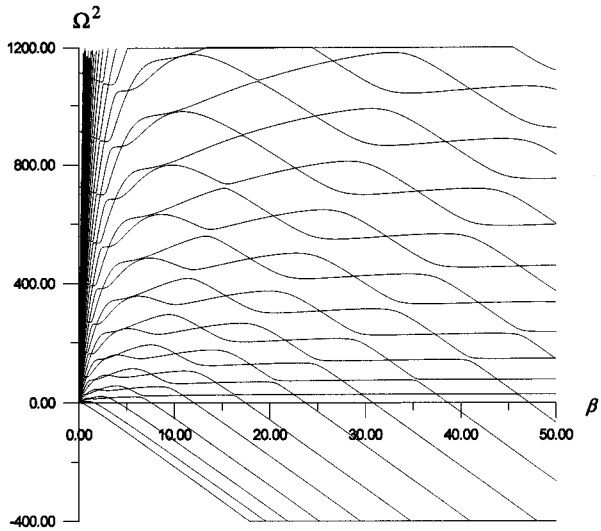

Fig. 9. β-dependent squared dimensionless eigenfrequencies Ω^2 (variable coefficients problem)

Fig. 10. β-dependent squared dimensionless eigenfrequencies Ω^2 (variable coefficients problem)

One can see that the part of branch crossings is splitted and another part is not splitted. The ballooning modes are subdivided into the branch pairs which interact between themselves but do not interact with the components of another pairs. One can see very well the deflected gaps — the ways from infinite β to the origin of coordinates without crossings with any branch of the spectrum.

We will try to explain such a behaviour of the spectrum. Let us simplify original problem again but by the less thoroughgoing way then before. Let us present the system of equations (1)—(2) in the form:

$$\begin{aligned} \Omega^2 F(\theta)\,\hat{\tau} &= A(\theta)\,\hat{\tau}'' + B(\theta)\,\hat{\tau}' + C(\theta)\,\hat{\tau} + D(\theta)\,\hat{\xi}' + E(\theta)\,\hat{\xi}, \\ \Omega^2 f(\theta)\,\hat{\xi} &= a(\theta)\,\hat{\xi}'' + b(\theta)\,\hat{\xi}' + c(\theta)\,\hat{\xi} + d(\theta)\,\hat{\tau}' + e(\theta)\,\hat{\xi}. \end{aligned} \tag{29}$$

Let us replace all its coefficients noted as $K(\theta)$ by $K(\theta;\sigma)$ where

$$K(\theta;\sigma) = (1-\sigma)\,K(0) + \sigma\,K(\theta). \tag{30}$$

It is clear, that at $\sigma = 0$ we obtain the constant coefficient system (4)—(5) and at $\sigma = 1$ we obtain the original one (1)—(2). We have complete information concerning the system (4)—(5) solutions because they can be obtained analytically, the original system (1)—(2) solutions can be obtained only numerically.

Let us attempt to solve the boundary eigenvalue problem with very small but positive σ. On the one hand, the presence of the nonzero σ which perturbs the constant coefficients is sufficient for the elimination of degeneration. On the other hand, such solutions and consequently the spectrum will slightly differ from the solutions and spectrum of problem with constant coefficients.

The spectrum of the problem with perturbed (lightly variable) coefficients ($\sigma = 0.01$) is shown on Figure 11. Let us enumerate the clearly visible branch splittings: 5_+ and 9_-, 5_+ and 7_-, 4_+ and 8_-, 4_+ and 6_-, 3_+ and 5_-, 2_+ and 4_- (twice). The assumption that splitting occurs at branch m_+ with branch $(m + 2l)_-$, $l = 1, 2,...$ crossing points seems to be verisimilar hypothesis. But why do the modes engage one another with step equal to two and why don't the adjoining modes interact? Let us decompose all the coefficients of system (29) into the Fourier series. If we go through this we will reveal that all the even coefficients are decomposable by cosines either by even powers or by odd powers and the odd

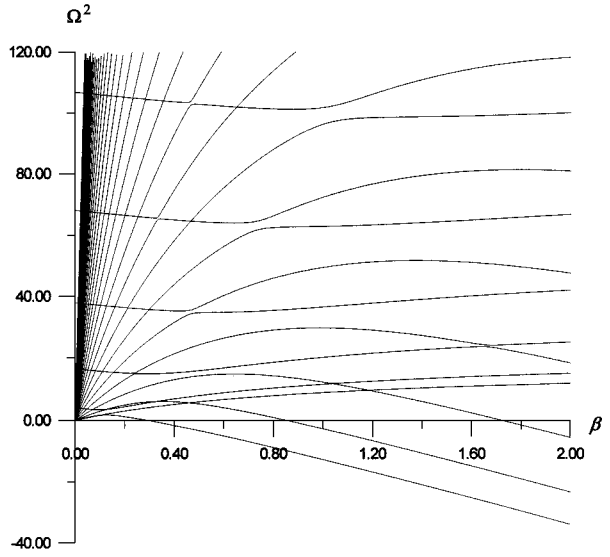

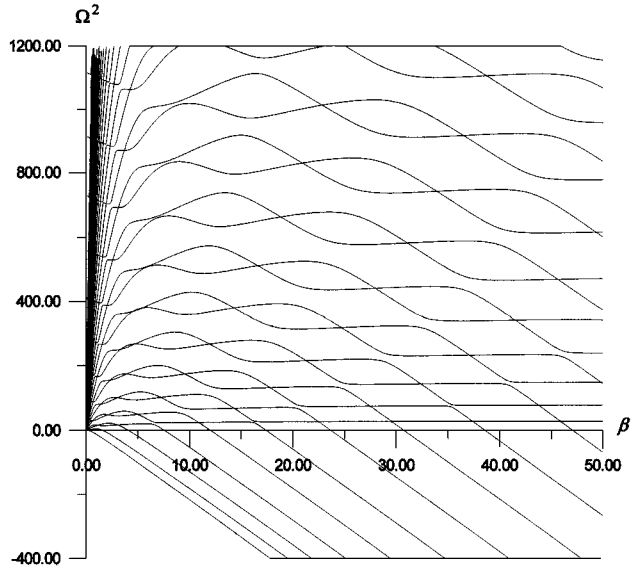

Fig. 11. β-dependent squared dimensionless eigenfrequencies Ω^2 (lightly variable coefficients problem, $\sigma = 0.01$)

Fig. 12. β-dependent squared dimensionless eigenfrequencies Ω^2 (variable coefficients Dirichlet problem (10))

coefficients are decomposable by sines of the same powers. This fact turns out to be forcible argument for the efforts to confirm the rule for the splitting and to estimate σ-dependent splitting parameter. Since the centres of global gaps pass through the crossing points of the splitted branches one can attempt to obtain them, at the least numerically. The successful realization of this scenario offers a valid explanation to the reason of (see Figure 10) why the initial problem spectrum has resolved into the set of disjoint «queues».

It might help in the interpretation of the original problem spectrum with Dirichlet-type boundary conditions (10)

$$\hat{\tau}(\pm\theta_0) = 0,$$
$$\hat{\xi}(\pm\theta_0) = 0,$$

which seem to be very natural but do not permit to simplify the original system. Figure 12 shows that the Dirichlet boundary conditions problem spectrum is similar enough to the boundary conditions (7) problem spectrum.

CONCLUSIONS

The system of equations which describes the MHD waves development in the dipole magnetic field was obtained there.

The system obtained was used for the description of disturbances in the near-equatorial region of plasmasphere.

It was noted that such disturbances first of all must occur at the radiation belts.

It was shown that advanced plasma pressure leads to the essential modification of spectrum:

— maghetosonic oscillation branch appears;

— unstable flute and ballooning modes appear.

It was shown that flute instability growth rate preponderate over the ballooning instability ones.

The flute mode and ballooning modes stability criterion was derived for the case of pressure which is not small.

There was obtained the β-dependent and L-dependent spectra of MHD modes suitable for the whole magnetic force line not only in the near-equatorial region.

It was shown that oscillation spectrum contains the gaps between magnetosonic modes and poloidal shear Alfven ones.

A lot of local gaps resulting from elimination of degeneration at non-constant coefficients of equations and the global gaps in the β-space were described.

REFERENCES

1. Burdo O. S., Cheremnykh O. K., Verkhoglyadova O. P. Study of Ballooning Modes in the Near Equatorial Region of the Earth Plasmasphere // Ukrainian J. Physics.—2000.—**45**, N 7.—P. 803—811 (in Ukrainian).
2. Burdo O. S., Cheremnykh O. K., Verkhoglyadova O. P. Study of ballooning modes in the inner magnetosphere of the Earth // Izvestiya Akademii nauk. Ser. Fizicheskaya.—2000.—**64**, N 9.—P. 1897—1901 (in Russian).
3. Lifshitz E. M., Pitayevskij L. P., Physical kinetics (Ser. Theoretical physics). — Moscow: Nauka, 1979.—Vol. 10 (in Russian).
4. Burdo O. S., Cheremnykh O. K., Verkhoglyadova O. P. Ballooning modes instability in the space plasmas. // Proc. 1998 Int. Congress on Plasma Physics, Praha, 23 June—3 Jule, 1998.
5. Burdo O. S., Cheremnykh O. K., Verkhoglyadova O. P. Theory of low-scale MHD waves in the inner magnetosphere of the Earth. // Proc. of Intern. Symp. From solar corona through interplanetary space, into Earth prime s magnetosphere and ionosphere: Interball, ISTP satellites, and ground-based observation, 1-4 February, 2000, Kyiv.
6. Cheng C. Z., Chang T. C., Lin C. A., Tsai W. H. // J. Geophys. Res.—1993.—**98**.—P. 11339.

Космічна наука і технологія. ДОДАТОК. 2001. Т 7. № 2. С. 84—88.

UDC 530.145

POSSIBLE PECULIARITIES OF SYNCHROTRON RADIATION IN STRONG MAGNETIC FIELDS

B. I. Lev[1], A. A. Semenov[1], C. V. Usenko[2]

[1]Institute of Physics, NAS of Ukraine, 46, Nauky pr., Kiev 03022, Ukraine
[2]Taras Shevchenko Kiev University, Physical Department, 6, Academician Glushkov pr., Kiev 03127, Ukraine

Relativistic quantum effects on physical observables of scalar charged particles are studied. Possible peculiarities of their behavior that can be verified in an experiment can confirm several fundamental conceptions of quantum mechanics. For observables independent of charge variable, we propose the relativistic Wigner function formalism that contains explicitly the measurement device frame. This approach can provide the description of charged particles gas (plasma). It differs from the traditional one but is consistent with the Copenhagen interpretation of quantum mechanics. The effects that are connected with this approach can be observed in astrophysical objects, i.e., neutron stars.

INTRODUCTION

The wave function nature has been considered as philosophical rather than physical question for a long time. However, it is very actual now because of the recent theoretical and experimental progress in quantum information [12].

In 1980, the specific behavior of the quantum systems that are described by the Einstein — Podolsky — Rosen (EPR) paradox was confirmed in an experiment [1]. It is very important that EPR correlation «distributes» in a space instantly. Nevertheless, if one adheres to the Copenhagen interpretation, there is no a casualty principle breaking.

In contrast, if one can try to hold an objective and deterministic description of quantum mechanics, then classical understanding of the casualty principle should be broken, because of the conflict between quantum mechanics and special relativity [2], [6]. In [4] the relativistic classical and quantum mechanics that generalizes the casualty principle was constructed. Such an approach follows from the Eberhard and Bell idea that correct description of quantum mechanics should contain a preferred frame.

This theory has a well definite position operator. In the preferred frame it coincides with the Newton — Wigner coordinate [7]. It means that measurement of the coordinate does not create a particle-antiparticle couple because there is no an odd part.

Hence, it is very important to find situations when the odd part of the position operator could manifest itself. However, unfortunately, such experiments are very difficult on the Earth because of necessity of a very strong field. There are such fields near the astrophysical objects, i.e., neutron stars. Therefore, it is interesting to find how the odd part of the position operator can influence the observable variables in a multy-body system (in a gas of charged particles or plasma).

The Wigner function formalism [14] is a convenient method to describe such systems. However, there are several problems of generalization for the relativistic case. The first problem is that the time is not a dynamic variable in the Weyl rule. In [5] this problem was solved by the generalization of the spatial integration over the whole space-time domain. The Wigner function formulated in a framework of the stochastic interpretation of quantum mechanics is also the Lorentz invariant [10].

Formalism of the matrix-valued Wigner function for spin S particles was developed in [8] by usual Weyl rule. Certainly, such equations are not the Lorentz invariant.

Next problem is the absence of well-defined position operator. In [13] the Wigner function formalism was developed by using the Newton — Wigner coordinate. The results of this approach differ

from the standard one. However, one can connect them with [4] where the correct definition of the position operator is possible.

The aim of this work is a formulation of the Wigner formalism for scalar charged particles in the approach [8]. In addition we try to find several peculiarities of the behavior of relativistic quantum system including the cases with the complicated structure of the position operator.

WIGNER FUNCTION FOR A FREE PARTICLE

To develop the Wigner function formalism one needs to formulate the Weyl rule. Following [8] one should take into account that classical variables are matrixes. However, we restrict ourselves with those proportional to the identity matrix. For a convenience we shall use the Feshbach — Villars representation [7]. The Weyl rule is defined by usual way:

$$A_\alpha^\beta = \int A(p, q)\hat{W}_\alpha^\beta(p, q)dpdq,$$

where $\alpha, \beta = \pm 1$, $A(p, q)$ is the classical variable, $\hat{A}_\alpha^\beta$ is the corresponding classical variable, $\hat{W}_\alpha^\beta$ is the density operator that can be presented by the displacement operator:

$$\hat{W}_\alpha^\beta(p, q) = \frac{1}{(2\pi h)^{2d}} \int \hat{D}_\alpha^\beta(P, Q)e^{\frac{i}{\hbar}(Qp - Pq)}dQdP. \tag{1}$$

In this representation the displacement operator can be expanded by eigenvectors of the momentum operators:

$$\hat{D}_\alpha^\beta(P, Q) = \int |p + P/2\rangle R_\alpha^\beta\left(p + \frac{P}{2}, p - \frac{P}{2}\right) e^{-\frac{i}{\hbar}Qp}dp\,\langle p - P/2|. \tag{2}$$

In contrast to [13] and for non-relativistic case there is the matrix-valued variable in (2):

$$R_\alpha^\beta(p_1, p_2) = \varepsilon(p_1, p_2)\delta_\alpha^\beta + \chi(p_1, p_2)\tau_{1\,\alpha}^\beta.$$

It contains even and odd parts and is expressed by the relativistic energy of a free particle $E(p)$:

$$\varepsilon(p_1, p_2) = \frac{E(p_1) + E(p_2)}{2\sqrt{E(p_1)E(p_2)}}, \qquad \chi(p_1, p_2) = \frac{E(p_1) - E(p_2)}{2\sqrt{E(p_1)E(p_2)}}. \tag{3}$$

Combining (1) and (2) we obtain now the formula for the density operator expansion:

$$\hat{W}_\alpha^\beta(p, q) = \frac{1}{(2\pi h)^d} \int |p + P/2\rangle R_\alpha^\beta\left(p + \frac{P}{2}, p - \frac{P}{2}\right) e^{-\frac{i}{\hbar}Pq}dP\langle p - P/2|. \tag{4}$$

The Wigner function is the average of this operator for an arbitrary state:

$$W(p, q) = \sum_{\alpha,\ \beta} \langle\psi_\beta|\hat{W}_\alpha^\beta(p, q)|\psi^\alpha\rangle.$$

This expression contains four terms. Two of them are the average of the even part of the density operator and two others are the average of the odd part. Now one can introduce the symbols:

$$W_\alpha^\beta(p, q) = \langle\psi_\beta|\hat{W}_\alpha^\beta(p, q)|\psi^\alpha\rangle. \tag{5}$$

It should be noted that $W_\alpha^\beta(p, q)$ is not the matrix-valued Wigner function in the sense of [8].

Using the expressions (4) and (5) the components of the Wigner function are obtained in the form:

$$W_\alpha^\alpha(p, q) = \frac{1}{(2\pi h)^d} \int \varepsilon\left(p + \frac{P}{2}, p - \frac{P}{2}\right)\psi_\alpha^*\left(p + \frac{P}{2}\right)\psi^\alpha\left(p - \frac{P}{2}\right) e^{-\frac{i}{\hbar}Pq}dP,$$

$$W_{\alpha}^{-\alpha}(p, q) = \frac{1}{(2\pi h)^{d}} \int \chi\left(p + \frac{P}{2}, p - \frac{P}{2}\right) \psi_{\alpha}^{*}\left(p + \frac{P}{2}\right) \psi^{-\alpha}\left(p - \frac{P}{2}\right) e^{-\frac{i}{h}Pq} dP.$$

One can obtain the quantum Liouville equation by standard way [14]:

$$\begin{aligned} \frac{\partial W_{\alpha}^{\alpha}(p, q, t)}{\partial t} &= \alpha \frac{2}{h} E(p) \sin\left\{-\frac{h}{2} \overleftarrow{\partial_p} \vec{\partial_q}\right\} W_{\alpha}^{\alpha}(p, q, t), \\ \frac{\partial W_{\alpha}^{-\alpha}(p, q, t)}{\partial t} &= i\alpha \frac{2}{h} E(p) \cos\left\{-\frac{h}{2} \overleftarrow{\partial_p} \vec{\partial_q}\right\} W_{\alpha}^{-\alpha}(p, q, t). \end{aligned} \tag{6}$$

The equation for the even part of the Wigner function coincides with the similar expression in the Newton — Wigner coordinate approach [13]. Hence dynamics of the distribution function in both cases is identical. The difference is in the constraints for the initial conditions. The physical variables that contain higher moments of the coordinate (for example, dispersion) differ from those in [13]. For one particle problem these peculiarities were developed in [3].

PARTICLES IN A HOMOGENEOUS MAGNETIC FIELD

The particles in external electromagnetic fields are more sensitive to the odd part of the coordinate. For example, in a uniform electric field the odd part of the position in the Hamiltonian of interaction results in the effects of particles creation from the vacuum [9]. The origin of this peculiarity is that even and odd parts of the Wigner function are entangled in equations like (6).

Here we shall study the behavior of particles in a time-independent and homogeneous magnetic field that is more typical for astrophysical objects. Following [11] we shall use the energy representation and so we have to consider quasi-particles rather than particles. Both the position and momentum operators have odd parts in this approach.

Further we do not take into account the particle motion along the magnetic field and consider only relativistic rotator.

Following the previous paragraph one can write the displacement operator in the energy representation:

$$D_{n,m;\alpha}^{\beta}(P, Q) = (\varepsilon_{n,m}\delta_{\alpha}^{\beta} + \chi_{n,m}\tau_{1\alpha}^{\beta}) D_{n,m}(P, Q),$$

where $D_{n,m}(P, Q)$ are the matrix elements of the usual displacement operator on the eigenfunctions of the harmonic oscillator [15]. $\varepsilon_{n,m}$, $\chi_{n,m}$ are defined like (3), but with the spectrum of the relativistic rotator in place of the energy of a free particle. Then, the density operator and the Wigner function are defined in the way presented in the previous paragraph. The final expressions for the even and odd components of the Wigner function are

$$W_{\alpha}^{\alpha} = \sum_{m,n} \varepsilon_{m,n} C_{n;\alpha}^{sup} * C_{m;}^{\alpha} T_{m,n}(p, q),$$

$$W_{\alpha}^{-\alpha} = \sum_{m,n} \varepsilon_{m,n} C_{n;\alpha}^{sup} * C_{m;}^{-\alpha} T_{m,n}(p, q),$$

Here $C_{n;\alpha}$ is the wave function in the energy representation, $T_{m,n}(p, q)$ is the matrix elements of the usual displacements operator

$$\hat{T}(p, q) = \frac{1}{(2\pi h)^{2d}} \int \hat{D}(P, Q) e^{-\frac{i}{h}(Pq - Qp)} dP dQ.$$

The equations for the Wigner function (12) can be obtained in the standard way too. Here the different components are not entangled. Hence there are no effects connected with vacuum instability [9]:

$$\frac{\partial W_{\alpha}^{\alpha}(p, q, t)}{\partial t} = \alpha \frac{2}{h} E(p, q) \sin\left\{\frac{h}{2}(\overleftarrow{\partial}_q \overrightarrow{\partial}_p - \overleftarrow{\partial}_p \overrightarrow{\partial}_q)\right\} W_{\alpha}^{\alpha}(p, q, t),$$
$$\frac{\partial W_{\alpha}^{-\alpha}(p, q, t)}{\partial t} = i\alpha \frac{2}{h} E(p, q) \cos\left\{\frac{h}{2}(\overleftarrow{\partial}_q \overrightarrow{\partial}_p - \overleftarrow{\partial}_p \overrightarrow{\partial}_q)\right\} W_{\alpha}^{-\alpha}(p, q, t). \quad (7)$$

In this expression we introduce the Weyl symbol for the Hamiltonian of the relativistic rotator in the energy representation (it should be redefined):

$$E(p, q) = mc^2 \sqrt{1 + \frac{2}{mc^2}\left(\frac{p^2}{2m} + \frac{\omega_c^2 m}{2} q^2\right)},$$

where $\omega_c = eB/m$ is the cyclotron frequency.

The odd part in the Wigner function definition describes interference effects between particles and antiparticles. Furthermore, the value ε_{nm} defines the specification of the initial conditions.

In [11] we studied dynamics of the one particle problem. It was shown that in fields less than critical ($h\omega_c < mc^2$) the mean radius of the trajectory oscillates with the frequency

$$\Omega = \frac{h\omega_c^2}{mc^2}.$$

This is essencially quantum relativistic effect. It can be observed as a low frequency modulation of synchrotron radiation. However, unfortunately such dynamical process is identical to both approaches and does not reveal the complicated structure of the position operator.

Let us consider now the dispersion of the orbit radius for the nonlinear coherent state [11]:

$$\overline{\Delta R^2} = \frac{h}{m\omega_c}\left[1 - |C_0|^2 \sum_n \frac{R^{2n}}{2^n n! [\varepsilon_n]!} \chi_n^2\right],$$

where C_0 is the normalization factor, and Q, P are the mean value of the position and momentum of the wave packet. It contains both the standard and additional terms. They result in the appearance of the states with formally broken uncertainty relation. One can expect that such effects take place for multi-body systems too.

CONCLUSION

The odd part of the position operator results in the non-standard behavior of the physical observables. The whole system has also peculiarities. However, it is observed not for all physical variables. For example, behavior of energy does not contain such peculiarities. Hence, one can expect these effects for the quadratic and higher moments of the coordinate and momentum.

Especially one should notice the effects connected with interference between particles and antiparticles. They result from the odd part of the Wigner function and can be observed in systems of particles with opposite charge signs.

Finally we briefly note that relativistic quantum mechanics in a Wigner formulation contains the measurement device frame. Actually, one can write the equation (6) and (7) using only four dimensional Lorentz invariant symbols. To make it possible one should incorporate into equations a certain time-like vector. It can be interpretated as a four-velocity of the frame where a wave packet reduction happens relative to the second (immobile) observer. It is very important that quantum mechanics equations contain explicitly the observer characteristics. This fact can serve as an additional argument in favor of the Copenhagen interpretations of quantum mechanics.

REFERENCES

1. Aspect A., Roger G., et. al. Time Correlations between Two Sidebands of the Resonance Fluorescence Triplet // Phys. Rev. Lett.—1980.—**45**.—P. 617;
Aspect A., Grangier P., Roger G. Experimental Test of Realistic Local Theories via Bell's Theorem // Phys. Rev. Lett.—1981.—**47**.—P. 460.
2. Bell J. S. Speakable and Unspeakable in Quantum Mechanics. — Cambridge: Cambridge Univ. Press, 1987.
3. Blokhintzev D. I. On localization relativistic micro particles in space and time // JINR, R-2631, Dubna, 1966 (in Russian).
4. Caban P., Rembielinski J. Lorentz-covariant quantum mechanics and preferred frame // Phys. Rev. A.—1999.—**59**.—P. 4187.
5. De Groot S. R., van Leeuwen W. A., Weert Ch. G. Relativistic kinetic theory. Principles and Applications. — Amsterdam: North-Holland, 1980.
6. Eberhard P.H. Bell's Theorem and the Different Concepts of Locality. // Nuov. Cim.—1978.—**46B**.—P. 392.
7. Feshbach H., Villars F. Elementary Relativistic Wave Mechanics of Spin 0 and Spin S Particles // Rev. Mod. Phys.—1958.—**30**.—P. 24.
8. Gerard P., Markovich P. A., Mauser N. J., et al. Homogenization Limits and Wigner Transforms // Comm. Pure Appl. Math.—1997.—**50**.—P. 0323.
9. Grib A. A., Mamaev S. G., Mostapenko V. M. Vacuum quantum effects in strong fields. — Moscow: Energoatomizdat, 1988 (in Russian).
10. Holland P. R., Kyprianidis A., Maric Z., et al. Relativistic generalization of the Wigner function and its interpretation in the casual stochastic formulation of quantum mechanics // Phys. Rev. A.—1986.—**33**.—P. 4380.
11. Lev B. I., Semenov A. A., Usenko C. V. Behaviour of $\pi\pm$ mesons and synchrotron radiation in a strong magnetic field // Phys. Lett. A.—1997.—**230**.—P. 261.
12. Menskii M. B. Quantum mechanics: new experiments, new applications, new formulations // Uspekhi fizicheskikh nauk.—2000.—**170**, N 6.—P. 631.
13. Mourad J. The Wigner-Weyl formalism and the relativistic semi-classical approximation. — E-print of LANL: /hep-th/9307135.
14. Moyal J. E. Quantum Mechanics as a Statistical Theory // Proc. Cambr. Phil. Soc.—1949.—**45**.—P. 99.
15. Perelomov A. M. Generalized coherent states and their applications. — Berlin: Springer, 1996.

Космічна наука і технологія. ДОДАТОК. 2001. Т 7. № 2. С. 89—92.

UDC 533.9

RADIATION SPECTRUM OF A RELATIVISTIC ELECTRON MOVING IN CURVED LINES OF MAGNETIC FIELD

Ya. M. Sobolev

Institute of Radio Astronomy, NAS of Ukraine, Kharkov, sobolev@ira.kharkov.ua

Radiation of ultra relativistic charged particles moving with small pitch angles along the spiral trajectory winded around curved magnetic force line is considered. The general radiation formulae, which can reduce to the formulae for either synchrotron or curvature radiation in the limiting cases, have been obtained. When the velocity of cyclotron rotation and the drift velocity are similar it is necessary to take into account the curvature of magnetic force line.

1. INTRODUCTION

Synchrotron radiation has broad application in investigation of laboratory plasma, plasma of solid bodies, in designing new apparatuses [7, 8]. Synchrotron radiation is among the most important in radio astronomy and astrophysics. Power law spectra of extragalactic radio sources corresponds to synchrotron radiation of ultrarelativistic electrons in cosmic magnetic fields [2]. The synchrotron radiation formulae are derived assuming a uniform and straight magnetic field. In the magnetosphere of a pulsar (Jupiter) charged particles are moving along curved magnetic field lines. Their trajectories are likely to be spiral curves along dipolar field lines. However, on calculating radio emission, many authors used the synchrotron radiation formulae for charged particles motion in uniform and straight magnetic field lines which may be correct or incorrect.

New radiation formulae for an ultrarelativistic charged particle motion along spiral trajectory with a small pitch angle to curved magnetic force line have been obtained in [1, 5, 6]. The case for which in the reference frame moving with the particle along magnetic force line the particle's energy is ultrarelativistic has been considered in [1, 4, 6]. This radiation was called as synchrotron curvature in [1]. The case when transverse energy is nonrelativistic in the particle system, and radiation is gathering from many particle cycles around force line was considered in [5] and called as the undulator curvature. The word «curvature» was added to distinguish between synchrotron and undulator radiation from charged particles in straight field lines and that from charged particles in curved magnetic field lines. Synchrotron radiation of relativistic electrons moving along spiral trajectory in tokamak was considered in [4]. When the drift velocity and cyclotron velocity of relativistic electrons are comparable it is necessary to take into account the curvature of magnetic field lines [6].

The radiated spectrum, polarization characteristics of the radiation emitted by the ultrarelativistic charged particle moving along spiral trajectory with small pitch angles in the curved magnetic field lines are obtained in the paper.

In the region in which radiation goes from magnetic field the lines are approximated by circular force lines with curvature radius R. The particle velocity along force line is equal to the light velocity, $v_{||} \to c$. Emitted energy losses are not taken into account.

2. SYNCHROTRON CURVATURE RADIATION

Spectral angular distribution of energy radiated by the charged particle in the wave zone (energy radiated in the range of solid angles between o and $o + do$, and in the unit frequency interval of the frequency

ω) can be written as [3]

$$dEdo\,d\omega = \frac{cR_0^2}{4\pi^2}|E(\omega)|^2, \tag{1}$$

where $E(\omega)$ is the Fourier component of an electric field in the wave zone

$$E(\omega) = \frac{-i\omega e}{cR_0}\exp\frac{i\omega R_0}{c}\int_{-\infty}^{+\infty}[n[n,\beta]]\exp i\omega(t - nr/c)dt. \tag{2}$$

Here R_0 is a distance to the observer, n is the unit vector pointing the observer, $\beta = v/c$, v is the particle velocity, r is the particle position vector, for which (in the approximation $r_B/R \ll 1$, where r_B is a Larmor radius) we have expression [6]

$$r = [-2\delta r_B\sin\omega_B t\cos\Omega t + (R + r_B\cos\omega_B t)\sin\Omega t]\mathbf{i} + [2\delta r_B\sin\omega_B t\sin\Omega t + (R + r_B\cos\omega_B t)\cos\Omega t]\mathbf{j} +$$
$$+ [v_D t - r_B\sin\omega_B t]\mathbf{k}, \tag{3}$$

where $\omega_B = eB/mc\gamma$, $\gamma \gg 1$ is a Lorentz factor, $\delta = \Omega/\omega_B \ll 1$, $\Omega \equiv v_{||}/R$ is an angular velocity of the motion along circular force line, $v_D = -\Omega^2 R/\omega_B$ is the drift velocity, $\mathbf{i}$, $\mathbf{j}$, $\mathbf{k}$ are the unit vectors of a coordinate system (magnetic force lines are localized in (x, y)-plane, and the magnetic surface axis is directed along z-axis), the magnitude (B) of the magnetic field is constant.

In order to calculate the spectral angular distribution of radiated energy given by equations (1), (2), we shall do as in the paper [6]. It is known that only a small part of the trajectory is effective in producing the narrow cone (with an apex angle $\propto 1/\gamma$) of radiation observed in the direction of the relativistic particle velocity. So at a given point the trajectory can be replaced by a circle, and the radiation formulae of the circular motion can be used.

The unit vectors in the plane perpendicular to the vector $\mathbf{n}$ pointing to the observer are defined as

$$\mathbf{e}_\sigma = [\mathbf{b},\mathbf{n}]/|[\mathbf{b},\mathbf{n}]|,\ \mathbf{e}_\pi = [\mathbf{n}[\mathbf{b},\mathbf{n}]]/|[\mathbf{b},\mathbf{n}]|, \tag{4}$$

where $\mathbf{b}$ is the unit vector of the binormal to the trajectory (3). The unit vector $\mathbf{e}_\sigma$ is perpendicular to the ($\mathbf{v}$, $\mathbf{n}$)-plane, and the vector $\mathbf{e}_\pi$ is placed in this plane.

To calculate the power radiated by a relativistic electron in the frequency range between the frequencies ω and $\omega + d\omega$, it is necessary to integrate the expression (1) over the solid angle and average it in time. The radiation is concentrated in the angular width $\delta\chi \propto 1/\gamma$ with respect to the surface being formed by the velocity unit vector $\tau = \mathbf{v}/v$, when the phase is changed in the interval $0 \le \omega_B t \le 2\pi$. The angle χ is counted in the direction perpendicular to this surface, the second angle μ is counted along the curve drawn by the end of the vector τ in the ($\mathbf{v}_y$, $\mathbf{v}_z$)-plane. The solid angle is $do = d\chi d\mu$, where $d\mu = = (1/v)(dv_y^2 + dv_z^2)^{1/2} = |v_D/v|\ (1 + q^2 + 2q\cos\omega_B t)^{1/2}d\omega_B t$, $q \equiv \omega_B^2 r_B/\Omega^2 R$ is the ratio of cyclotron velocity to the magnitude of the drift velocity. The cyclotron period $2\pi/\omega_B$ was taken as a time interval.

After that, the spectral power radiated by the charged particle in π- and σ-polarization can be written as

$$\frac{dP_\pi}{d\omega} = \frac{3\sqrt{3}}{8\pi}\frac{1}{\gamma^3}\int_0^{2\pi}\frac{d\omega_B t}{2\pi}\frac{W}{kc}y\left[\int_y^\infty dxK_{5/3}(x) - K_{2/3}(y)\right],$$
$$\frac{dP_\sigma}{d\omega} = \frac{3\sqrt{3}}{8\pi}\frac{1}{\gamma^3}\int_0^{2\pi}\frac{d\omega_B t}{2\pi}\frac{W}{kc}y\left[\int_y^\infty dxK_{5/3}(x) + K_{2/3}(y)\right], \tag{5}$$

where $y = \omega/\omega_S$, $\omega_S = (3/2)\gamma^3 kc$, $W = (2/3)(e^2/c)k^2c^2\gamma^4$ is a total power radiated by the electron, which carries out circular motion with the curvature radius $1/k$, $kc = \Omega(1 + q^2 + 2q\cos\omega_B t)^{1/2}$.

The total radiated power, calculated from equations (5) [6], is

$$\frac{dP}{d\omega} = \frac{3\sqrt{3}}{4\pi}\frac{1}{\gamma^3}\int_0^{\pi}\frac{d\omega_B t}{\pi}\frac{W}{kc}y\int_y^{\infty}dxK_{5/3}(x). \tag{6}$$

It should be noted that the formula (6) can be derived from the expression (15) of the paper [4], in which the method based on the consideration of the rate at which the electron accomplishes work in the electromagnetic field was used. Thus, the formula (6) has been obtained by using two methods: on calculating the flux of the radiated power in the wave zone and by considering the work of the radiation field.

On performing the integration over the frequency in equations (5), we obtain $P_{\pi} = (1/8)P$ and $P_{\sigma} = (7/8)P$, where the total radiated power is given by

$$P = \frac{2}{3}\frac{e^2}{c}\gamma^4\Omega^2(1+q^2). \tag{7}$$

It is shown from equation (7) that the total power radiated by an electron in the curved magnetic field consists of both the curvature radiation losses (the first term in (7)) and the synchrotron radiation losses (the second term in (7)).

The formulae (5), (6) can be simplified by changing the order of integration, and they are reduced to

$$\frac{dP_i}{d\omega} = \frac{P}{\omega_1}f_i(y_1, q),\ i = \pi, \sigma, \text{tot}, \tag{8}$$

where $f_i(y_1, q)$ is given by

$$f_i(y_1, q) = \frac{(1+q)^2}{1+q^2}\frac{9\sqrt{3}}{8\pi}y_1\left\{\int_{y_1\frac{1+q}{|1-q|}}^{\infty}dxF_i(x) + \int_{y_1}^{y_1\frac{1+q}{|1-q|}}dxF_i(x)\frac{2}{\pi}\arcsin\frac{1+q}{2\sqrt{q}}\sqrt{1-\frac{y_1^2}{x^2}}\right\}. \tag{9}$$

In which $y_1 = \omega/\omega_1$, $\omega_1 = (3/2)\gamma^3\Omega(1+q)$, $F_{\pi,\sigma}(x) = (1/2)(K_{5/3}(x) \pm dK_{2/3}(x)/dx)$ (plus is related to π-polarization), $F_{\text{tot}} = F_{\pi} + F_{\sigma} = K_{5/3}$. The function (9) has property $f_i(y_1, q) = f_i(y_1, 1/q)$.

Therefore, the universal function of synchrotron radiation in a uniform magnetic field [3, 7]

$$f(y) = \frac{9\sqrt{3}}{8\pi}y\int_y^{\infty}dxK_{5/3}(x) \tag{10}$$

is replaced by expression (9).

The figure gives a graphical representation of the function (9) for different values of the parameter q.

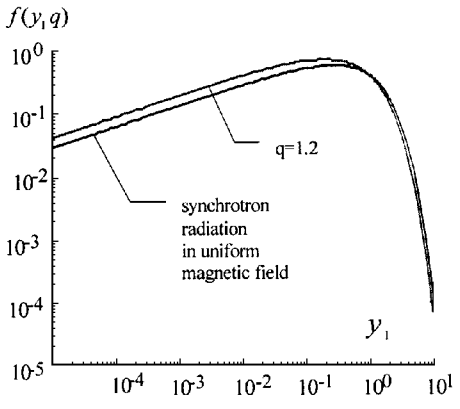

Figure. The function of synchrotron radiation in curved magnetic field

3. DIFFERENT CASES OF SYNCHROTRON RADIATION

Let's classify different cases of the radiation in curved magnetic field with respect to the parameter q and the ratio of the Lorentz factors γ and $\gamma_{\|}$, where

$$\gamma = (1/\gamma_{\|}^2 - \beta_{\perp}^2 - \beta_{\mathrm{D}}^2)^{-1/2}, \qquad \gamma_{\|} = (1 - v_{\|}^2/c^2)^{-1/2},$$
$$\beta_{\perp} = |\omega_{\mathrm{B}}| r_{\mathrm{B}}/c, \qquad \beta_{\mathrm{D}} = |v_{\mathrm{D}}|/c.$$

The charged particle is moving at the constant angle to the guiding center trajectory. The angle between this trajectory and the magnetic force line is $\sim \beta_{\mathrm{D}} = \Omega/\omega_{\mathrm{B}}$.

We have the following limiting cases:

1. When $q = |v_{\perp}/v_{\mathrm{D}}| > 1$ and $\gamma \gg \gamma_{\|} \gg 1$, the radiation is concentrated between two surfaces which have the apex angles $\propto 1/\gamma_{\|}$. The angular width between these surfaces is $1/\gamma$. The picture is analogous to the straight magnetic field. If $\gamma \sim \gamma_{\|}$ and $\beta_{\perp} < 1/\gamma_{\|}$, we have the case of undulator curvature radiation [5].

2. When $q \sim 1$ and $\gamma \gg \gamma_{\|} \gg 1$, the apex angle of the radiation cones is $\propto 1/\sqrt{2}\gamma_{\|}$ with respect to the direction of the guiding center trajectory. The angular width between cones is $\propto 1/\gamma$. The curvature of magnetic field lines is essential, the radiated spectral power is described by equations (8), (9). For $\gamma \sim \gamma_{\|}$ one needs to consider an undulator radiation case.

3. When $q < 1$, the apex angle of the radiation cone is less than the angle between the force line and the guiding center trajectory. If $\gamma \gg \gamma_{\|} \gg 1$, $\beta_{\mathrm{D}} \sim 1/\gamma_{\|}$, the apex angle of the radiation cone is $1/\gamma_1 = (1/\gamma_{\|}^2 - \beta_{\mathrm{D}}^2)^{1/2} \ll 1/\gamma_{\|}$. If also $\beta_{\perp} \sim 1/\gamma_1$, then $\gamma \gg \gamma_1$, and we have the usual picture of synchrotron radiation. The case $\beta_{\perp} < 1/\gamma_1$ needs additional consideration. If $\gamma \approx \gamma_{\|}$ it is the case of curvature radiation.

Therefore, there exist the correct formulae of synchrotron radiation of a relativistic charged particle moving at small pitch angles along curved magnetic field lines. The universal function (10) of synchrotron radiation in a uniform magnetic field is replaced by formula (9), which can be identical to either synchrotron or curvature radiation in certain parametric regions. The curvature of magnetic force line is essential when the parameter $q = |v_{\perp}/v_{\mathrm{D}}| = \omega_{\mathrm{B}}^2 r_{\mathrm{B}}/\Omega^2 R \sim 1$.

REFERENCES

1. Cheng K. S., Zhang J. L. General radiation formulae for a relativistic charged particle moving in curved magnetic field lines: the synchrocurvature radiation mechanism // Astrophys. J.—1996.—**463**, N 1.—P. 271—283.
2. Ginzburg V. L. Theory physics and astrophysics. — M.: Nauka, 1987.—488 p.
3. Landau L. D., Lifshits E. M. The field theory. — M.: Nauka, 1973.—504 p.
4. Pankratov I. M. Towards analyses of runaway electrons synchrotron radiation spectra. // Fizika Plazmy.—1999.—**25**, N 2.—P. 165—168.
5. Sobolev Ya. M. Towards radiation theory of a relativistic charged particle in curved magnetic field // Radio Physics and Radio Astronomy.—2000.—**5**, N2.—P. 137—147.
6. Sobolev Ya. M. Drift trajectory and synchrotron radiation of an ultrarelativistic electron moving in magnetic field with curved force lines // Voprosi Atomnoj Nauki i Tekhniki. Ser.«Plasma electronics and new acceleration methods»—2000.—N 2.—P. 27—30.
7. Sokolov A. A., Ternov I. M. Relativistic electron. — M: Nauka, 1983.—304 p.
8. Ternov I. M., Mikhailin V. V. Synchrotron radiation. Theory and experiment. — M.: Energoatomizdat, 1986.—96 p.

Космічна наука і технологія. ДОДАТОК. 2001. Т 7. № 2. С. 93—95.

PROPAGATION OF ELECTRON BEAMS IN SOLAR CORONAL LOOPS

V. N. Mel'nik

Radio Astronomy Institute of National Academy of Sciences of Ukraine, Kharkov, Ukraine
melnik@ira.kharkov.ua

It is shown that electron beams propagate into coronal loops as accelerated beam-plasma structures. Definitions of electric fields in loops from observed asymmetry of X-ray emission generated by fast electron beams as well as plasma temperature from electron beam velocity are proposed.

It is thought [3] that energy is released during solar flare in the cusp of coronal loops. High energy electrons accelerated in the flare propagate through plasma in the form of simple beams [2]. It is known that under such conditions beam instability occurs and the Langmuir waves are generated. In turn these waves influence electron dynamics.

In recent papers [4, 6, 8] it was shown that for quasilinear approximation electrons propagate as a nonlinear object of beam-plasma structure, consisting of electrons and the Langmuir waves. The velocity of the structure is constant and equals half maximum of electron velocity determined by electron distribution function for plateau in velocity space. Formation of this soliton-like object takes place because of generation and absorption of the Langmuir waves, correspondingly, at front and back of the structure.

The presence of electric fields in the coronal loops must be taken into account in analysis of quasilinear propagation of electrons. In 1967 Ryutov [9] considered the problem, in which he studied plateau formation at electron distribution function in an external electric field. However, it can be shown that for solar conditions quasilinear relaxation is a fast process and electron movement in electric field is a slow one. So, we suppose that the plateau of the electron distribution function is instantly

$$f(v, x, t) = \begin{cases} p(x, t), & v < u(x, t), \\ 0, & v > u(x, t), \end{cases}$$

established at every point and height $p(x, t)$ and maximum velocity $u(x, t)$ is changing slowly under electric field. The spectral energy density of the Langmuir waves is generated in the form

$$W(v, x, t) = \begin{cases} W_0(v, x, t), & v < u(x, t), \\ 0, & v > u(x, t). \end{cases}$$

For functions $p(x, t)$, $u(x, t)$, and $W_0(v, x, t)$ the gas-dynamic equations

$$\frac{\partial p}{\partial t} + \frac{u}{2}\frac{\partial p}{\partial x} = 0,$$

$$\frac{\partial u}{\partial t} + u\frac{\partial u}{\partial x} - \gamma = 0,$$

$$\frac{\partial}{\partial v}\frac{1}{v^3}\frac{\partial W_0}{\partial t} = \frac{m}{\omega_{pe}}\left(\frac{\partial p}{\partial t} + v\frac{\partial p}{\partial x}\right)$$

with boundary conditions

$$\frac{\partial W_0}{\partial t} = 0, \qquad v = u, \qquad \frac{\partial u}{\partial t} W_0 = 0, \qquad v = u$$

are derived from the quasilinear equations

$$\frac{\partial f}{\partial t} + v\frac{\partial f}{\partial x} + \frac{eE}{m}\frac{\partial f}{\partial v} = \frac{4\pi^2 e^2}{m^2}\frac{\partial}{\partial v}\frac{W}{v}\frac{\partial f}{\partial v},$$

$$\frac{\partial W}{\partial t} = \frac{\pi\omega_{pe}}{n}v^2 W\frac{\partial f}{\partial v}, \quad \omega_{pe} = kv$$

by standard way [6].

The solution of these equations in the case of boundary monoenergetic beam

$$f_b(v, t) = f(v, x, t)\Big|_{x=0} = f_0\delta(v - v_0)\psi(t)$$

is [7]

$$pl(x, t) = p(T) = \begin{cases} \dfrac{f_0 v_0 \psi(-T)}{(v_0 - \gamma T)^2(v_0 - 2\gamma T)}, & T < 0, \\ \dfrac{f_0(_0 + 4\gamma T)\psi(T)}{v_0^2(v_0 + 2\gamma T)}, & T > 0, \end{cases} \tag{1}$$

$$T = t - \frac{2}{\gamma}(u - v_0), \tag{2}$$

$$u = \sqrt{2\gamma x + u_0^2}, \tag{3}$$

$$W_0(v, x, t) = \frac{m}{\omega_{pe}}\left[p(x, t)v^4\left(1 - \frac{v}{u}\right) + \frac{v^5}{u}p\left(\frac{v_0 - u}{\gamma}\right)\right]. \tag{4}$$

If electrons are injected during time tau and the source function $\psi(t)$ can be presented as

$$\psi(t) = \exp(-t/\tau),$$

then we find solution of the equations (1)—(4) in the form of accelerated beam-plasma structure. Indeed, it follows from (1) that maximum electron density propagates according to law

$$x = \frac{\gamma t^2}{8} + \frac{u_0 t}{2}.$$

That is to say, the acceleration of beam-plasma structure is four times smaller than for a single particle.

Electron number in the structure

$$N = \int dx \int dv f$$

is proportional to $u^2(x, t)$ owing to both structure width and plateau width in velocity space and proportional to $u(x, t)$. An increase of particle number in accelerating field is connected with phenomenon of «pulling out» particles from the thermal region. In decelerating field electron number in beam-plasma structure is decreased because of electron slowing down to thermal velocity. Variations of fast electron density can be exhibited in the asymmetry of hard X-ray emission from footpoints of magnetic loops. For asymmetry $\rho = \dfrac{F_+ - F_-}{F_+ + F_-}$ (F_+, F_- are X-ray intensities of footpoints where electrons are accelerated and decelerated, correspondingly). Taking into account that $F \propto n©\sigma v$, where $\sigma \propto 1/E \propto 1/v^2$ we find

$$\rho \approx \frac{|\gamma|(x_+ + x_-)}{2v_0^2}. \tag{5}$$

The electric fields in coronal loops can be estimated from observed asymmetry ρ and distance $d = x_+ + x_-$ between loop footpoints

$$E = \frac{2m}{e}\frac{\rho v_0^2}{d}.$$

From data presented in [1] we derived the electric fields in the range from 10^{-8} to $7 \cdot 10^{-8}$ CGSE.

As it was shown in [5] nonlinear processes of the Langmuir wave scattering on plasma ions ($l + i = l + i$) limit the maximum velocity of the beam-plasma structure

$$v_{pl} \approx 14 v_{Te}(1 + T_e/T_i)^{1/2}, \quad (6)$$

where T_e, T_i are temperatures of electrons and ions, correspondingly. For the isothermal plasma this enables to find plasma temperature knowing beam velocity. For example, for electron velocity $v_{pl} = 5 \cdot 10^9$ cm/s in the magnetic loops [2] we derive $T_e = 4 \cdot 10^5$ K from (6).

This work was partially supported by INTAS (grants No. 96-0183 and No. 97-1964)

REFERENCES

1. Abramenko V. I., Gopasyuk C. I., Ogyr M. B. On the opportunity to define electric field in flare loops from X-ray observations // Izvestiya Krao.—1993.—**87.—P. 3—11.**
2. Benz A., Magun A., Stehling W., Su H. Electron beams in the low corona // Solar Phys.—1992.**141**.—P. 335—348.
3. Benz A. Plasma astrophysics. Kinetic processes in solar and stellar coronae. — Dordrecht: Kluwer, 1993.—299 p.
4. Kontar E. P., Lapshin V. I., Mel'nik V. N. Propagation of monoenergetic electron beams in plasma: numerical and analytical consideration // Fizika plazmy.—1998.—**24**, N 9.—P. 832—836.
5. Mel'nik V. N. Properties of Type III bursts in gas-dynamic model of propagation electron beams in plasma // Kinematika i fizika nebesnych tel.—1991.—**7**, N 3.—P. 59—68.
6. Mel'nik V. N. On the «gas-dynamic» flying off fast electron flux in plasma // Fizika plazmy.—1995.—**21**, N 1.—P. 94—96.
7. Mel'nik V. N. About influence of electric field on propagation of electron beams in solar magnetic loops // Radiofizika i radioastronomiya.—1997.—**2**, N 3.—P. 298—301.
8. Mel'nik V. N., Lapshin V. I., Kontar E. P. Propagation of a Monoenergetic Electron Beam in the Solar Corona // Solar Phys.—1999.—**184**, N 2.—P. 353—362.
9. Ryutov D. D. Quasilinear theory of running away electrons // Zhurn. Eksp i teor fiz.—1967.—**52**.—P. 1378—1385.
10. Vedenov A. A., Ryutov D. D. // Voprosy teorii plasmy.—1972.—**6**.—P. 3—69.

Космічна наука і технологія. ДОДАТОК. 2001. Т 7. № 2. С. 96—100.

UDC 324.35-4

ULTRA RELATIVISTIC EXPLOSION IN MOVING MEDIA AS A MODEL OF SUPER-LUMINAL RADIO JETS

V. N. Pasyuga

Research and Technological Institute of Transcription, Translation and Replication, Kharkov, Ukraine, pas@insurance.kharkov.ua

Super-luminal components of radiojets are identified with luminous segments of ultrarelativistic shock fronts (further SF), moving to the observer, in particular, they can be a vicinity of their leading point. The cases of a local hydrostatic equilibrium, accretion and wind flows of a nonperturbed medium in a field of central object («a black hole»?) are investigated. In the case of the noncentral explosion in a medium, being in a state of a local hydrostatic equilibrium [4], the apparent superluminal velocity (further β_{app}) of a leading point movement of a shock front (further SF) is asymptotically constant and proportional to a total energy of explosion, according to observational data [2]. In cases of accretion and wind flows the dependences β_{app} on the distance from a leading point to the nucleus are obtained. In the case of explosion with an energy pumping from a central source we manage to identify the observable times of acceleration of radiojets components with the duration of energy pumping from flares correlating with components [5] according to data [8]. The movement influence of a nonperturbed medium upon the shift of superluminal radiocomponents in a picture plane is discussed.

1. INTRODUCTION. SUPERLUMINAL RADIO JETS

The components of jets moving with (apparent) superluminal velocities at VLBI observations in a series of radiosources [7] are observed. The observed superluminal (further SL) movement velocities of components are explained by relativistic effects at moving with the major Lorentz-factors under a small angle to the direction of sight. The correlation between occurrence of SL components and optical flares for ultra relativistic (further UR) jets in quasars 3C 345 and 3C 273 [1] was detected. Subsequently the similar correlation was observed also by others [8]. The model, in which the optical flares are identified with off-center UR explosions in a vicinity of AGN, is offered [4]. The superluminal velocities of components are asymptotically constant and they correlate with an energy release in flares [2], that can be explained within the framework of the offered model. The acceleration and further deceleration of SL components of a radiojet 3C 345 is observed, which can be explained by an energy pumping from optical flares and the variability of an exponent in the law of decrease of a medium density in a vicinity of AGN at initial times. The movement of SL components of radiojets in a picture plane is observed, that can be explained by movement of a nonperturbed medium.

2. THE ULTRA RELATIVISTIC SHOCK WAVE

The model of UR adiabatic explosion in a vicinity of AGN is discussed. The movement of SF will be ultrarelativistic in the case, if the total energy of explosion E is great enough in comparison with rest energy of a medium confined in the volume V restricted by SF

$$E \gg \rho V c^2, \tag{1}$$

where c is the light velocity.

In the case of UR adiabatic explosion within a frame of a nonperturbed medium, the boundary conditions on SF are

$$p_2 \equiv e_2/3 \equiv 2\Gamma^2 w_1 c^2, \qquad n_2' \equiv n_2\gamma^2 = 2\Gamma^2 n_1, \qquad \gamma_2^2 = \Gamma^2/2, \tag{2}$$

where $\Gamma = \sqrt{1 - v^2/c^2}$ is the Lorentz-factor SF; p_2, e_2, n_2 are the pressure, density of an energy and concentration of particles, measured in the system of the post-shock flow; n_2', γ_2 and w_1 are the concentration of particles, the Lorentz-factor of a pre-shock flow and the density, measured for the rest system of a nonperturbed medium.

For determination of the Lorentz-factor SF (further Γ) we use the Kompaneyets approximation for UR explosion [6]. The given approximation adequately describes the SF movement at exponents in the law of a density decrease of a nonperturbed medium $n \leq 3$. In the given approximation the pressure p_2 uniform along the SF and proportional to the average density of the explosion enegy $p_2 = \lambda\Gamma/V$, is suggested where the constant of proportionality λ is determined from self-similar solutions [4]. The Kompaneyets equation for SF in cylindrical coordinats (r, z) looks like

$$\dot{r}/\sqrt{1 + (r'_z)^2} = -[1 - \Gamma^{-2}]^{1/2}, \tag{3}$$

the left-hand side of this relations is a movement velocity SF, directed along a normal line to the front.

From conditions on SF (2), using the Kompaneyets approximation we obtain the expression for Γ:

$$\Gamma^2 = 3\lambda E/2w_1 V(t)c^2, \tag{4}$$

where $w_1 = \rho_0(R_0/R')^n$ is density of a nonperturbed medium, R_0 is the distance from AGN up to the point of explosion, R' is the distance from the nucleus to the explosion point, ρ_0 — is the medium density in the point of explosion.

In the UR limit the SF becomes spherical $V(t) \approx 4\pi R^3/3$. In view of the latter, the expression for Γ looks like

$$\Gamma^2 = 9\lambda E R_0^n R'^n/8\pi\rho_0 c^2 R^3. \tag{5}$$

At transition to a frame moving perpendicularly to SF with a velocity β_1 and the Lorentz-factor γ_1, Γ varies according to the law

$$\Gamma' = \gamma_1\Gamma(1 \pm \beta'\beta_1) \approx \Gamma\gamma_1(1 \pm \beta_1). \tag{6}$$

where the sign + corresponds to the frame moving in the direction of SF propagation.

In case of the movement a unshocked medium for the Lorentz-factor of a leading point vicinity of SF from (4) taking into account (6) we obtain

$$\Gamma'^2 = 3\lambda E\gamma_1^2(1 \pm \beta_1)^2/2w_1 V(t)c^2. \tag{7}$$

As a first approximation, at nonrelativistic movement in a vicinity of AGN the relation (7) passes to (4). In this case the medium movement influences SF movement according to the law of a medium decrease in the vicinity of AGN.

3. ULTRA RELATIVISTIC EXPLOSION IN A VICINITY OF AGN
A LOCAL HYDROSTATIC EQUILIBRIUM OF A RELATIVISTIC MEDIUM IN THE VICINITY OF AGN

The guessed law of a relativistic medium decrease is

$$w_1 = \rho_0(R_0/R')^3, \tag{8}$$

The asymptotic constancy GAMMA follows from the expression (5) at major times [4]

$$\Gamma^2 \underset{t \to \infty}{\longrightarrow} \text{const} = 1/2B, \tag{9}$$

where $B = 4\pi\rho_0 c^2/9\lambda E$.

For a source moving under a small angle α in the direction of sight [7]

$$\beta_{app} = \beta \sin\alpha/(1 - \beta\cos\alpha), \tag{10}$$

where the angle α meets the requirement

$$1/\Gamma^2 \ll \alpha \ll 1.$$

For a vicinity of a leading point SF moving under a small angle α, we have from (9)

$$\beta_{app} \approx 2\alpha\Gamma^2, \tag{11}$$

where $1/\Gamma^2 \ll \alpha \ll 1/\Gamma$.

As we see from (11), in a vicinity of a leading point SF β_{app} is asymptotically constant and proportional to a total energy of explosion. This result is in accordance with the observational data for jets 3C 345 and 3C 273.

A WIND FLOW

The outflow velocity of a nonperturbed medium is v_1 = const, the density decreases by the inverse quadratic law $w_1 = \rho_0(R'/R_0)^{-2}$. According to (7), the Lorentz-factor of movement of a vicinity of a leading point looks like

$$\Gamma'^2 = 3\lambda E\gamma_1^2(1 + \beta_1^2)/2Vw_1, \tag{12}$$

where $\beta_1 = v_1/c$ and γ_1 — is the velocity and the Lorentz-factor of movement of the outflow of the nonperturbed medium correspondingly.

For major times from the relation (12) the asymptotics for Γ' is:

$$\Gamma'^2 \approx \gamma_1^2(1 + \beta_1^2)/2BR. \tag{13}$$

Taking into account (13) we obtain from the expression (11)

$$\beta_{app} \approx \alpha E\gamma_1^2(1 + \beta_1^2)^2/AR, \tag{14}$$

where $A \equiv EB = 4\pi\rho_0 c^2/9\lambda R_0^2$.

In the case of the outflow of a medium from the AGN with constant velocity β_{app} is proportional to an energy of explosion and asymptotically decreases with the distance between the leading point and the nucleus as R^{-1}.

AN ACCRETION FLOW

The slow accretion (ADAF) on the central compact object («a black hole») is presupposed. The dependence of a density w_1 and the velocity v_1 medium upon the distance from the nucleus

$$w_1 = \rho_0(R_0/R')^{3/2}, \qquad v_1 = V_0(R_0/R'^{1/2}. \tag{15}$$

In a vicinity of the leading point SF, according to (7), the Lorentz-factor SF is determined by the relation

$$\Gamma'^2 \approx (R')^{3/2}\gamma_1^2(1 - \beta_1)^2/2BR^3. \tag{16}$$

Within the first approximation, when the velocity of accretion movement is small in comparison with the light velocity, the expression (16) becomes

$$\Gamma'^2 \approx (R')^{3/2}/2BR^3. \tag{17}$$

From the expression (17) the asymptotics follows for Γ at major times

$$\Gamma'^2 \approx 1/2BR^{3/2}. \tag{18}$$

For a superluminal velocity β_{app} from the relation (18) we obtain

$$\beta_{app} \approx \alpha E/AR^{3/2}, \tag{19}$$

where $A = 4\pi\rho_0 c^2/9\lambda R_0^{3/2}$.

In the case of slow accretion of the relativistic medium on central compact object the apparent superluminal velocity of a leading point SF asymptotically decreases with the distance as $R^{-3/2}$.

4. ACCELERATION OF SUPERLUMINAL COMPONENTS OF RADIOJETS

The case of an energy pumping to SF from a central source by an energy flow $L(t)$ with the Lorentz-factor $\Gamma_L \gg \Gamma$ is considered. The power law of an energy pumping and stratification of a nonperturbed medium is supposed

$$L(t) = L_0 t^q, \qquad w_1 \approx (R')^{-n}. \tag{20}$$

Time dependence of the Lorentz-factor on the SF leading point vicinity [3] looks like

$$\Gamma^2 \approx t^{-m}, \qquad m = \frac{q + k - 2}{q + 2}. \tag{21}$$

As we can see from (21), SF will be accelerated at $q \sim+\sim k > 2$. Optical flares correlating with superluminal components of radiojets, were identified according to the energy pumping to SF. In this case, the duration of an optical flares τ_* is the duration of the presupposed energy pumping. As a result of the delivery delay of the emitted energy portion to SF, the time of pumping τ_* is not equal to the duration of SF pumping

$$\tau \sim \tau_* 2\Gamma^2(\tau). \tag{22}$$

The observable time of acceleration is equal to the duration τ_* of an energy pumping (flares) for the remote observer under a small angle of which the leading point moves. As it was shown, for a radiojet 3C345 [5] the estimates of the observable times of acceleration coincide with the duration of optical flares that may confirm the offered model.

The monotonic increase of X-coordinates and cyclic variability of Y-coordinates of the components in a picture plane is observed. The offered explanation of observable motions of components of SF by involvement rotating medium of an accretion disk is given. The apparent periods T_{app} of a presupposed rotation of the C4, C5 and C7 components are 12, 20 and 4 years, correspondingly. The true period T for the components rotations is $T \cong \overline{T}_{app}\overline{\beta}_{app}/\alpha$, where the upper line means average value on a phase. For a thin disk $T \sim T_k$, where T_k is the Keplerian period of a disk rotation. We have $\overline{\alpha} \sim 0.001$. The sufficient condition of a monotonicity of x coordinates is $\Omega_k < c\ (\alpha_1 - \alpha_2)/4R$, where α_1 and α_2 are the angles between the direction of sight and a disk axis and between a disk axis and the line of a component movement. We guess $\alpha_2/\alpha_1 \sim 0.1$, then $\alpha_1 - \alpha_2$ and a requirement of monotony is $(R_g/R)^{1/2} < \overline{\alpha}/4$, R_g is the gravitational radius of AGN. The given inequality is valid for C4 and C5. However, inequality is not valid for C7. The latter can be explained by the decrease of a medium reversion frequency $\Omega < \Omega_k$ with the component removal from a disk plane.

5. CONCLUSION

1. In the case of a local hydrostatic equilibrium of a relativistic medium in a vicinity of AGN the asymptotic constancy of an observable superluminal velocity β_{app} and its proportionality of a total energy of the explosion is obtained, in accordance with the observational data [2]. In the case of accretion and wind flows in the vicinity of AGN the dependences β_{app} upon the distance from the nucleus have been obtained.

2. In the case of explosions with an energy pumping from a central source the observable duration of acceleration of superluminal components of radiojets is possible to identify with the duration of energy pumping from optical flares.

3. The explanation of the movement of superluminal radiojets components in a picture plane of a nonperturbed medium movement in a vicinity of an accretion disk is offered.

The obtained data are in accordance with the observational data for superluminal radiojets 3C 345 and 3C 273 [2, 8].

REFERENCES

1. Babadzhanyanz M. K., Belokon' E. T. Optical manifestation of superluminal motion in the quasar 3C 345 // Astrofizika.—1985.—**23**.—P. 459—471.
2. Babadzhanyanz M. K., Belokon' E. T. The new testimonies of a reality of 13-year's phase in optical variability of a quasar 3C 273 and its correlation with observable parameters of a parsec-scale radiojet // Astronomicheskiy Zhurnal.—1993.—**70**, N 2.—P. 241—257.
3. Blandford R. D., McKee C. F. Fluid dynamics of relativistic blast waves // Physic of Fluids.—1976.—**19**, N 8.—P. 1130—1138.
4. Kontorovich V. M., Pasyuga V. N. A shock wave theory of super-luminal outburst from AGN // Odessa Astron. Publ.—1999.—**12**.—P. 90—93.
5. Kontorovich V. M., Pasyuga V. N., Pimenov S. F. To the shock wave theory of super-luminal jets from AGN // JENAM 2000: Abstracts Book. — 2000.—P. 152.
6. Shapiro P. R. Relativistic blast waves in two-dimensions. I. The adiabatic case // Astrophys. J.—1979.—**233**, N 3.—P. 831.
7. Vermeulen R. C., Cohen M. H. Superluminal motion statistics and cosmology // Astrophys. J.—1994.—**430**, N 1.—P. 467—494.
8. Zensus J. A. Parsec-scale jets in extragalactic radio sources // Annu. Rev. Astron. and Astrophys.—1997.—**35**.—P. 607—636.

Космічна наука і технологія. ДОДАТОК. 2001. Т 7. № 2. С. 101—104.

UDC 533.6

THE OVERFLOW OF DENSITY SINGULARITY BY SHOCK GENERATED BY STRONG EXPLOSION

S. I. Shelyag

Institute of Radio Astronomy of National Academy of Science, Kharkov, Ukraine
e-mail: Sergey Shelyag@mail.ru

Cosmological nature of the GAMMA-Ray Bursts means that energy discharged from the GRB is greater than energy emitted from supernova explosion, and is enough to make shock reach neighbouring stars or gas clouds and remain strong. It implies the possibility of using the Kompaneets strong explosion approximation for analysis of «hypernovae» remnants shapes, which may correspond to the Gamma-Ray Bursts. Forms of the shock generated by a strong explosion in a medium with quadratic law of density decrease and coming to constant on big distances are analysed. The overflow of density singularity is observed. Obtained results are compared with observational data about hypernova explosions.

The revelation of GAMMA-Ray Bursts cosmological nature in the recent couple of years means that in a nature the explosions of stars are much more powerful than the explosions of supernovae (with the energy approximately 10^{53} erg) [7]. In its turn, it means that like supernovae remnants existing during tens of thousands years, the remnants of these more powerful explosions — hypernovae — are also to exist too. At present the objects NGC5471B, MF83 are considered as pretenders [1, 9].

The energy emitted by hypernova explosion in principle is sufficient to make the blast wave reach neighbouring stars and remain strong enough. In doing so the rounding of obstacle [6] (star, cloud) has to arise, reminding characteristic detail in the image of presupposed remnant of hypernova [1].

The case of enlarging of the shock wave in a radially stratified medium with quadratic density decrease (similar to peripheral regions of sun corona) and coming to the constant corresponding to average density of an interstellar medium is the most interesting. Direct solution of the problem for this case is difficult, but it is possible to obtain it using transformation suggested by V. Kontorovich and S. Pimenov [4, 5], for shock front generated by a strong blast in the flat-stratified medium with positive exponential index and coming to the constant in negative z region:

$$\varphi(z) = \beta\, e^{\alpha z} + c. \tag{1}$$

So, using transformation [4, 5]

$$\ln\frac{R}{a} = \frac{z}{z_0},\ z_0\chi = r,\ \Psi(R) = \varphi\left(z_0 \ln\frac{R}{a}\right)\frac{z_0^2}{R^2}, \tag{2}$$

where $\Psi(R)$ is the dependence of density on distance to density singularity, a is the distance from singularity to the explosion in radially stratified medium, $\varphi(z)$ is the density function in flat-stratified medium, z_0 is the scale of the medium nonhomogeneity, general form of the density function from distance to singularity is obtained:

$$\varphi(z) = \beta\, e^{\alpha z} + c \Leftrightarrow \Psi(R) = \frac{\beta\, z_0^2}{a^{\alpha z_0}} R^{\alpha z_0 - 2} + c\frac{z_0^2}{R^2}. \tag{3}$$

One can see from (3), $\alpha z_0 = 2$ corresponds to coming to the constant in (1). In this way obtain the law of the dependence of density on distance, required for solution of the problem ($z_0 = 1$, $\alpha = 2$):

$$\Psi(R) = \frac{\beta}{a^2} + \frac{c}{R^2}. \tag{4}$$

Solutions for the blast wave in the medium (1) for equation proposed by Kompaneets,

$$\left(\frac{\partial r}{\partial y}\right)^2 - \frac{1}{\varphi(z)}\left[\left(\frac{\partial r}{\partial z}\right)^2 + 1\right] = 0, \tag{5}$$

where $r = r(z, y)$ is the function describing the form of the shock wave front, and generalized «time» y of the shock wave distribution is introduced accordingly to

$$dy = \sqrt{\frac{\lambda(\gamma^2 - 1)E}{2\rho_0}}\,\frac{dt}{\sqrt{V(t)}}, \tag{6}$$

where t is the time, $V(t)$ is the volume bounded by the shock front in time moment t, γ is the adiabat index, λ is the constant, taking into account the deviation of pressure directly beyond the front from average pressure by volume, built analogously [3—5, 8] by division of variables method:

$$\frac{\partial r}{\partial y} = \xi, \qquad \frac{\partial r}{\partial z} = \pm\sqrt{\xi^2(\beta e^{\alpha z} + c) - 1}, \tag{7}$$

$$\begin{gathered} r = \int_0^z \sqrt{\xi^2(\beta e^{\alpha z} + c) - 1}\, dz + \xi y + b(\xi), \\ \frac{\partial r}{\partial \xi} = 0 = y + \int_0^z \frac{\xi(\beta e^{\alpha z} + c)}{\sqrt{\xi^2(\beta e^{\alpha z} + c) - 1}}\, dz + \frac{db}{d\xi}. \end{gathered} \tag{8}$$

Integrating by using condition of sphericity of the shock wave in small y and z ($b(\xi) = 0$) analogously to Silich and Fomin [8], and applying transformation (2) to obtained solutions, we obtain complete parametrical form of solution for the required density dependence:

$$\begin{gathered} \chi(R, \xi) = \frac{1}{\sqrt{1 - c\xi^2}}\left[\arccos\sqrt{\frac{1 - c\xi^2}{\xi^2\beta}} - \arccos\left(\frac{a}{R}\sqrt{\frac{1 - c\xi^2}{\xi^2\beta}}\right)\right], \\ y(R, \xi) = \frac{1}{\xi}\left[\sqrt{\xi^2(\beta + c) - 1} - \sqrt{\left(\xi\frac{R}{a}\right)^2\beta + c\xi^2 - 1}\right] + \chi\, c\xi, \end{gathered} \tag{9}$$

in region

$$R \le R_-, \qquad \frac{1}{\beta(R/a)^2 + c} \le \xi^2 < \infty; \tag{10}$$

$$\begin{gathered} \chi(R, \xi) = \frac{1}{\sqrt{1 - c\xi^2}}\left[\arccos\left(\frac{a}{R}\sqrt{\frac{1 - c\xi^2}{\xi^2\beta}}\right) - \arccos\sqrt{\frac{1 - c\xi^2}{\xi^2\beta}}\right], \\ y(R, \xi) = \frac{1}{\xi}\left[\sqrt{\xi^2(\beta + c) - 1} - \sqrt{\left(\xi\frac{R}{a}\right)^2\beta + c\xi^2 - 1}\right] + \chi\, c\xi, \end{gathered} \tag{11}$$

in region

$$R \ge R_+, \qquad \frac{1}{\beta + c} \le \xi^2 < \infty. \tag{12}$$

In region

$$R_- \ge R \ge R_+,$$

$$\eta(z)\frac{1}{\beta + c} + \eta(z)\frac{1}{\beta(R/a)^2 + c} \le \xi^2 < \infty, \tag{13}$$

the front of the shock is described by solution (with $b(\xi) \neq 0$, where $b(\xi)$ is chosen from the continuity condition of χ and y):

$$\chi(R,\xi) = \frac{1}{\sqrt{1-c\xi^2}}\left[\arccos\left(\frac{a}{R}\sqrt{\frac{1-c\xi^2}{\xi^2\beta}}\right) + \arccos\sqrt{\frac{1-c\xi^2}{\xi^2\beta}}\right],$$
$$y(R,\xi) = \frac{1}{\xi}\left[\sqrt{\xi^2(\beta+c)-1} + \sqrt{\left(\xi\frac{R}{a}\right)^2\beta + c\xi^2 - 1}\right] + \chi\, c\xi. \tag{14}$$

The bounds of the regions R_+ and R_- follow from real-validity and continuity of χ and y [8], and are defined by equations

$$y = \sqrt{\beta}\left[\sqrt{1-\left(\frac{R_-}{a}\right)^2} + \frac{c}{\beta}\frac{a}{R_-}\arccos\frac{R_-}{a}\right], \tag{15}$$

$$y = \sqrt{\beta}\left[\sqrt{\left(\frac{R_-}{a}\right)^2 - 1} + \frac{c}{\beta}\arccos\frac{a}{R_+}\right], \tag{16}$$

which follow from (9) and (11) correspondingly.

Ultra relativistic shock wave is formed in the initial stage of expansion in the case of analysis of the shock waves, generated by energy emission of hypernova order. It's velocity of spreading in any point of the front equals light speed.

Blandford — Mac-Kee formula, which describes the behaviour of the ultra relativistic shock wave front in the homogeneous medium, is used for analysis of initial stage of shock wave expansion:

$$\Gamma^2 = \frac{E}{\rho\, c^2 V}, \tag{17}$$

where $V = \frac{4\pi}{3}(ct)^3$ is the volume bounded by shock front. So, the time expended on the ultra relativistic stage of expansion (at $\Gamma^2 \geq 1$) is expressed in energy of blast and density of medium:

$$t_{ur} = \sqrt[3]{\frac{3E}{4\pi c^5 \rho}}, \tag{18}$$

and full time of the shock front expansion presented in form of a sum of times expended to ultra relativistic and non-relativistic stages of expansion accordingly to (6) and (18):

$$t_f = t_{ur} + \sqrt{\frac{2\rho_0}{\lambda(\gamma^2-1)E}}\int_{y_{ur}}^{y}\sqrt{V(y)}\,dy, \tag{19}$$

where y_{ur} — such «time» moment y, that $V(y) = \frac{4\pi}{3}(ct_{ur})^3$.

In Fig. 2 one can see the remnant of hypernova blast and calculated form of shock front in the «time» instant $y = 8.5$ corresponding to the real time $t \sim 30000$ years, passed since the moment of the blast with energy $E \sim 10^{48}$ J, which took place on a distance 500 light years from the density singularity.

In Fig. 2 it is noticeable the correspondence of the forms of the shock waves overflowing density decrease, which in this case can correspond to the dense cloud of the interstellar gas with size $R \sim 0.5$ light years and density $\rho \sim 10^{-21}$ kg/m^3 [2]. Also, there are many formations similar to one described above here in the left-hand side of

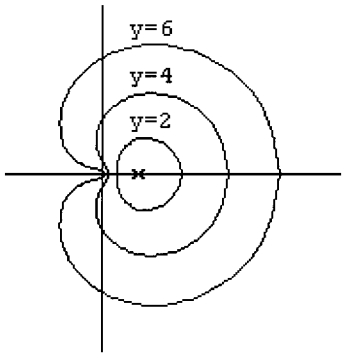

Figure 1. Cross section of a shock wave front in thee successive «time» moments y

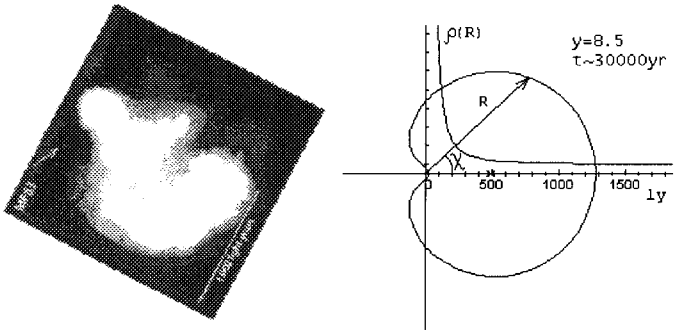

Figure 2. Image of the intended hypernova remnant MF83 (on the left side) and calculated form of a shock wave front (in the right side). Object, which can correspond to density singularity is marked by arrow (in the right figure density singularity is situated in the coordinate center), and overflow of a shock wave front is observed around it, shown in the right-hand side of the figure. Red color on the left figure corresponds to ionized sulfur, green — H_α-emission. Explosion point R = 500 light years is marked up by cross.

Fig. 2. These formations may be shown as a result of the overflow of the shock wave front on stars and interstellar gas clouds situated nearby the hypernova explosion.

REFERENCES

1. Energetic evidence for Hypernovae // Sky and Telescope.—1999.—July.—P. 25—27.
2. Binovaty-Kogan G. S., Silich S. A. Shock wave propagation in the nonuniform interstellar medium // Rev. Mod. Phys.—1995.—**67**, N 3.—P. 661—712.
3. Kompaneets A. S. Point explosion in nonuniform atmosphere // Dokl. AN SSSR.—1960.—**130**, N 5.—P. 1001—1003.
4. Kontorovich V. M., Pimenov S. F. Exact solution of Kompaneets equation for a strong point explosion in a medium with quadratic density decrease // Izv. VUZov RADIOFIZIKA.—19???.—**41**, N 6.—P. 683—698.
5. Kontorovich V. M., Pimenov S. F. Investigation of shock wave in an inhomogeneous solar atmosphere // Solar Physics.—1997.—**172**.—P. 93—101.
6. Korykansky D. G. An off-center point explosion in a radially stratified medium: Kompaneets approximation // Astrophys. J.—1992.—**398**.—P. 184—189.
7. Paczynski B. Gamma-Ray Burst — Supernova Relation. astro-ph/9909048.
8. Silich S. A., Fomin P. I. Point explosion in exponential atmosphere with nonzero asymptote // Dokl. AN SSSR.—1983.—**268**, N 4.—P. 861—864.
9. Wang Q. D. Detection of X-ray emitting hypernova remnants in M101 // Astrophys. J.—1999.—**517**.—P. L27—L30.

Космічна наука і технологія. ДОДАТОК. 2001. Т 7. № 2. С. 105—109.

UDC 524.7

THE DIFFUSION MODEL OF EXTRAGALACTIC RADIO SOURCE EXTENDED COMPONENTS

F. M. Kolesnikov

Institute of Radio Astronomy NANU, Kharkov, Ukraine
koles@ira.kharkov.ua

INTRODUCTION

The diffusion model is applied to extragalactic radio source extended components for modelling of radio source component images. It is assumed that the radio source hot spots (injection regions) are sources of relativistic electron plasma (accelerated by shocks). Electrons of plasma propagate due to the diffusion, lose the energy because of the synchrotron emission, and form the lobes (radio emitting clouds). The motions of the injection regions are introduced and it naturally explains the lobes size asymmetry and the displacement of the hot spots with respect to the center of the lobes [8]. There is the kinetic equation to be considered. The kinetic equation describes the diffusion of plasma relativistic electrons analytically and synchrotron losses are taken into account. The injection spectrum of the hot spots is taken as the power-law dependence on the energy within the given energy interval, the diffusion coefficient and the magnetic field are assumed to be dependent on coordinates. From the transfer equation the radio emission of electrons is found numerically, the reabsorption being taken into account. The Stoks parameters for plasma electrons are found from the formulas for the synchrotron emission. Velocities of the radio source hot spots and the diffusion velocity of plasma electrons determine the correlation of transverse and longitudinal lobe sizes. Observed changes of lobes at various frequencies accord with the diffusion model [3]. The reabsorption in the lobes leads to their asymmetry, depending on source rotation relative to the line of sight [6]. The distributions on a source of the polarized emission intensity, radio images at various frequencies and sources' spectra are received. The results are compared with the centimeter and decameter wavelengths observational data.

DIFFUSIONAL MODEL

The distribution function $N(E, \mathbf{r}, t)$ for the relativistic electrons satisfies the kinetic equation with a moving source:

$$\frac{\partial N}{\partial t} - \frac{\partial}{\partial E}(\beta E^2 N) - D\Delta N = Q\delta(x - Vt)\delta(y)\delta(z)E^{-\gamma_0}\Theta(t)\Theta(E_2 - E)\Theta(E - E_1).$$

The second term in the equation describes the synchrotron and the Compton losses with the synchrotron losses factor: $\beta = \left(\frac{32\pi}{9}\right)\left(\frac{e^2}{mc^2}\right)\frac{\omega_H + \omega_r}{m^2c^3}$, where $\omega_H + \omega_r$ is the energy density of the magnetic field and the emission. To simplify the model, disregard the possible coordinate dependence of the diffusion coefficient D, and the magnetic field H, the power-law dependence on the energy is taken for the diffusion coefficient: $D = D_0(E/E_D)^{\mu}$. The right-hand part of the kinetic equation corresponds to the point source of relativistic electrons (the hot spot) moving along the x-axis with the velocity V; the injection spectrum is taken as the power-law dependence on the energy $E^{-\gamma_0}$ in the range $E_1 < E < E_2$ and zero outside it. Here γ_0 is the injection index corresponding to acceleration in shocks ($\gamma_0 = 2$ in our calculations). The expression for the distribution function is given in the appendix. The Stoks parameters

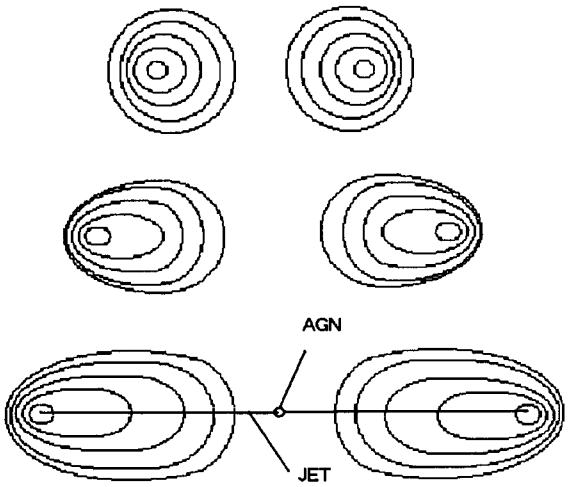

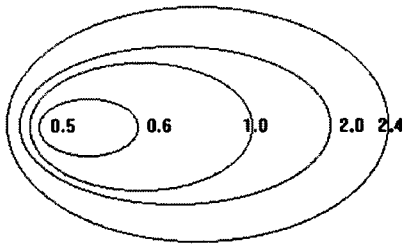

Figure 1. Radio source images for various correlations of hot spot velocity in the mapping plane and the electron diffusion velocity: $V/V_{\text{diff}} = 1, 4, 8$. $\gamma_0 = 2$; contour levels are 2, 4, 6, 8, 10 dB

Figure 2. The distribution of the spectral index α; $V/V_{\text{diff}} = 8$, $\gamma_0 = 2$; every contour conforms to a particular spectral index: 0.5, 0.6, 1.0, 2.0, 2.4

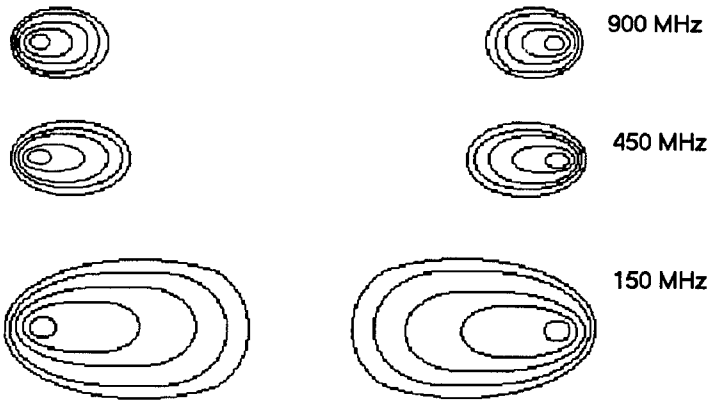

Figure 3. Radio source images obtained at three frequencies: 150 MHz, 450 MHz, 900 MHz; $\gamma_0 = 2$, $V/V_{\text{diff}} = 8$; contour levels are 2, 4, 6, 8 and 10 dB

for electrons are found from the formulas for the synchrotron emission [4], [5]:

$$I_\nu = I(\nu, \mathbf{r}, t) = \frac{\sqrt{3}e^3}{mc^2} \int dEdRN(E, \mathbf{r}, t) H \sin\chi \frac{\nu}{\nu_c} \int_{\nu/\nu_c}^{\infty} K_{5/3}(\eta) d\eta,$$

$$Q_\nu = Q(\nu, \mathbf{r}, t) = \frac{\sqrt{3}e^3}{mc^2} \int dEdRN(E, \mathbf{r}, t) H \sin\chi \cos 2\tilde{\chi} \frac{\nu}{\nu_c} K_{2/3}(\nu/\nu_c),$$

$$U_\nu = U(\nu, \mathbf{r}, t) = \frac{\sqrt{3}e^3}{mc^2} \int dEdRN(E, \mathbf{r}, t) H \sin\chi \sin 2\tilde{\chi} \frac{\nu}{\nu_c} K_{2/3}(\nu/\nu_c).$$

$\int dR$ ... corresponds to the integration along the line of sight, χ is the angle between the magnetizing force and the line of sight, $\tilde{\chi}$ is the angle between the mapping plane projection of the magnetic field H_{plane} and the biggest axis of the electric vector oscillation ellipse, ν_c is the cyclotron frequency: $\nu_c = = \frac{3eH_{\text{plane}}}{4\pi mc}\left(\frac{E}{m}\right.$

As to parameter V_ν it turns out to be zero in the ultrarelativistic approach. Figures 1—4 show examples

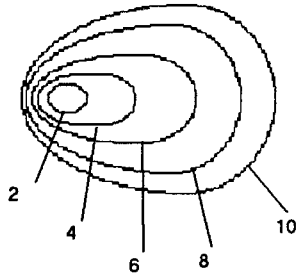

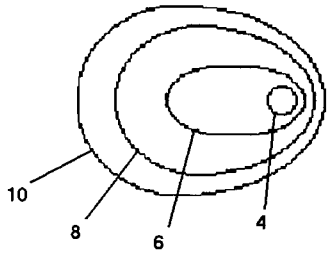

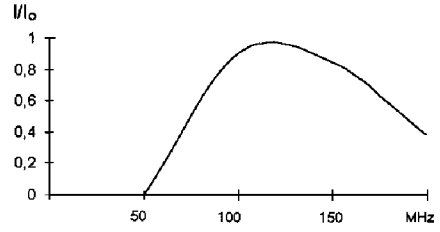

Figure 4. Images of radio source at 150 MHz rotated at 10 degrees (the left-hand lobe is closer to the observation point). The reabsorbtion is taken into account; $\gamma_0 = 2$, $V/V_{\text{diff}} = 8$; contour levels are 2, 4, 6, 8 and 10 dB

Figure 5. The radio source (the right-hand component, figure 4) spectra with account of reabsorption

of radio images for various values of parameters, reabsorption and the distribution of the spectral index are taken into account. Another example is the spectrum of a source with the reabsorption (figure 5). The spectrum has a typical abatement at low frequencies.

3C286

3C286 (1328+307) is a powerful radio source identified as a quasar at $z = 0.849$ [2]. The radio source has a steep spectrum which turns over at about 100 MHz. Subarcsecond resolution radio images show a misaligned triple structure, the central component of which accounts for at least 95 % of the total flux density at all frequencies. 3C286 is one of the strongest extragalactic sources in polarized emission (0.84 Jy at 5 GHz and 1.41 Jy at 1.4 GHz) and with a rotation measure close to zero. Hence, the observed orientation of the electric field vector is essentially independent of frequency. The polarized image reveals strong linear polarization, with the magnetic field which has dominant component which is perpendicular to the source axis (Fig. 6a). The former interpretation of the morphology of 3C286 was

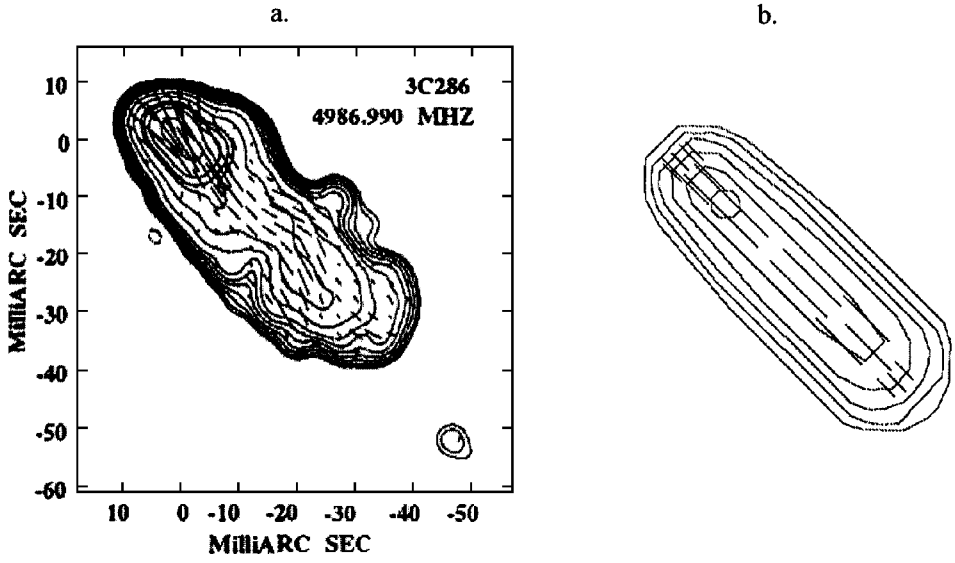

Figure 6. a: EVN polarizaton image of 3C286 [2], contour levels are −3.0, 3.0, 4.2, 6, 8.4, 12, 16.8, 24, 45, 90, 180, 240, 360, 750 mJy/beam and the peak is 1.0 Jy/beam; the vectors represent the projected orientation of the electric vector; their length is proportional to the polarized flux density; b: polarization image at 5000 MHz obtained in the diffusion model, contour levels are 2, 4, 8, 12, 16, 20 dB

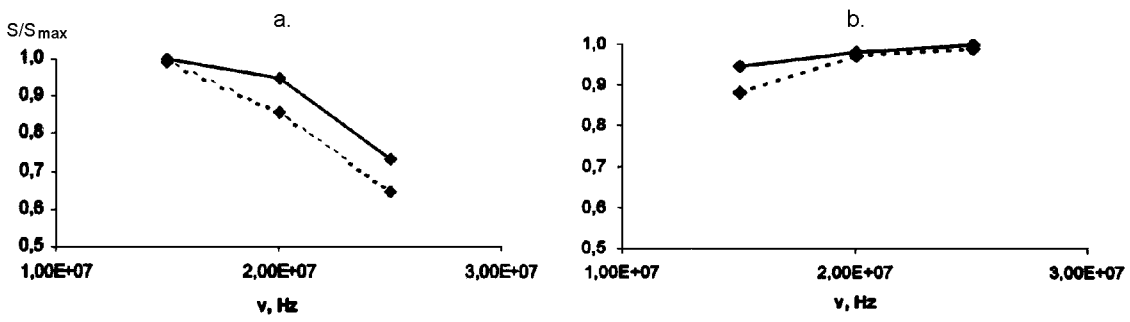

Figure 7. 3C196 components' spectra; a: the extended component spectrum; b: the compact component spectrum; dash lines correspond to the observation data and solid lines are model curves

that the brightest region of 3C286 harbours the core, and the overall arcsecond morphology is that of a misaligned, asymmetric and core-dominated triple. However, on mas scales the cores of quasars are rarely strongly polarized (at most 2 %) and the magnetic fields in the jets of quasars are often quite closely parallel to the jet axes. Moreover, the lack of reported significant variability in the total flux density of 3C286 implies that the source orientation is near the plane of the sky and that the core has a steep high frequency spectrum. There is the possibility that the brightest region of 3C286 is a lobe with the hot-spots in an asymmetric, compact FR II radio source. A steep radio spectrum, high fractional polarization and the perpendicular field orientation are in agreement with the observed properties of the hot-spot regions of FR II sources, where the high polarization and transverse field are originated by a compression shock. The strong asymmetry between the sizes and flux densities of the two lobes may be due to different local environments, and the main lobe would apper brighter and smaller due to a stronger confinement of the radio emitting plasma. It was obtained a polarization image of the 3C286 southwest component at 5 GHz in the model numerically (Fig. 6b).

3C196

3C196 (z = 0.871) is one of the brightest radio source of the south sky. At high frequencies the 3C196 radio images commonly consist of two compact components. The angular structure study of the radio emission was carried out by URAN-1 and URAN-4 radio interferometers at 25, 20 and 16.7 MHz [7]. As it has been found the angular structure at high frequencies and at decameters were noticeably different. Only one compact component was observable at decameters and an extended component was detected. At three frequencies (25, 20 and 16.7 MHz) the extended and compact component fluxes and spectral indexes (between 25 and 20 MHz) were obtained. In the diffusion model network we computed component spectra and spectral indexes. The extended component spectral index is 1.14 (1.25 is observed) and −0.08 for the compact component (−0.08 is observed).

APPENDIX

The distribution function $N(E, \mathbf{r}, t)$:

$$N(E, \mathbf{r}, t) = \frac{Q_0 E^{-2}}{8\pi^{3/2}\beta}\left(\frac{\beta(1-\mu)E_D^{\mu}}{D_0}\right)^{\{}(\gamma_0 - 1)(1-\mu)(1-\mu)\times$$

$$\times \int_{\lambda^2(E_2)}^{\lambda^2(E)} \frac{d\lambda_0^2 \lambda_0^{2(\gamma_0-1)(1-\mu)-2}}{(\lambda^2-\lambda_0^2)^{3/2}} \Theta[tD_0-(\lambda^2-\lambda_0^2)] \exp\left\{\frac{-\left[x-V*t+\frac{v}{D_0}(\lambda^2-\lambda_0^2)\right]^2-y^2-z^2}{4(\lambda^2-\lambda_0^2)}\right\}.$$

In this expression for the distribution function $\lambda^2 = D_0 E^{\mu-1}/(1-\mu)E_D^{\mu}\beta)$ is the square of the diffusion length [1]. We see from expressions for the distribution function and the radio spectrum (4) that the external shape of radio lobes is determined by the relation between the electron diffusion velocity $V_{diff} = = D_0/\lambda$ and the velocity of the source V in the mapping plane.

REFERENCES

1. Berezinskiy V. S., Bulanov S. V., Ginzburg V. L., et al. Astrophysics of cosmic rays. — Moscow: Nauka, 1984.—358 p.
2. Dallacasa D., Schilizzi R. T., Sanghera H. S., et. al. 5GHz EVN polarization of 3C286. Extragalactic radio sources // IAU.—1996.—**175**.—P. 85-87.
3. Gestrin S. G., Kontorovich V. M., Kochanov A. E. The diffusion model of extended radiocomponents and jets with the moving source of accelerated particles // Kinematica i Fizika Nebesnykh Tel.—1987.—**3**, N 4.—P. 57—67.
4. Ginzburg V. L. Theoretical Physics and Astrophysics. — Moscow: Nauka, 1987.—488 p.
5. Ginzburg V. L., Syrovatskii S. I. Origin of cosmic rays. — Moscow: Nauka, 1963.—384 p.
6. Kontorovich V. M., Kolesnikov F. M. The images of extragalactic radio sources in the diffusion model // Gamov Memorial International Conference.—1999.—**45**.—P. 87—89.
7. Men' A. V., Braude S. Ya., Rashkovskij N. K., et al. Radio emission of the quasar 3C196: the angular structure // Izvestiya Vysshikh Uchebnykh Zavedeniy, Radiofizika.—1990.—**33**, N 5.—P. 523—533.
8. Valtaoja E. Diffusion of electrons in radio galaxies // Astron. and Astrophys.—1982.—**111**, N 2.—P. 213—219.